Analysis of atmospheric VSLS measurements during the DRIVE campaign in the tropical East Atlantic

Diploma thesis

by

Steffen Fuhlbrügge

MATHEMATISCH – NATURWISSENSCHAFTLICHE FAKULTÄT DER
CHRISTIAN – ALBRECHTS – UNIVERSITÄT ZU KIEL

ERSTELLT AM LEIBNITZ – INSTITUT FÜR MEERESWISSENSCHAFTEN

FORSCHUNGSBEREICH 1

MARITIME METEOROLOGIE

KIEL, JULI 2011

Abstract

This diploma thesis investigates variations in mixing ratios of very short lived substances (VSLS) during the DRIVE (Diurnal and Regional Variability of halogen Emissions) campaign in the tropical East Atlantic conducted during P399 2/3 from May to June 2010. The main focus lies on the diurnal and regional variability of three halocarbons influenced by meteorological factors at six 24 h stations. For this reason, regular ship measurements of temperature, wind, air pressure and humidity were complemented by radiosonde launches and air samples for the trace gas investigation. According to the radiosonde measurements a changeover between tropical and extra tropical air masses is observed at about 30° N. In contrast to the dominating trade wind regime with northeasterly winds, the ship cruise was mainly exposed to north-northwesterly winds with moderate weather conditions. In addition, the height of the atmospheric boundary layer is determined from the atmospheric profile, ranging from 500 m – 1700 m over open ocean. At coastal areas, especially at the Mauritanian upwelling, the boundary layer stays at the surface. For an evaluation of the wind measurements, wind speed and direction are compared to a high resolution ERA-Interim data set and, to NCEP/NCAR Reanalysis Project 1 Data (NNRP-1). In situ ship measurements show higher correlations for the wind speed (ERA-Interim: r = 0.91, NNRP-1: r = 0.79) than for the wind direction (ERA-Interim: r = 0.69, NNRP-1: r = 0.67). Recalculating the correlation coefficients for the same temporal resolution (6-hourly) results in an improvement of the correlations, indicating a good agreement between the observed and simulated wind. For the determination of potential source regions, the trajectory model HYSPLIT is used to investigate the origin of the observed air masses. The air mass history is analyzed 315 h backwards, indicating an air mass origin mainly above the North Atlantic during leg 2 but also above the Arctic Ocean during leg 3. During the 24 h stations close to the coast predominantly younger and local sources seem to influence the observed trace gas mixing ratios (mean $CH_2Br_2/CHBr_3$ ratio: 0.4) with a partly strong dependency on the wind direction ($r > 0.81$). Especially the methyl iodide mixing ratios show a strong relation to air masses originating at the Banc d'Arguin National Park. In contrast to that, bromoform and dibromomethane show an increase of the mixing ratios connected to trajectories passing the coastal areas of Mauritania and Western Sahara. Increased mixing ratios of the observed trace gases concentrations with highest values of 8.9 ppt (bromoform), 3.31 ppt (dibromomethane) and 1.25 ppt (methyl iodide) are observed in combination with lowest boundary layer heights. With correlation coefficients of r = -0.90 (bromoform), r = -0.91 (dibromomethane) and r = -0.63 (methyl iodide) especially the mixing ratios of the longer lived bromocarbons seem to be strongly connected to the boundary layer height. However, the highest atmospheric bromoform mixing ratio of 9.8 ppt was not observed at the Mauritanian upwelling (leg 2), but close to Lisbon (leg 3) with the Rio Tejo as a potential source region. This implies the significance of regional sources as well as the consideration of the current lower atmospheric state for the variations of the VSLS mixing ratios.

Zusammenfassung

Diese Diplomarbeit untersucht die Variabilität in den Mischungsverhältnissen sehr kurzlebiger Spurengase (VSLS) innerhalb der DRIVE (Diurnal and Regional Variability of halogen Emissions) Kampagne während P399 2/3 im tropischen Ostatlantik von Mai bis Juni 2010. Dabei richtet sich der Blick insbesondere auf die täglichen und regionalen Variationen dreier sehr kurzlebiger halogenierter Spurengase durch meteorologische Faktoren, während sechs 24 h Stationen. Hierfür wurden an Bord des Schiffes, neben Radiosondenaufstiegen zur Untersuchung der vertikalen Struktur der Atmosphäre, regelmäßige Messungen von Temperatur, Wind, Druck und Feuchte, sowie Luftprobennahmen zur Messung der atmosphärischen Mischungsverhältnisse vorgenommen. Anhand der Radiosondenaufstiege lässt sich ein Übergang zwischen tropischen und extratropischen Luftmassen bei ca. 30° N feststellen. Entgegen des eigentlichen Passatwindregimes mit überwiegend nordöstlichen Winden, war die Fahrt überwiegend durch eine ruhige Wetterlage mit nordnordwestliche Winden bestimmt. Aus dem Profil der Atmosphäre wird die Höhe der atmosphärischen Mischungsschicht bestimmt, welche über dem offenen Ozean zwischen 500 m und 1700 m variiert und in Küstennähe, speziell im Bereich des Mauretanischen Auftriebs, den Boden erreicht. Für eine objektive Einschätzung der jeweiligen Genauigkeit von Windgeschwindigkeit und Richtung werden die Schiffsmessungen mit hochaufgelösten ERA-Interim Daten und mit NCEP/NCAR Reanalyse Daten (NNRP-1) verglichen. Hier zeigen sich für die in situ Schiffsmessungen höhere Übereinstimmungen in der Windgeschwindigkeit (ERA-Interim: r = 0.91, NNRP-1: r = 0.79) im Vergleich zur Windrichtung (ERA-Interim: r = 0.69, NNRP-1: r = 0.67). Eine Neuberechnung der Korrelationskoeffizienten bei gleicher zeitlicher Auflösung (6 stündlich) resultiert in einer Verbesserung der Korrelationen, was auf eine gute Übereinstimmung der beobachteten Windverhältnisse mit den simulierten schließen lässt. Für die Bestimmung möglicher Quellregionen werden mithilfe des Trajektorienmodells HYSPLIT die Ursprungsgebiete der untersuchten Luftmassen ermittelt. Hierbei wird der in den vergangenen 315 h zurückgelegte Weg der Luftmassen ermittelt, welche ihren Ursprung hauptsächlich im Nordatlantik (Leg 2), sowie im Arktischen Ozean (Leg 3) haben. Während der 24 h Stationen in den küstennahen Auftriebsregionen ergeben sich jedoch überwiegend jüngere und lokale Quellen für die gemessenen Spurengase (mittleres $CH_2Br_2/CHBr_3$ Verhältnis: ~ 0.4), mit einer teils starken Abhängigkeit von der Windrichtung ($r > 0.81$). Besonders die Methyljodidkonzentrationen zeigen eine starke Verbindung zu Luftmassen mit dem Banc d'Arguin National Park als Ursprungsgebiet. Im Gegensatz dazu zeigen Bromoform und Dibrommethan eine Konzentrationszunahme in Verbindung mit Trajektorien über den Küstengebieten Westsaharas. Erhöhte Mischungsverhältnissen der Spurengaskonzentrationen mit maximalen Werten von 8.9 ppt (Bromoform), 3.31 ppt (Dibrommethan) und 1.25 ppt (Methyljodid) treten in Zusammenhang mit geringen atmosphärischen Mischungsschichthöhen auf. Die Korrelation der Spurengase mit der Mischungsschichthöhe ergibt r = -0.90 (Bromoform), r = -0.91 (Dibromomethane) und r = -0.63 (Methyljodid), und zeigt damit insbesondere für die bromierten Kohlenwasserstoffe eine Verbindung zwischen Mischungsverhältnis und Mischungsschichthöhe. Das höchste atmosphärische Bromoformmischungsverhältnis von 9.8 ppt wurde jedoch nicht im Mauretanischen Auftrieb (Leg 2) gemessen, sondern nahe Lissabon (Leg 3), wo der Rio Tejo als mögliche Ursache in Frage kommt. Dies impliziert sowohl die Wichtigkeit von regionalen Quellen

als auch die Berücksichtigung des aktuellen Zustands der unteren Atmosphäre auf die Variationen der VSLS Mischungsverhältnisse.

Table of contents

1. Introduction

Ozone depletion in the atmosphere is mainly caused by anthropogenic sources of chlorine and bromine (WMO, 2007). Although the bromine concentrations in the stratosphere are about two orders of magnitude lower than those of chlorine, it has a much higher ozone depleting efficiency (up to 50 times) on a per atom basis (Sinnhuber and Folkins, 2006). Besides the anthropogenic sources, naturally produced halocarbons can also be an intense source for the organic halogen content in the atmosphere (WMO, 2007; Salawitch, 2006). Studies have shown distinctive emissions in tropical coastal regions due to high biological productivity, e. g. by macro algae, seaweed and phytoplankton (Zhou et al., 2005). The VSLS are predominantly transported into the upper troposphere and lower stratosphere by deep convection especially at the tropics Warwick et al., 2006). Exposed to ultraviolet radiation from the sun, inorganic bromine (Br_y) is converted to more reactive gases and are estimated to contribute 20 - 30 % of the tropospheric and stratospheric ozone depletion (Salawitch et al., 2005; Warwick et al., 2006). Impacts on emission and production fluxes of these compounds or on the deep convection due to climatic changes could significantly influence tropospheric and stratospheric ozone (Quack et al., 2004; Salawitch, 2006; WMO, 2011).

Recent studies (Quack et al., 2004, 2007; O'Brien et al., 2009) have shown high emission rates of reactive bromine and iodine at the area of the Mauritanian upwelling. Quack et al. (2004) suggested regionally enhanced biogenic production in the water column of the Mauritanian upwelling and the resulting high sea-to-air fluxes of VSLS to be responsible for very high tropospheric VSLS mixing ratios in this region. The shelf waters have been identified as a source of bromocarbon compounds for the atmosphere and enhanced sea-to-air emissions. For a better understanding of present and future atmospheric trace gas impact, and the determination of physical feedbacks between chemical emissions of marine short lived substances and transport processes in the atmosphere, the DRIVE campaign examines the further role of coastal areas in the North East Atlantic for the formation and emission of halocarbons and reactive inorganic halogen compounds, especially their diurnal and regional variability. This diploma thesis evaluates the meteorological conditions during DRIVE and investigates potential influences on the atmospheric VSLS mixing ratios, in particular those of bromoform, dibromomethane and methyl iodide. A special focus lies on their relation to the mixed layer height. The meteorological fundamentals and the trace gases of interest, in combination with their potential to ozone depletion are introduced in Chapter 2. Chapter 3 describes the numerical data and methods used for the investigation of air mass origins. The ship cruise is described in Chapter 4, highlighting first meteorological and chemical results for both cruise legs. Chapter 5 investigates and evaluates the VSLS measurements in combination with an analysis of the air mass origin by HYSPLIT backward trajectories, especially at the 24 h stations of leg 2. Afterwards, correlations between both, the meteorological and the VSLS measurements, and the VSLS themselves are shown. Finally the results of this thesis are discussed and the conclusions for the observations are drawn.

2. Fundamentals

This chapter provides an overview of the meteorological, oceanographical and chemical basics used for this diploma thesis. Especially for the investigation of the trace gases and the evaluation of their observed mixing ratios, the atmospheric boundary layer and its determination play an important role and will be explained in detail. First the vertical structure of the atmosphere and the predominant wind regimes during the ship cruise are introduced, followed by a description of the Mauritanian upwelling. Finally the chemical background about very short-lived substances (VSLS) in particular bromoform, dibromomethane and methyl iodide and their contribution to ozone depletion, is given.

2.1. Structure of the atmosphere

The word atmosphere derives from the Greek words atmós (“vapor”) and spheira (“sphere”) and describes the aerially shell above the earth’s surface. It is equilibrated by the gravitation of Earth and the proper motion of molecules and atoms. Without gravitation, the gases would escape into space as a consequence of diffusion due to the proper motion of the gas particles.

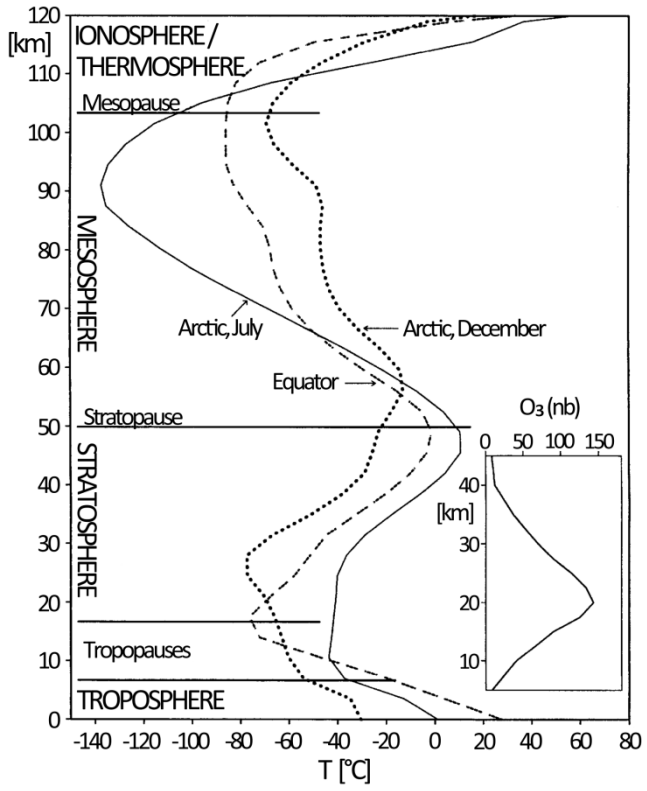

Figure 2-1: Vertical temperature profiles for Equator and Arctic, July and December. The lower right-hand side of the figure shows Partial pressure of ozone (nb) with height in February at about 50° N (Labitzke, 1999).

According to the mean temperature profile (Figure 2-1) the atmosphere can be distinguished between 4 different layers: the troposphere, the stratosphere, the mesosphere and the ionosphere. For this diploma thesis the troposphere and the stratosphere are mainly important and will be discussed in the following.

2.1.1. The troposphere

The first layer from the Earth's surface is the troposphere, which demonstrates decreasing temperature with height. "Troposphere" derives from the Greek word tropé ("twist", "turn"). About 90 % of the total mass and 99 % of the total water vapor of the whole atmosphere exist in the troposphere. It is also the "weather" layer, where the formation of clouds and precipitation as a result of solar insolation and convection takes place. In contrast to the other atmospheric layers, higher vertical wind speeds due to convection and turbulence are found within the troposphere. The thermal and dynamic behavior is caused by the absorption of shortwave radiation at the first heating layer, the surface, and the roughness of the surface itself. The temperature profile of the troposphere can be explained due to transport of latent and sensible heat and by successive transformation of this thermal energy into potential energy as well as due to radiative processes, such as radiative cooling through emission of infrared radiation by water vapor. The troposphere itself can be divided into the atmospheric boundary layer from the surface to about 2 – 3 km height and the free atmosphere above. The atmospheric boundary layer is discussed in detail in the next section.

The temperature profiles of the air for different locations and seasons are shown in Figure 2-1. The temperature decreases from the surface with a rate of about -0.5 to -1 K/100 m to -55 ° to -35 °C at altitudes of 8 km in the Arctic and -80 °C at altitudes of 18 km in the Tropics. This first temperature minimum is called the tropopause and it is located as a kind of intersection layer with a roughly constant temperature between the troposphere and the stratosphere. A few different definitions of the tropopause exist, e. g. the lapse rate tropopause (LRT) which is used by the World Meteorological Organization (WMO):

> "The lowest level at which the lapse rate decreases to 2 °C/km or less, provided that the average lapse rate between this level and all higher levels within 2 km does not exceed 2 °C/km."
>
> (Roe and Jasperson, 1981)

but least physical meaning in the Tropics and the cold point tropopause (CPT):

> "The CPT is defined as the position of the minimum temperature in the vertical temperature profile."
>
> (Highwood and Hoskins, 1998)

which is commonly used for the detection of the tropical tropopause (Highwood and Hoskins, 1998; Labitzke, 1999; Kraus, 2000; Klose, 2008).

2.1.2. The stratosphere

The layer above the troposphere between the tropopause and the stratopause is called stratosphere after the Latin word stratus ("stratified"). It is the second heating layer and as shown by Figure 2-1 it extends from the tropopause to about 50 km of height, where the temperature maximum of about 0 °C is reached. The temperature profile in the stratosphere is mainly defined by the radiation equilibrium of heating by absorption of solar radiation through ozone and cooling through infrared emission. Two main layers can be observed. The first and lower one reaches from the tropopause to about 30 km of height with a temperature gradient of roughly 1 K/100 m and the second one from about 30 km to 50 km of height with a temperature gradient of about 2.5 K/100 m. The lower right-hand side of Figure 2-1 shows the vertical ozone concentration in nanobar (nb) of the lowest 45 km of the atmosphere in February at 50° N. Obviously the temperature maximum at 50 km lies above the ozone peak at 20 km height. The available ozone above the ozone maximum already filters large amounts of solar radiation and therefore heats the upper stratosphere (Labitzke, 1999; Klose, 2008; Roedel and Wagner, 2011).

2.2. Atmospheric boundary layer

The atmospheric boundary layer is the layer between the Earth's surface and the free atmosphere at about 3 km. It responds to forces like frictional drag, evaporation and heat transfer with a timescale of about one hour or less. Consequently, it can be described as the layer where interactions between the Earth's surface and the large scale atmospheric flow take place. In addition to the transfer of sensible and latent heat it also transfers momentum and atmospheric constituents (gases, aerosols and others) between the surface and higher atmospheric levels. The energy transfer is partly accomplished by turbulent eddies. Atmospheric turbulence itself is produced by two different mechanisms in the atmospheric boundary layer: On the one side by wind shear due to surface friction, baroclinity or certain mesoscale phenomena like low level jets or flow channeling, and on the other side by buoyancy due to heating from the ground, radiative cooling of elevated cloud layers, or even by overturning of gravity waves. Substances emitted into this layer are gradually dispersed horizontally and vertically so that they become completely mixed within the atmospheric boundary layer. As a result the terms "mixed layer" and "mixing layer" have become customary in air pollution meteorology, whereas "mixing" describes more commonly the physical process than the result. If the atmospheric boundary layer is defined as the turbulent domain of atmosphere adjacent to the ground, it coincides with the mixed layer. Consequently it influences the near-surface atmospheric mixing ratios of the trace gases by determining the available volume of air into which the trace gases are emitted. In this thesis the boundary layer is declared as the mixed layer. According to the dominant developing mechanism of the turbulence, two basic atmospheric boundary layer regimes can be distinguished: the convective (Figure 2-2) and the stable boundary layer (Figure 2-3) (Stull, 1988; Seibert et al., 1997).

2.2.1. Convective boundary layer

The main source of turbulence in the convective boundary layer (CBL) is positive buoyancy at the Earth's surface, caused by thermal heating due to strong solar insolation. Characteristically the CBL exhibits organized convective structures ("thermal plumes"), which generate an intense vertical exchange of energy and matter. This results in a well-mixed CBL, limited in its vertical extension by a stable layer above with typical height levels of a few hundred meters to 2 - 3 km above the ground, depending on the location and season.

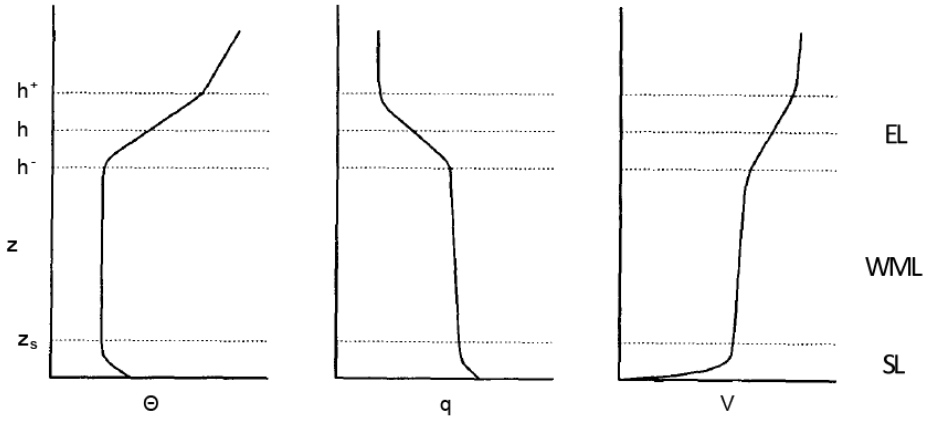

Figure 2-2: Idealized structure of the convective boundary layer, from left to right: potential temperature *Θ*, specific humidity *q* and wind speed *V* against height *z*. The height of the surface layer is indicated by z_s and the mixed layer height by *h* with extreme definitions h^- and h^+. *SL* stands for surface layer, *WML* for well-mixed layer and *EL* for entrainment layer (Seibert et al., 1997).

Figure 2-2 shows idealized cases of the vertical profiles of potential temperature *Θ*, specific humidity *q* and wind speed *V*. *h* marks the mixed layer height with extreme definitions h^+ and h^-. The CBL can be divided into 3 sub layers. The lowest layer is the "surface layer" (SL), covering about 5-10 % of the whole CBL and characterized by a super adiabatic lapse rate, a decrease of specific humidity with height and a significant vertical wind shear. The upper limit of the surface layer is marked in Figure 2-2 by z_s. The next higher layer is the so-called "well-mixed layer" (WML), extending from z_s to h^-. This layer embeds about 50-80 % and therefore the major part of the CBL. Intensive vertical mixing leads to a roughly constant vertical profile of most mean meteorological variables with height in this layer. The third and topmost layer is the "entrainment-layer" (EL) which forms a transition zone between the well-mixed layer and the free atmosphere above while covering about 10-30 % of the whole CLB. Referring to Figure 2-2 it can be defined as the layer h^- - h^+. The entrainment-layer is specified by a positive lapse rate, for idealized cases by a sudden increase of potential temperature after a nearly constant linear trend, a sharp decrease of specific humidity and sometimes by a vertical wind shear (Seibert et al., 1997).

2.2.2. Stable boundary layer

The stable boundary layer occurs under stable conditions, when wind shear becomes the only mechanism creating turbulence. The combination of stable background stratification and negative buoyancy, due to radiative cooling, acts as a sink for turbulent kinetic energy. This results in a sensitive equilibrium between development and vanishing of turbulence in the stable boundary layer. Therefore turbulence does not occur continuously but with an intermittent character. The consequence of a weak level of turbulence is a variety of stable boundary layer structures due to the effects of radiative cooling, gravity waves, advection and subsidence. Figure 2-3 shows three different cases for the vertical potential temperature profile: 1) weak horizontal pressure gradients and weak surface winds, 2) an increase of vertical mechanical turbulence and 3) weak radiative cooling and strong winds. Radiative cooling leads to near surface inversions in all cases and especially for the first one in combination with weak mechanical turbulence production to a stable layer with no observable mixed layer height (Figure 2-3-1). For the second case (Figure 2-3-2) two different layers can be distinguished at least, a lower layer with nearly linear increase of potential temperature due to the combination of radiative cooling of the surface and turbulent exchange and an upper layer with much weaker potential temperature gradients caused by radiative cooling of the atmosphere itself. The third and last case (Figure 2-3-3) shows the profile of the potential temperature for strong winds and less radiative cooling leading to a slight increase with height and a layer with relative effective mixing close to the ground.

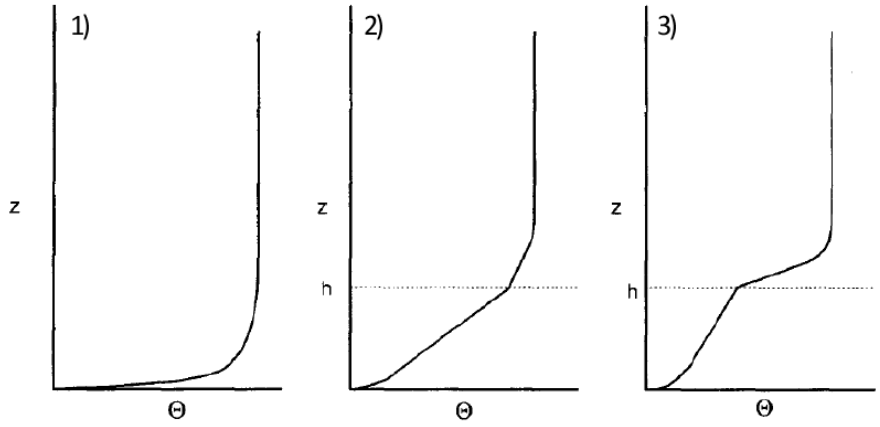

Figure 2-3: Vertical potential temperature profiles in the SBL: 1) weak wind, strong stability, 2) moderate wind, 3) strong wind. *h* marks the height of the mixed layer (Seibert et al., 1997).

2.2.3. Theoretical determination

In order to determine the mixed layer height theoretically it is helpful to use the concept of the Richardson number, which considers the turbulent kinetic energy. For less turbulence as found under stable conditions or close to the top of the boundary layer near the free atmosphere, turbulence has to perform work against the restoring force of gravity. The ratio of the buoyant

developing and destruction of turbulent kinetic energy to the generation by shear is called the flux Richardson number Rif:

$$Ri_f = \frac{g}{T_0} \frac{\langle w'\Theta' \rangle}{\langle u'w' \rangle \ \partial u/\partial z + \langle v'w' \rangle \partial v/\partial z} \ ,$$

with

	g	acceleration of gravity,
	T_0	sea surface temperature,
	u, v	x, y-components of the horizontal wind vector,
	z	height coordinate,
	<$w'\Theta'$>	(potential) momentum flux,
	<$u'w'$>	zonal momentum flux,
	<$v'w'$>	meridional momentum flux.

With the use of the flux-gradient scheme for the parameterization of turbulent fluxes with the eddy diffusivity coefficients for heat K_H and momentum K_M and a first approximation that K_H and K_M are equal, Ri_f becomes the gradient Richardson number Ri:

$$Ri = \frac{g}{T_0} \frac{\partial\Theta/dz}{(\partial u/\partial z)^2 + (\partial v/\partial z)^2} \ .$$

Under homogeneous and quasi-stationary conditions, turbulence vanishes if the Ri number exceeds a critical value $Ri_c \approx 0.25$, as was shown by theory and observations (Seibert et al., 1997).

2.2.4. Practical determination

Radiosoundings are the most common source of data to use for determining the mixed layer height practically. The measurements can be investigated for temperature inversions and temperature lapse conditions in the lower part of the atmosphere. In the convective boundary layer, the mixing height is often identified with the base of a stable layer (elevated inversion) or a significant reduction in air moisture. According to Stull (1988) the CBL height can be identified as the base of an inversion increased by half of the depth of the inversion layer. In addition the virtual potential temperature Θ_v is a common variable based on conserved quantities to identify the mixed layer height. It is analogous to the potential temperature, which is per definition the temperature dry air must have to equal the density of moist air at the same pressure, but neglects temperature variations due to changes in pressure altitude of an air parcel.

Thus the virtual potential temperature is a necessary variable and is derived as follows:

$$\Theta_v = \Theta \cdot (1 + 0.61 \cdot r_{sat} - r_L) \ ,$$

with Θ potential temperature,
r_{sat} water vapor saturation mixing ratio,
r_L liquid-water mixing ratio.

Evidence for the mixed layer height due to virtual potential temperature observations are positive lapse rates after a roughly constant linear trend (Stull, 1988, Seibert et al., 1997).

Together with the gradient Richardson number *Ri* and the wind speed, these quantities are analysed to determine the mixing height from the radiosondes launches along DRIVE (section 4.3.2).

2.3. General Circulation

The general circulation is the summary of large-scale atmospheric circulation systems including horizontal and vertical winds and resulting from the latitudinal varying solar insolation. The Earth is heated by incoming solar radiation. Averaged over a year, it is in a nearly radiative equilibrium, incoming radiation equals outgoing radiation. Taking a look at the global distribution of incoming and outgoing radiation as shown in Figure 2-4, the Earth has an energy surplus of incoming solar radiation in the tropics and a deficit at the poles, where more energy is emitted than absorbed. This imbalance creates temperature gradients from the equator to the poles and results in a rise of air pressure over heated surfaces and a decline of air pressure over cooling surfaces.

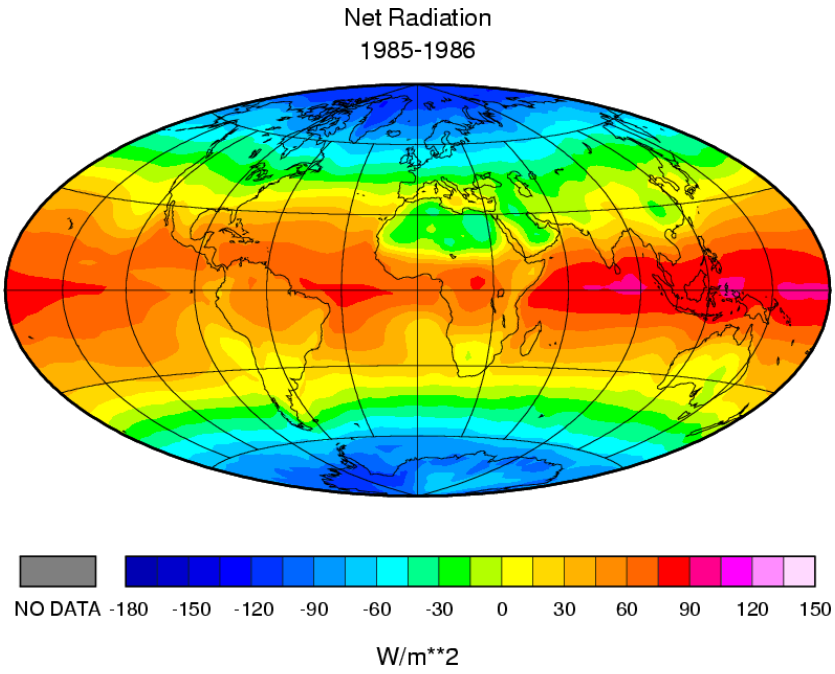

Figure 2-4: Annual mean net radiation balance with positive values for net energy entering the earth and negative values for leaving it, as observed from the earth Radiation Budget Experiment (ERBE) 1985-1986. Source: Graphic by Hartmann and Michelsen, University of Washington.

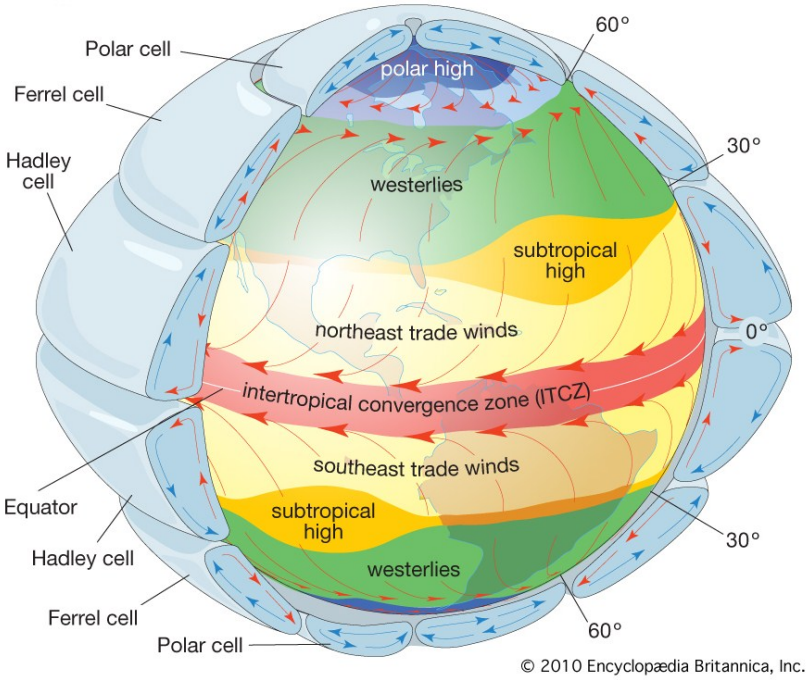

Figure 2-5: General schemata of the global atmospheric circulation. Source: http://media-3.web.britannica.com/eb-media//00/102500-050-2A2E7E20.jpg

The consequential pressure gradient forms a meridional circulation with winds from the equator to the poles at higher altitudes and winds from the poles to the equator at the ground due to continuity reasons. This so-called thermal direct circulation is often named after its discoverer G. Hadley, the “Hadley cell”. For a non-rotating Earth, one Hadley cell would be able to gain the heat balance. Given the rotation of the Earth, a three-cell circulation forms with two thermal-direct cells, the Hadley cell in the tropics and the polar cell in polar regions, and one resulting thermal indirect cell (“Ferrel cell”) in between. The resulting general circulation for the Earth with actual continents and oceans is shown in Figure 2-5. Due to the Coriolis force, resulting from the rotation of the Earth, air parcels are deflected to the right on the northern hemisphere (NH) and to the left on the southern hemisphere (SH). This slows the heat exchange down and makes it inefficient. The meridional temperature gradient in the mid-latitudes increases until a supercritical baroclinity forces the Hadley cell to collapse. Strong insolation at the equator (Figure 2-4) heats the air close to the ground and forces it to ascend, forming the intertropical convergence zone (ITCZ) at the ground. This equatorial trough coincides with the thermal equator and is found at about 5° N on annual average. Apart this fact, the ITCZ also shows a distinct seasonal shift as pointed by Figure 2-6, connected to the varying solar zenith from 23° N (northern midsummer) to 23° S (southern midsummer). Due to the much higher heat capacity of the oceans compared to the continents and the thus resulting less emission of incoming solar energy as sensible heat, the shift of the ITCZ over the oceans is not as intense as it is over land. The current location of the ITCZ over oceans therefore differs just about ± 5° from the mean position at 5° N. Over land variations up to ± 25° depending on the season are observable.

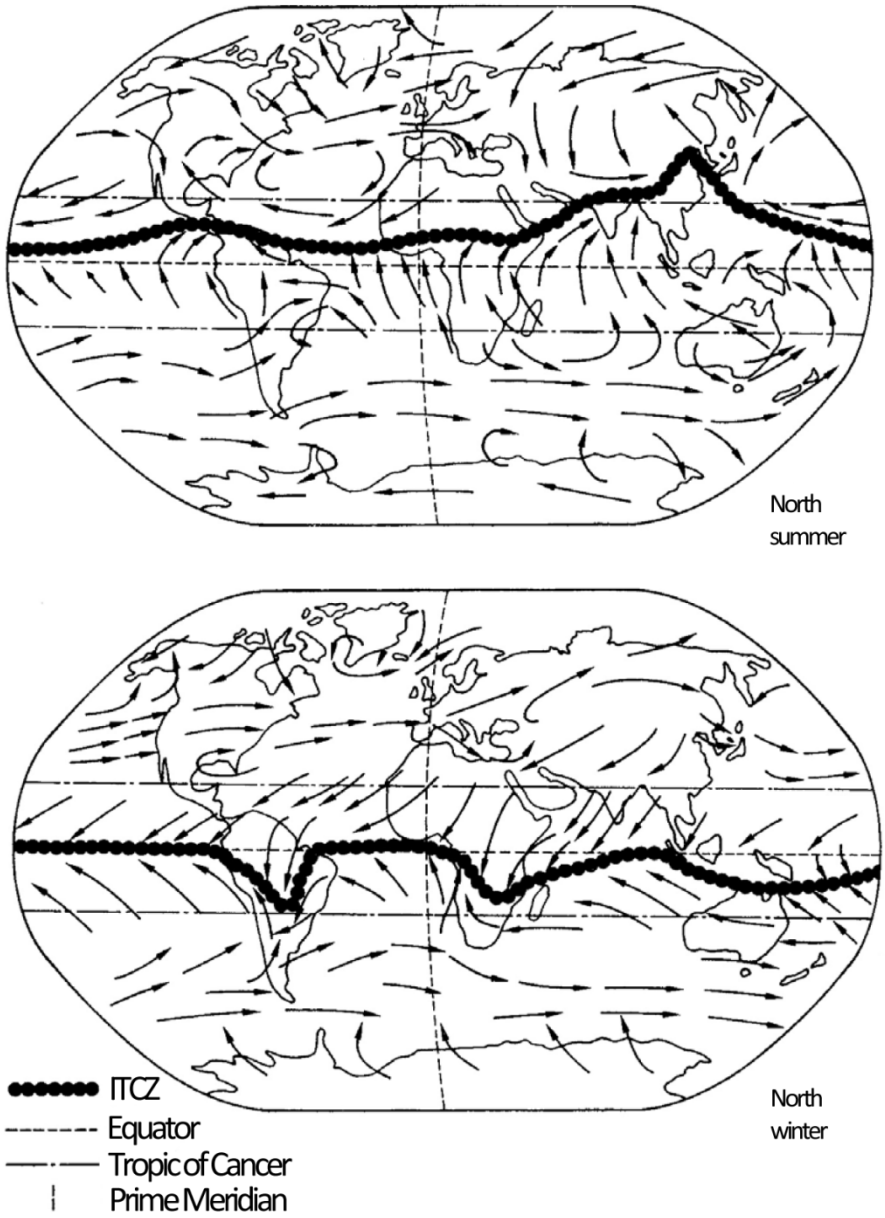

Figure 2-6: Predominant surface winds and the shift of the ITCZ for northern summer and northern winter (Roedel and Wagner, 2011).

After a moist adiabatic ascend in the Tropics, the air reaches the Tropopause at about 18 km of height and diverges to the north and south due to increasing temperatures in the stratosphere, preventing further ascent. The air masses flow poleward and are deflected by the Coriolis force. The resulting wind is called antitrade wind. With increasing latitude, the air cools due to less solar insolation (Figure 2-4) and descends due to the increasing air density. In certain cases a trade inversion develops at 1 – 2 km altitude (Figure 2-7). This is caused by the dry adiabatic warming of the descending air over colder ground level air layers. At about 20 - 30° N/S the air masses reach the ground, forming the so-called “subtropical high-pressure belt” with subtropical highs (Figure 2-5) and flow back to the equator due to continuity. On their way to the equator, the air parcels are again deflected by the Coriolis force, resulting in the trade-wind regime with

predominant winds from the north-east on the NH and south-east on the SH. A meridional schematic pattern of the Hadley Cell is shown in Figure 2-7 together with the trade inversion, the Tropopause and the subtropical jet (STJ) a maximum in the horizontal wind, resulting from the supercritical baroclinity in the mid-latitudes. According to the tropical Hadley cell a polar Hadley cell called “Polar cell” (Figure 2-5) exists as well with predominant easterly winds at the poles. The meridional heat transfer at the mid-latitudes is mainly accomplished by cyclones and anticyclones. Westerly winds characterize this cell (Etling, 2008; Klose, 2008; Roedel and Wagner, 2011).

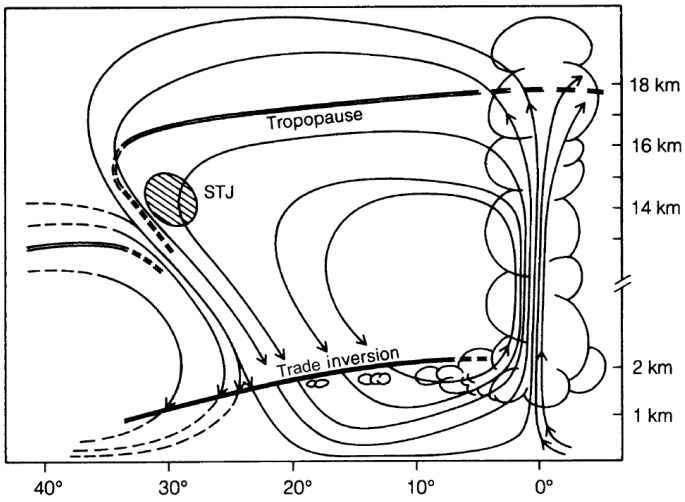

Figure 2-7: Schematic profile of the Hadley cell with warm rising air at the ITCZ (right), the connection to the Ferrel cell at higher latitudes (left), the subtropical jet (STJ), the Tropopause and the trade inversion (Roedel and Wagner, 2011).

2.4. Mauritanian upwelling

For a better understanding of the geographical and hydrological conditions at the northwest African coast, the Mauritanian upwelling, together with the Banc d’Arguin is described in this subsection. Coastal upwelling occurs within a narrow bend of 10 km from 10° N to 25° N (Tomczak and Godfrey, 2005) and therefore within the cruise track of the ship. As a consequence of the dominating trade wind regime, blowing southwest along the northwest coast of Africa, surface waters are transported offshore by Ekman transport (Mittelstaedt, 1986). Friction of the horizontal winds with the water surface results in a generation of wind stress with a shift of 15° to the right of the wind direction by the Coriolis force on the northern hemisphere. A so-called Ekman-spiral develops. The net mass transport is shifted to the right of the surface wind direction by 90°. In combination with western coasts on the northern hemisphere, upwelling occurs along the coastline (Tomczak and Godfrey, 2005). As a result of the trade winds, the Mauritanian upwelling is coupled to the seasonal variations of ITCZ, too. South of 20° N upwelling occurs during winter and spring with a highest intensity during February and March. Further north between 20° N and 25° N upwelling prevails throughout the year with a maximum

intensity during spring and autumn. North of 25° N upwelling arises predominantly during summer and autumn (Mittelstaedt, 1983).

2.4.1. The Banc d'Arguin

The Banc d'Arguin is an area of 491 km² with tidal flats and shallow inshore waters, which borders the Saharan desert at Mauritania at about 20.4° N and 16.1° W (Figure 2-8). Roughly 193 km² are estimated to be covered by dense seagrass beds and about 219 km² to consist of muddy flats with a less dense seagrass cover. The shallows of the area are influenced by the upwelling system at the Mauritanian coast, however the conditions differ from those in the upwelling area. The wind regime is mainly influenced by the trade winds and averaged monthly air temperatures range from 18 °C to 23 °C with hardly any surface run-off or precipitation (Wolff and Smit, 1990).

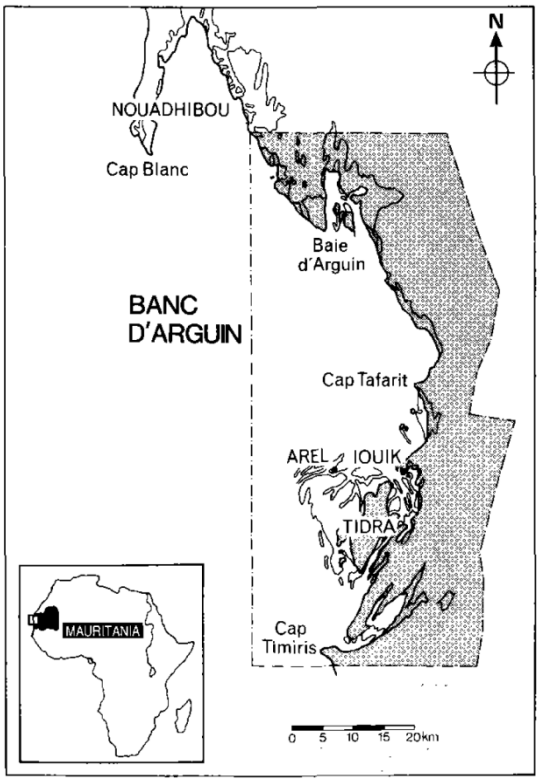

Figure 2-8: Schematic map of the Banc d'Arguin (Wolff and Smit, 1990).

2.5. Very short lived substances

Referring to the WMO (2007) very short-lived substances (VSLS) are "trace gases whose local tropospheric lifetimes are comparable to, or shorter than, tropospheric transport time scales, such that their tropospheric distributions are non-uniform". Typical lifetimes of VSLS are considered be less than half a year in practice (WMO, 2011).

2.5.1. Bromoform

The largest single source of organic bromine for the atmosphere is bromoform ($CHBr_3$). In terms of ozone depletion it is highly important as a source of reactive halogens to the troposphere and lower stratosphere and mainly produced from natural sources in the marine environment (WMO, 2007) especially by macroalgal and planktonic organism. With a mean atmospheric lifetime of 2 – 4 weeks, depending on temperature, location, zenith angle actinic flux and oxidant concentrations, it is able to reach the stratosphere under strong convective conditions, as they are found in the tropics (Barrie et al., 1988; Dvortsov et al., 1999; Schauffler, et al., 1999; Sturges et al., 2000; Nielsen and Douglass, 2001; Montzka et al., 2003; Quack and Wallace, 2003). Together with the degradation products it's photolysed and oxidized (Figure 2-9) both in the lower troposphere and in upper atmospheric layers, where it delivers three reactive bromine species (BrOx: Br + BrO) to the atmosphere (Barrie et al., 1988; Moortgat et al., 1993; DeMore et al., 1997, Kurylo et al., 1999; McGivern et al., 2000, 2002; Quack and Wallace, 2003). The global bromoform sea to air flux has been estimated to about 10 (3 – 22) Gmol Br yr^{-1} due to natural sources (e.g. macroalgal and emissions of polar microalgae) and anthropogenic sources (water chlorination and ozonation) (Blake et al., 2003; Quack and Wallace, 2003). Anthropogenic sources are estimated to about 0.3 (to 1.1) Gmol Br yr^{-1} and can be locally significant but negligible for global estimations (Quack and Wallace, 2003). The largest contribution (60 %) of the global macroalgal bromoform production is performed by brown algae and has been estimated to be 1.6 (0.4 – 2.7) Gmol Br yr^{-1} (Carpenter and Liss, 2000). Quack and Wallace (2003) estimated, that narrow nearshore regions with only 0.3 % of the global ocean area are responsible for 23 %, and continental shelves with 12 % of ocean area contribute about 48 %, to the global total bromoform emission. In contrast to that, the open ocean with 88 % ocean area is estimated to contribute just 29 % of the overall emission. These estimations are associated with significant uncertainties due to the short lifetime and the spatially and temporally variable production and emission rates, as well as atmospheric distributions (Zhou et al., 2008) with a range from 0.2 to >> 100 ppt $CHBr_3$ and typical background mixing ratios of 0.5 – 1.5 ppt in the marine boundary layer (Quack and Wallace, 2003).

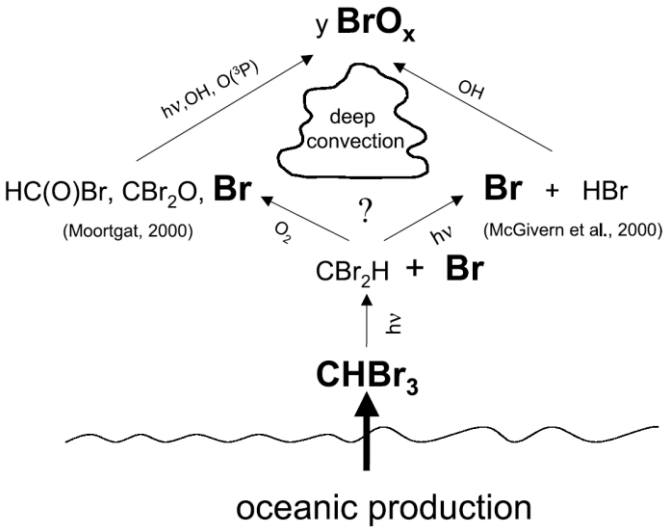

Figure 2-9: Photodissociation of bromoform: primary and secondary processes (Quack and Wallace, 2003).

2.5.2. Dibromomethane

Dibromomethane (CH_2Br_2) is a predominantly marine derived brominated compound without any known anthropogenic sources and a surface lifetime of about 2 - 3 months. It was found as by-product during the formation of $CHBr_3$ in phytoplankton and macro algal cultures (Manley et al., 1992; Tokarczyk and Moore, 1994) and during the process of reductive hydrogenolysis as a possible product from $CHBr_3$ (Vogel et al., 1987; Tanhua et al., 1996). Together with bromoform it's a source of reactive radical species BrO_x (Br + BrO) to the atmosphere (Carpenter and Liss, 2000; McGivern et al., 2000; Quack and Wallace, 2003). Because of its longer lifetime dibromomethane appears not as variable as bromoform but well mixed throughout the troposphere (WMO, 2003). Estimations for global oceanic emissions are about 0.67 – 3.5 Gmol Br (CH_2Br_2) yr^{-1}, which is about 15 – 25 % of the global $CHBr_3$ flux. Global emission ratios for dibromomethane / bromoform on the basis of atmospheric sink estimates, have been estimated to be 0.29 – 0.38 (WMO, 2003). Carpenter et al. (2003) and Yokouchi et al. (2005) report emission ratios of 0.11 – 0.25 in coastal regions increasing up to 0.5 – 1 over open ocean. Due to the longer lifetime of dibromomethane in contrast to bromoform, a concentration ratio of both compounds ($CH_2Br_2/CHBr_3$) gives evidence about the age of encountered air masses, with lower values for younger and higher values for older air masses.

2.5.3. Methyl iodide

Methyl iodide (CH_3I) is a trace gas with predominant natural marine but also anthropogenic origins. As a source of iodine radicals it is of interest in the upper troposphere and lower stratosphere for ozone depletion. It is known to be produced by marine seaweeds (Manley and Dastoor, 1987, 1988), phytoplankton (Moore et al., 1996a; Manley and de la Cueste, 1997) and by photochemical production (Moore and Zafiriou, 1994). These natural emissions contribute to elevated CH_3I in coastal environments and warm ocean surface waters (Bell et al., 2002), but they appear to be negligible on a global scale. Terrestrial emissions are due to rice paddies, natural wetlands and biomass burning. The global methyl iodide sea-to-air flux is estimated to be 0.9 – 2.5 Gmol yr^{-1} with uncertainties because of limited spatial and temporal data (Bell et al., 2002). Atmospheric CH_3I mixing ratios are typically less than or about 3 pptv over most of the Earth's surface and decreasing to less than half the value above the boundary layer. Higher values of about 10 – 20 pptv of CH_3I have been observed near oceanic regions with high biomass productivity, giving methyl iodide a key role in atmospheric chemistry (Rasmussen et al., 1982). A large portion of the global CH_3I is believed to come from these regions (Rasmussen et al., 1982). After reaching the atmosphere methyl iodide is rapidly broken down by photolysis due to ultraviolet radiation. The mean lifetime averages about 5 days (Lovelock et al., 1973; Zafiriou, 1974).

2.5.4. Contribution of VSLS to ozone depletion

The photochemistry of ozone in the upper troposphere and lowermost stratosphere is significantly altered by reactive organohalogens with atmospheric lifetimes of weeks. Depending on emission location and time, the VSL source gases are transported into the stratosphere (source gas injection) where they react and release halogen atoms. In addition also gases produced in the troposphere are transported into the stratosphere, called product gas injection. These product gases are either intermediate products (i.e. organic) or final products (i.e. inorganic) (WMO, 2007).

Short-lived bromine compounds are estimated to contribute 20 – 30 % of tropospheric and stratospheric ozone depletion by delivering their bromine content as inorganic bromine BrO_x (Br + BrO) to higher altitudes (Salawitch et al., 2005; Yang et al., 2005). Particularly after major volcanic eruptions, followed by times of high aerosol loading, enhanced levels of bromine lead to greater efficiency for ozone loss by the BrO + ClO catalytic cycle (Salawitch et al., 2005; Sinnhuber et al., 2006). Synergistic coupling between atmospheric bromine and chlorine cycles produces additional free bromine and chlorine atoms. These can, for moderate mixing ratios of stratospheric bromine, enhance ozone depletion due to chlorofluorocarbons up to 20 % (Wofsy et al., 1975; Yung et al., 1980; McElroy et al., 1986; Anderson et al., 1989; WMO, 1995, 1999; Quack and Wallace, 2003). Effects on tropospheric ozone by inorganic bromine from halogenated VSLS are largely regional in nature, but they have implications on global scale ozone concentrations (WMO, 2007). Further the ozone depleting effectiveness of bromine is about 60 times greater on a mole-for-mole basis than that of chlorine (WMO, 2007; Sinnhuber et al., 2009). Further representative of halogenated VSLS are iodine source gases with significant emissions (WMO, 2007). Stratospheric iodine is predominantly supplied by methyl iodide (Davis et al., 1996). Nevertheless, ozone destruction due to catalytic cycles involving iodine in the lower stratosphere is still poorly understood (WMO, 2007).

3. Data and Methods

This chapter describes the meteorological assimilations ERA-Interim and NCEP/NCAR Reanalysis Project 1 (NNRP-1) used for the comparison with ship and radiosonde measurements, and for the trajectory calculations. In the following, a description of the National Oceanic and Atmospheric Administration (NOAA) Hybrid Single Particle Lagrangian Integrated Trajectory (HYSPLIT) model, which is used for the backwards trajectory calculations, is given. Finally, the radiosondes used during the campaign are described.

3.1. ERA-Interim

The ERA-Interim project was conceived as a bridge between the ERA-40 atmospheric reanalysis and future generations of reanalysis to be produced at the ECMWF (http://www.ecmwf.int). Covering the period from January 1st 1989 onwards, it is extended forward in near real time. The reanalysis between 1979 and 1989 is currently in preparation. In contrast to the 6 hourly three-dimensional variational data assimilation system (3D-Var) of ERA-40, the core component of the ERA-Interim data assimilation system is a 12 hourly 4D-Var (horizontal, vertical and temporal component), which uses the forecast model to constrain the state evolution within each analysis window. The horizontal resolution of the current model is T255 (nominally 0.70° ≈ 79 km), resulting in 512 zonal and 128 meridional grid points with 60 vertical model levels up to 0.1 hPa. It uses mostly the input data acquired for ERA-40 and assimilates the latest generation of satellite data such as radio occultation measurements. The current archive contains 6-hourly gridded estimates of three dimensional meteorological variables and 3-hourly estimates of a large number of surface parameters (Dee et al., 2011). For an evaluation of the surface wind ship measurements, they are compared with 6-hourly u- and v-winds from ERA-Interim. The results are shown in section 4.4.

3.2. NCEP/NCAR Reanalysis Project 1

The NCEP/NCAR Reanalysis Project 1 is a joint project between the National Center for Environmental Prediction (NCEP) and the National Center for Atmospheric Research (NCAR), with the goal to produce new atmospheric analysis using historical data from 1948 onwards and to produce analyses of the current atmospheric state. It is based on the NCEP operational model of 1995 and covers 6-hourly daily values from January 1st 1948 to present. The reanalysis system has a horizontal triangular truncation of 62 waves (T62), with a horizontal resolution of 208 km and a vertical resolution of 28 levels with a model top at about 3 hPa. The data is distributed in a 2.5 ° latitude x 2.5 ° longitude global grid with 144x73 grid points. The analysis scheme is a 3D-Var (horizontal and vertical) scheme cast in spectral space, according to Parrish and Derber (1992) called Spectral Statistical Interpolation. For the reanalysis rawinsonde observations of temperature, horizontal wind and specific humidity of upper air are assimilated, as well as operational TOVS vertical temperature soundings from NOAA polar orbiters over ocean, winds

by cloud tracking from geostationary satellites and observations of wind and temperature by aircrafts. In addition, land and sea surface pressures as well as oceanic reports of temperature, horizontal wind and specific humidity are assimilated, too (Kalnay et al., 1996; Kistler et al., 2001). For the evaluation of the backward trajectories, ship and radiosonde measurements are compared with the 6-hourly u- and v-winds of NNRP-1 at the ground and at the 925 hPa and 850 hPa pressure levels due to their height within the mixed layer.

3.3. Trajectory Model: HYSPLIT

For the investigation of the air mass history, backward trajectories are calculated by the NOAA HYSPLIT model (Version 4.9). The HYSPLIT model is suited for computing simple trajectories to complex dispersion and deposition simulations, using previously gridded meteorological data sets. The calculation method of the model is a hybrid between the Eulerian approach, using a fixed 3D grid as a reference frame, and the Lagrangian approach, using a moving reference frame as the air parcels move from their initial location. The Eulerian approach is used for the calculation of pollutant concentrations and the Lagrangian approach for the calculation of advection and diffusion (Draxler and Hess, 2004). Besides a downloadable PC version, HYSPLIT is an online tool with the option to use different assimilation data sets, such as GDAS (Global Data Assimilation System), EDAS (ETA Data Assimilation System), NAM (North American Mesoscale model) or NCEP/NCAR Reanalysis data.

For the air mass analysis in this thesis the NCEP/NCAR Reanalysis data set is used to calculate backward trajectories. The maximum duration of the trajectories is limited by HYSPLIT to 315 h (13 days and 3 hours) with hourly time steps. For the starting height, the surface level and 1000 m height are chosen to consider different origins of the air masses within the mixed layer. For the final analysis of the air mass origin, the trajectories are plotted with a MATLAB Mapping toolbox.

3.4. Radiosondes

Radiosondes are used to investigate different parameters of the atmosphere and can reach the lower to mid stratosphere, depending on the capacity of the balloon. The 41 DFM-06 radiosondes launched during the DRIVE campaign are manufactured by GRAW, factory calibrated and designed to measure atmospheric pressure, temperature, relative humidity, wind speed and wind direction. The measurements were sent down to a receiver on the ship by a radio-telemetry link. Unfortunately, all radiosoundings, sampled during DRIVE, show artificial temperature oscillations with increasing amplitudes up to ± 3 °C above 25 km height. Although these oscillations seem not to affect the overall temperature profile, they make it difficult to determine the mixed layer height and the tropopause. Due to the relative small oscillations close to the ground, inversions are still identifiable and make it possible to derive the mixed layer height from the temperature measurements. In contrast to that, the oscillations between 15 and

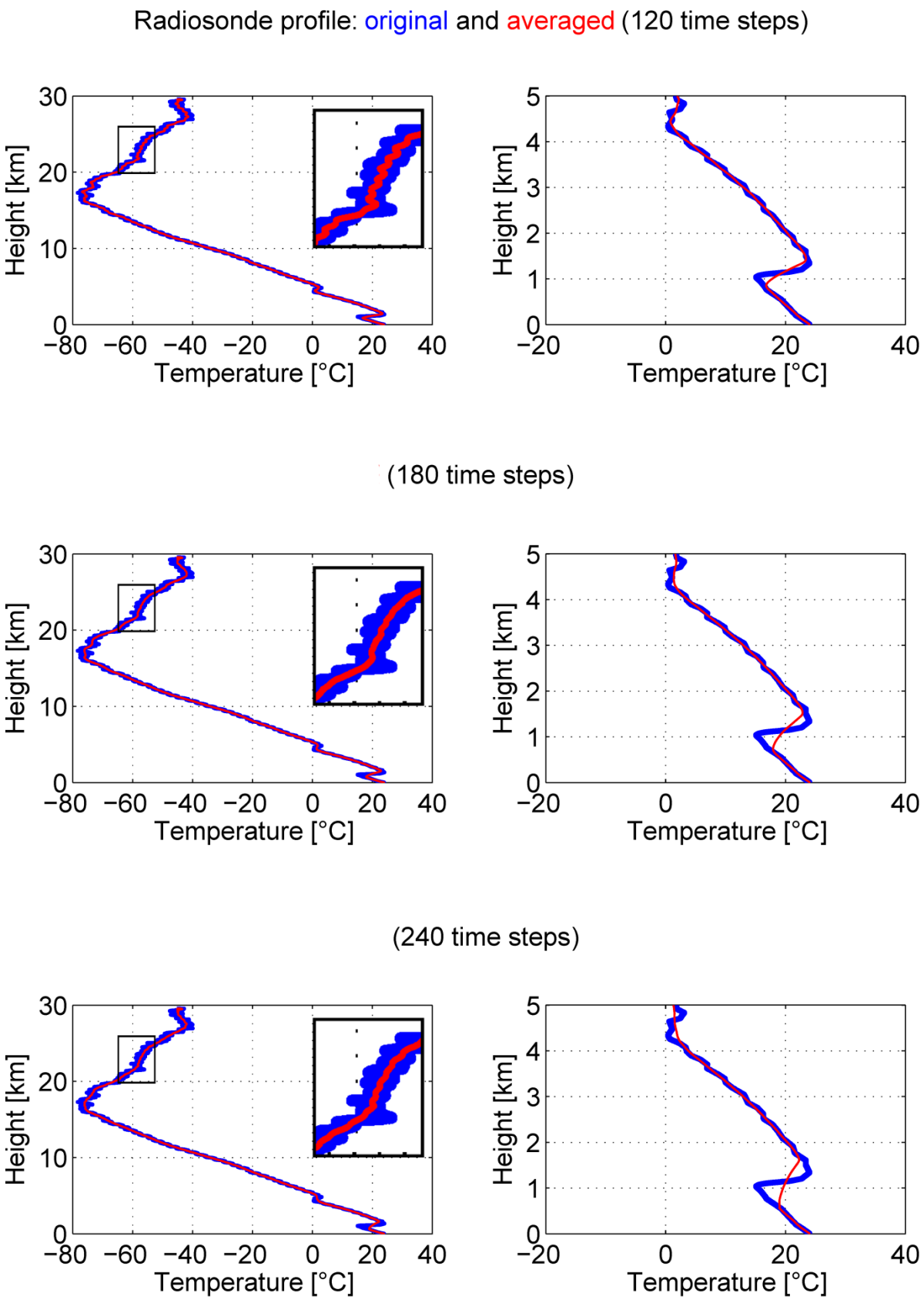

Figure 3-1: Radiosounding on 04.06.2010 12 UTC, original (blue line) and averaged (red line) for 120, 180 and 240 time steps.

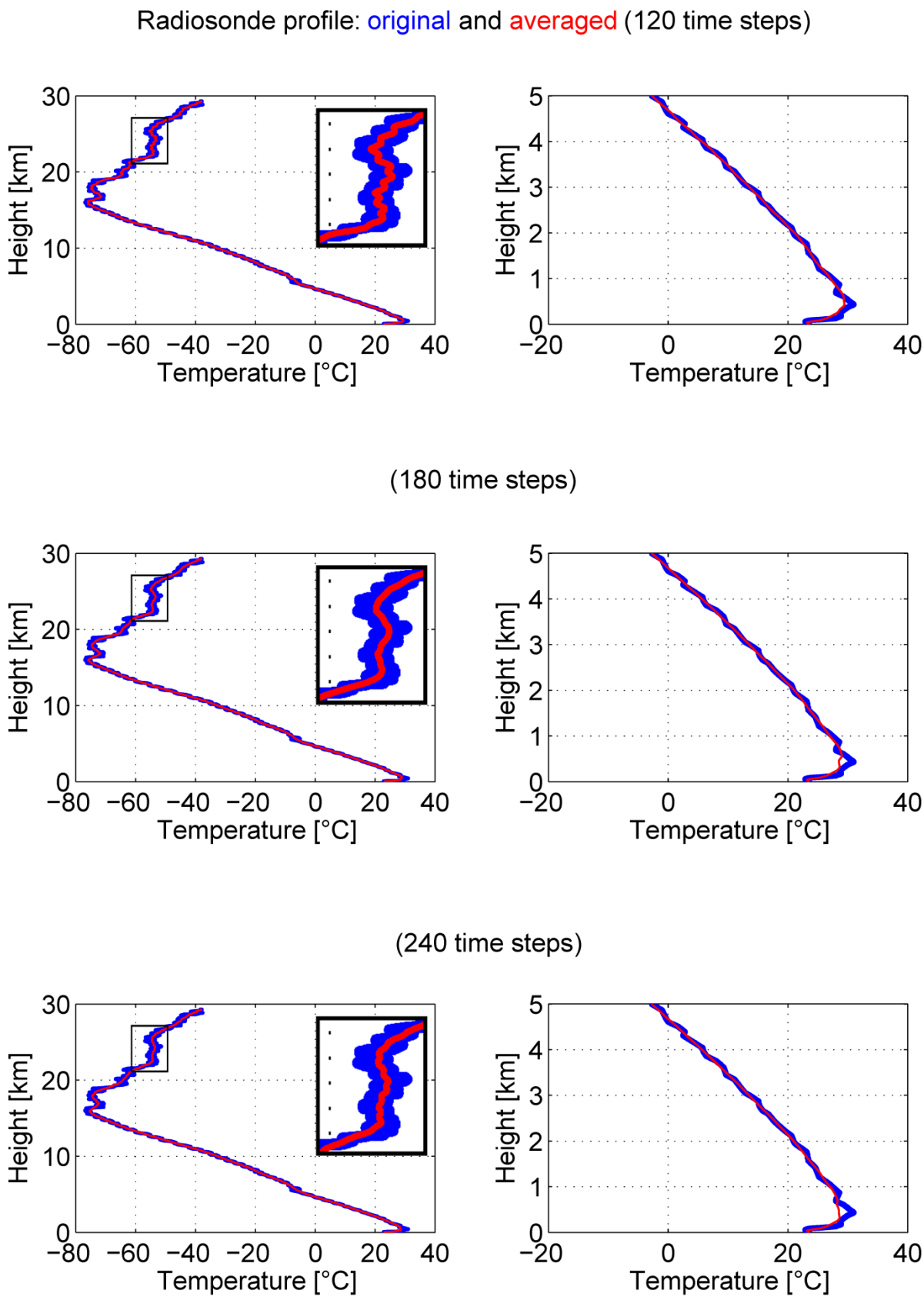

Figure 3-2: As Figure 3-1 for 10.06.2010 18 UTC.

20 km height are too intense to derive the tropopause height according to the tropopause definitions in section 2.1.1. For this reason a running mean MATLAB routine to filter out the artificial oscillations is written. The radiosonde output is given every second, still allowing a high frequency smoothing. Different time steps (120 s, 180 s and 240 s) are tested for the running mean approach. Figure 3-1 and Figure 3-2 show radiosoundings from 04.06.2010 12 UTC and 10.06.2010 18 UTC. The complete ascent is shown on the left and the lower 5 km on the right side, for the different time steps. The overall agreement between smoothed and original temperature profiles is good. For the 120 time steps averaging, oscillations are still visible above 15 km height. These are filtered out in the 180 time steps and the averaged profile still reflects the original temperature profile quite well. The 240 time steps plot already averages the original profile too much, and thus smears out inversions as for example the surface inversions. Consequently 180 time steps are chosen to average the temperature for the tropopause determination and the overall vertical temperature structure during DRIVE. Cold point and lapse rate tropopause are determined analogously to their definitions (section 2.1.1). The influence of the running mean routine on the surface inversions is shown by the plots on the right side of Figure 3-1. With increasing time steps, the intensity of the inversion weakens, but the vertical extensions increase. Therefore the temperature profiles are not averaged for the mixed layer height determination (see section 4.3.2).

4. The ship cruise

The following chapter introduces the ship cruise and the meteorological and chemical measurements carried out. The meteorological observations are compared with assimilation data, which are used for the air mass analyses. Finally an overview of the air mass origin during leg 2 and 3 is shown.

4.1. DRIVE campaign

The ship cruise belongs to the DRIVE campaign, where DRIVE stands for "Diurnal and Regional Variability of halogen Emissions". The research cruise is divided into two parts P399/2 (31.05.2010 – 17.06.2010, leg 2) and P399/3 (19.06.2010 – 23.06.2010, leg 3) and belongs to the BMBF[1] joint project SOPRAN. The scientific aims of SOPRAN are an enhanced understanding of climate important emissions from the surface ocean, such as CO_2, O_2, N_2O, halogenated and other reactive organic compounds. Also the effects of increasing CO_2 levels and climate-mediated changes in the input of atmospheric dust on the sensitivity of surface marine ecosystems and key biogeochemical cycles are assessed. In addition an improved understanding of exchange processes between surface ocean and the atmosphere and feedback mechanism between climate change, dust input, associated biological productivity and the physical transports of the eastern North Atlantic is aspired. Several SOPRAN-partners work together on this objective. During DRIVE, the daily and regionally variability of the halocarbons at six 24 h stations (see Figure 4-1 and Table 1), on which the ship remained on its position, were investigated.

The target area is the upwelling region near the coast of Mauritania. The choice of this area results from the geographical conditions. On the one hand dust from the closer Sahara is transported to the offshore and nutrient-poor tropical north-east Atlantic (Signorini et al., 1999) by the north-east trade winds, which influence the biological processes due to nutrient input (iron, etc.). On the other hand high nutrient mixing ratios can be found at the inshore Mauritanian upwelling area, forming the basement of one of the most biologically productive oceanic region all over the globe and thus an important source for a number of biologically produced climate-relevant trace gases (Minas et al., 1982; Quack et al., 2004, 2007). Therefore the 24 h stations were distributed over the nutrient-rich regions at the coastal upwelling near the Mauritanian coast and the nutrient-poor regions near Cape Verde, to contrast the different influences on the trace gases. When these trace gases, especially the halocarbons, access the atmosphere, they can contribute to ozone depletion. Active upwelling occurs within a narrow band along the continental margin from about 10° N to 26° N due to offshore Ekman transport by the trade wind belts of the subtropics (Schemainda et al., 1975; Hagen, 2000; Sawadogo et al., 2009).

[1] Bundesministerium für Bildung und Forschung

In order to investigate the distribution of trace gases in the atmosphere and in the ocean, air and water samples have been taken continuously on the ship. For the characterization of the atmospheric composition and the determination of halocarbons, air samples were taken on the upper bridge for trace gases and separately for isotope investigations. In addition a MAX-DOAS instrument of the University Heidelberg was installed on the upper bridge as well, to measure the mixing ratios of bromine- and iodine oxide (BrO, IO). Dust- and aerosol entries were collected by daily filter samples and the vertical structure of the atmosphere was observed with radiosonde launches.

4.2. Cruise track

The following cruise track description is based on the weekly reports of the P399 2/3 of Hermann Bange (http://www.ifm-geomar.de/index.php?id=5790). The cruise started on May 31th 2010 at about 08 UTC at Las Palmas de Gran Canaria (28.1° N, 15.4° W). Figure 4-1 shows the whole cruise track, including leg 2 and 3. Table 1 gives an overview of the positions and dates of the 24 h stations. After a straight south west heading the ship reached the TENATSO[2] station on June 3 and started with the first 24 h station.

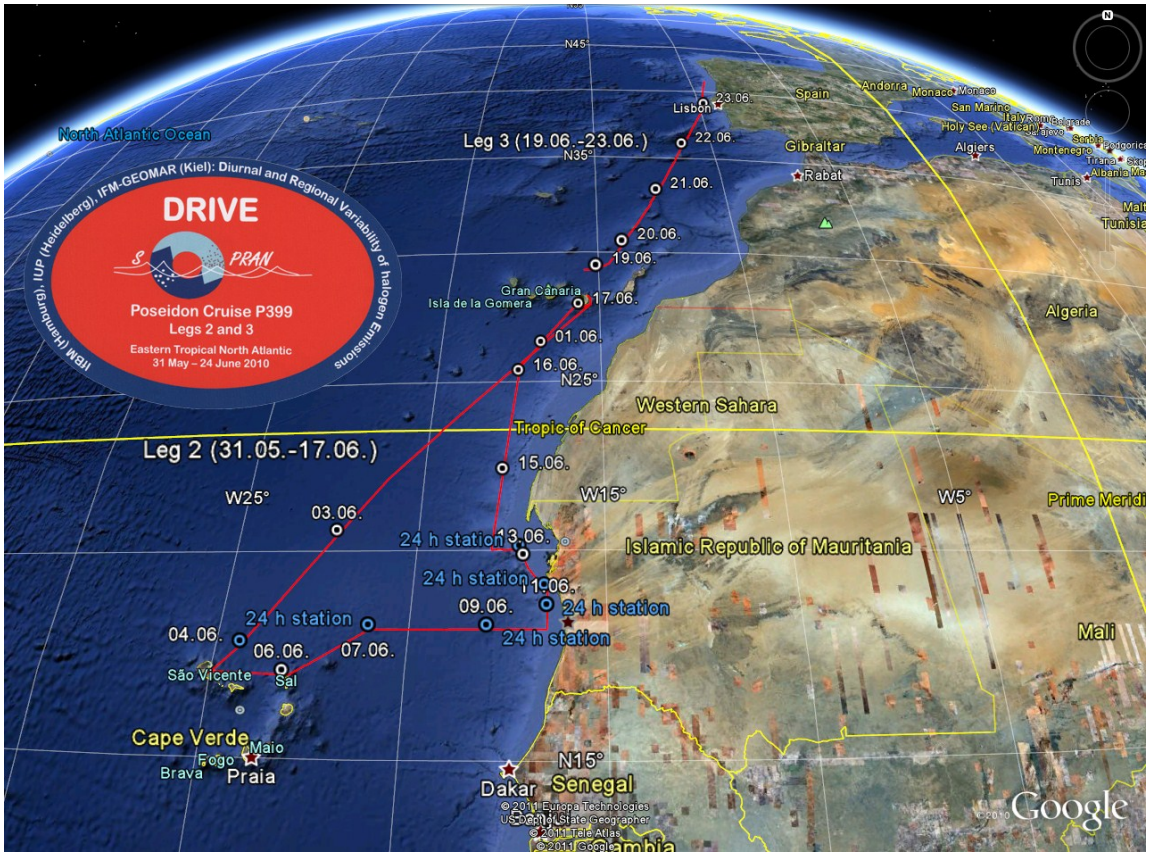

Figure 4-1: P399 cruise track: leg 2 (31.05.-17.06.) with 24 h stations & leg 3 (19.06.-24.06.) near the West African coast illustrated in Google Earth.

[2] Tropical Eastern North Atlantic Time-Series Observatory (16° N, 24° W)

Table 1: DRIVE: 24 h stations with positions and date.

Station	Position	Date
1st 24 h station	16° N, 24° W	June 3 – June 4 2010
2nd 24 h station	18° N, 21° W	June 6 – June 7 2010
3rd 24 h station	18° N, 18° W	June 8 – June 9 2010
4th 24 h station	18.5° N, 16.5° W	June 10 – June 11 2010
5th 24 h station	19° N, 16.5° W	June 11 – June 12 2010
6th 24 h station	20° N, 17.25° W	June 13 – June 14 2010

Mindelo (Cape Verde; 16.9° N, 25° W) was reached two days later and after a short stop in the port and a crew change the campaign continued along 18° N towards Mauritania. Two more 24 h stations were completed until the ship reached the Mauritanian coast and headed northwards. On June 10 at about 07 UTC the ship reached the Mauritanian coast and changed heading to North. On June 11 2010 at about 12 UTC the Mauritanian upwelling, characterized by the appearance of cold and nutrient-rich water, was reached. The surface water temperature began to drop from 23.5 °C to about 20 °C and a day later to 18 °C at 20° N and 17.25° W (Figure 4-2). This was a clear evidence for the Mauritanian upwelling. In addition a further increase of the nutrient mixing ratios was denoted. On June 17 2010 the ship reached the port of Las Palmas again after about 2100 nm and finished P399/2.

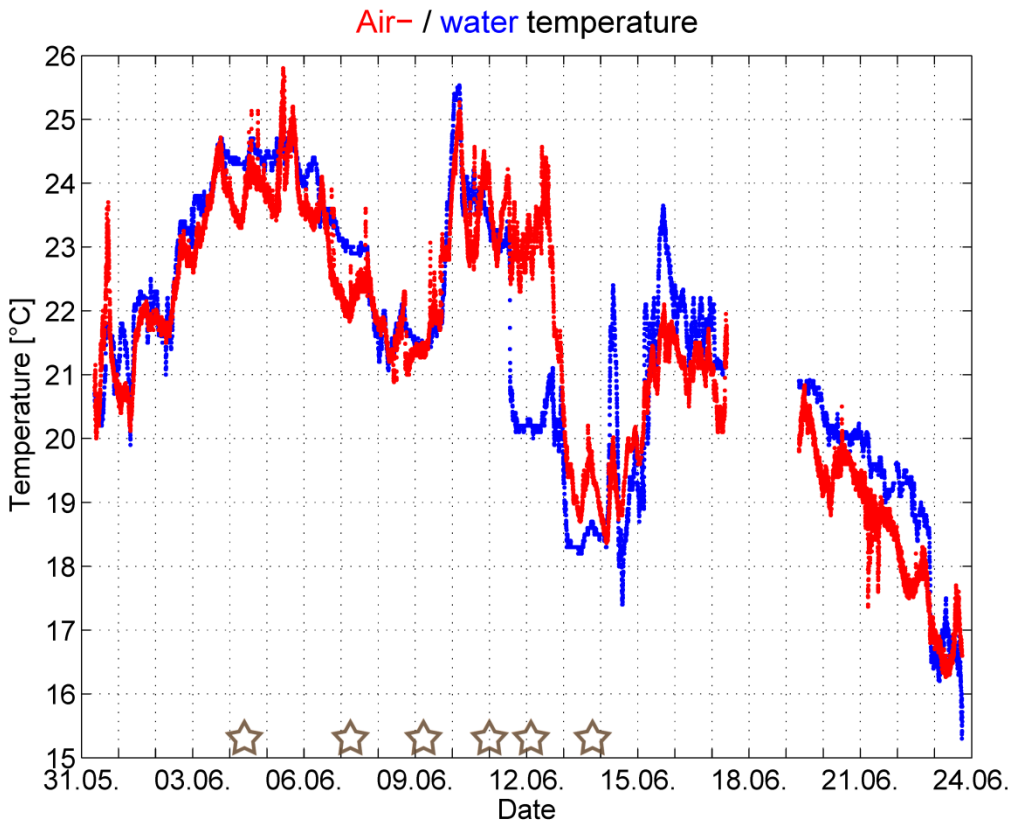

Figure 4-2: Air-(red line) and water (blue line) temperature measured on POSEIDON during the DRIVE campaign 2010 with a gap between leg 2 and 3. The stars indicate the 24h stations.

Leg 3 of the P399 ship cruise started on June 18 2010 at Las Palmas with a northward heading to Vigo, Portugal. After a short stop at the time series station ESTOC[3], about 100 km north of Gran Canaria Island, Vigo at the east coast of Portugal was reached on June 24 2010 after another 1000 nm and a whole cruise time of three and a half weeks.

4.3. Meteorology

With a velocity of 16.9 m/s the highest wind speed of the whole cruise was measured immediately after the start of P399/2 near Gran Canaria Island. This value lies by 9 m/s above the mean wind speed of 7.8 m/s (Leg 2: 7.38 m/s, Leg 3: 9.27 m/s) and forms together with stronger winds on June 14 the only velocities above 16 m/s. Contrary to the prior wind direction of the trade winds and the Westerlies, the mean measured absolute wind direction was NNW (Leg 2: 348°, Leg 3: 343°). A ten minute average of wind speed and direction is shown in Figure 4-3 for every three hours along the ship cruise. Most of the time maritime air masses influenced the ship measurements. Figure 4-2 shows a time series of the measured air and water temperature. A first intense increase of air temperature coincides with a collapse of the wind speed and a change of the wind direction to east on May 31 (Figure 4-4). This wind speed collapse follows the maximum measured wind speed of the whole cruise just by about 4 hours. As the ship cruise started towards the equator, the air and water temperature increased until the maximum air temperature of 25.8 °C is recorded right after the stop at Mindelo. In the following both temperatures began to fall for the first time. This might be caused by northerly winds, which transported cold water and air masses from the Mauritanian upwelling southwards to the ship. ERA-Interim surface winds confirm this assumption (Figure 4-5). Right after the third 24 h station and close to the Mauritanian coast, air and water temperatures increased again. On June 11 the ship reached the Mauritanian upwelling at 18.75° N, 16.5° W. This is distinguishable from the abrupt decrease of the water temperature, followed by a drop of the air temperature with a time lag of about one day until both stabilize between 18 °C and 20 °C. On June 14 2010 a certain increase of the water temperature to about 23.5 °C is distinguishable from Figure 4-2. This increase coincides with the second wind speed maximum of about 16 m/s (Figure 4-4) from the north. Warmer water masses from outside the Mauritanian upwelling may be transported towards the ship at this time, or the ship actually left the small upwelling belt, until the water temperature dropped again to about 18 °C. On June 15 2010 the ship left the area of upwelling water, indicated by the increasing air and water temperature until both decreased again with increasing latitude. The total air pressure difference of 13.35 hPa shows, that the crew and the ship were exposed to relatively calm weather during the campaign (Figure 4-6 and Figure 4-7 respectively). The lowest value of 1007.6 hPa was reached near the Mauritanian coast on June 11th 2010 when the ship reached the edge of a low pressure system, originated on the African onshore at the boarder of Senegal and Mauritania (Figure 4-8). This was the only day some dust from the Sahara was found in the air filter, as reported by the crew. The highest air pressure value of 1021 hPa was observed on June 19 during leg 3.

[3] European Station for Time Series in the Ocean (29.2° N, 15.5° W)

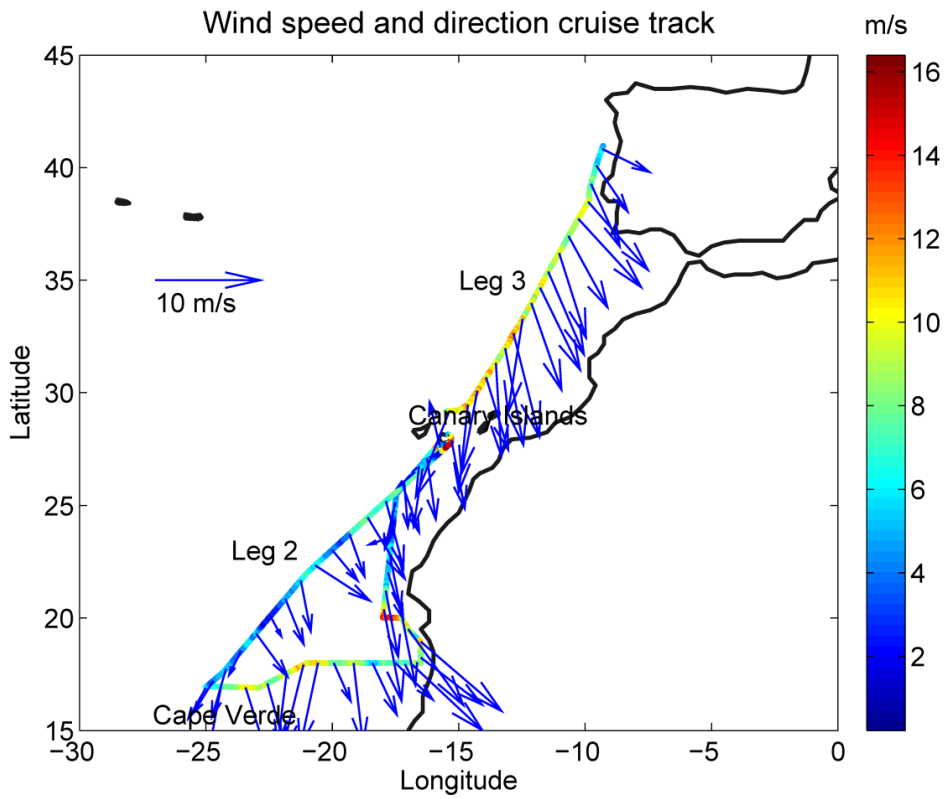

Figure 4-3: Ten minute average of wind speed and direction ship measurements for every six hours, except 24 h stations. The arrows indicate wind direction and speed. In addition the color of the cruise track indicates the wind speed as well.

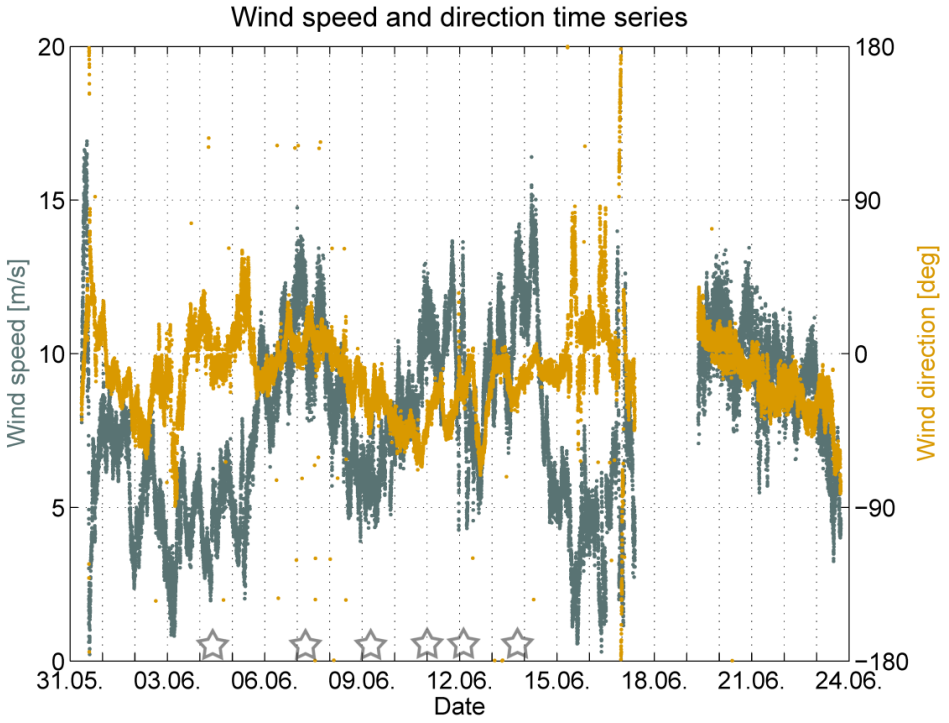

Figure 4-4: Time series of wind speed and wind direction measured on POSEIDON during the DRIVE campaign 2010 with a gap between leg 2 and leg 3. Stars indicate the 24 h stations.

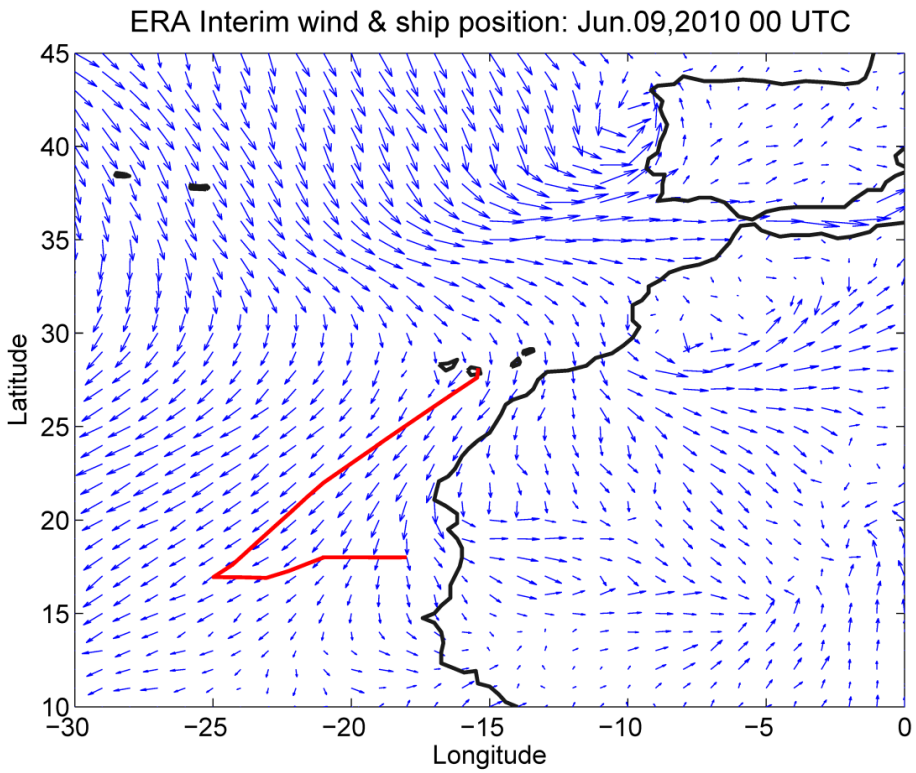

Figure 4-5: Surface winds of ERA Interim with covered ship track (red) of DRIVE campaign on June 9th 2010, 00 UTC.

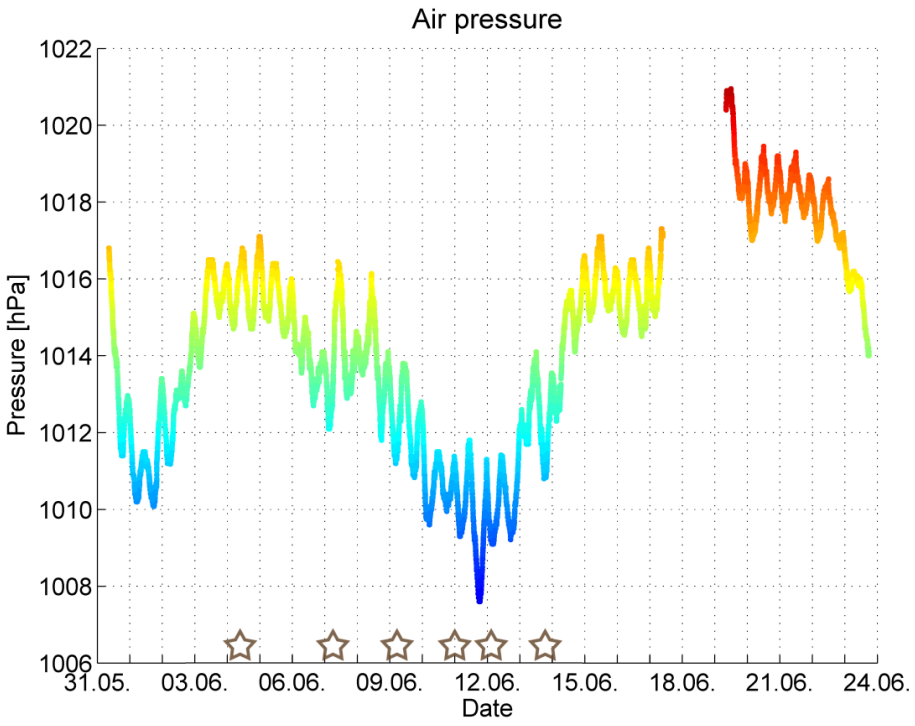

Figure 4-6: Time series of air pressure measured on POSEIDON during the DRIVE campaign 2010 with a gap between leg 2 and leg 3. Stars indicate the 24 h stations.

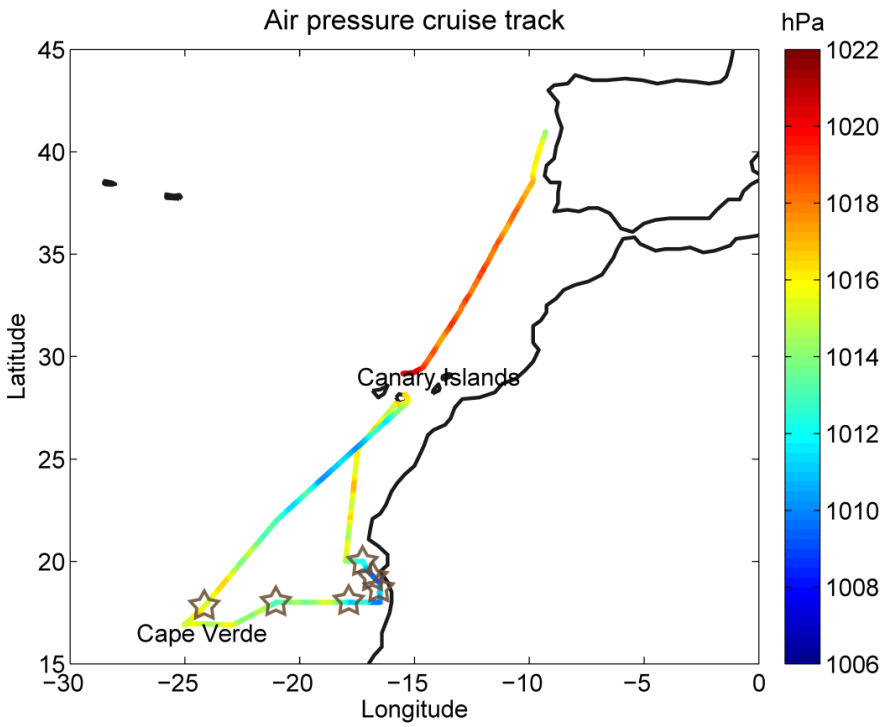

Figure 4-7: Cruise track of air pressure measured on POSEIDON during the DRIVE campaign 2010. Stars indicate 24 h stations.

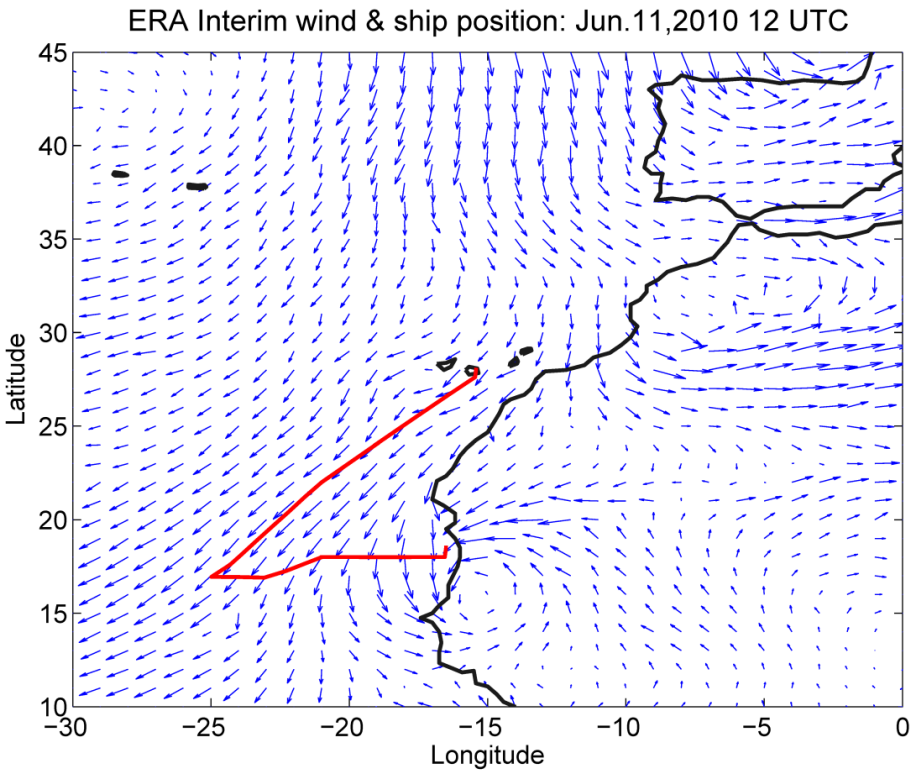

Figure 4-8: Surface winds of ERA Interim with covered ship track (red) of DRIVE campaign on June 11th 2010, 12 UTC.

4.3.1. Radiosoundings

During the DRIVE campaign 41 radiosondes have been launched to investigate the vertical structure from the surface to the mid stratosphere. The radiosondes were started every day at 12 UTC and during the 24 h stations at 00, 06, 12 and 18 UTC. The resulting profiles are shown in Figure 4-9 for temperature, Figure 4-10 for zonal wind, Figure 4-11 for meridional wind and Figure 4-12 for relative humidity respectively. The determined lapse rate (LRT) and cold point tropopause (CPT) (see section 2.1.1) are marked by the continuous and dashed-dotted lines. Both tropopause definitions show short-timed variations in height. Except from 06.06.2010 to 09.06.2010 were the CPT is about 2 km higher than the LRT, both definitions show heights of 16 – 17 km from 03.06.2010 to 15.06.2010. After June 15 2010 the height of the LRT in contrast to the CPT decreases to 15 km, while passing the Tropic of Cancer and entering the extratropics. Due to the less physical meaning of the CPT outside the tropics this is an evidence for the changing atmospheric regime. This assumption is founded by the appearance of the maximum zonal wind speed, hence the subtropical jet (STJ) in the radiosonde measurements (Figure 4-10). An abrupt increase of the zonal wind speed with a maximum of 48 m/s between 10 and 15 km height is found on 16.06.2010 accompanied by an increasing northern wind component up to 15 m/s (Figure 4-10 and Figure 4-11). As shown by Figure 2-7 the STJ is generally found at these altitudes, followed by a descent of the tropopause height towards increasing latitude.

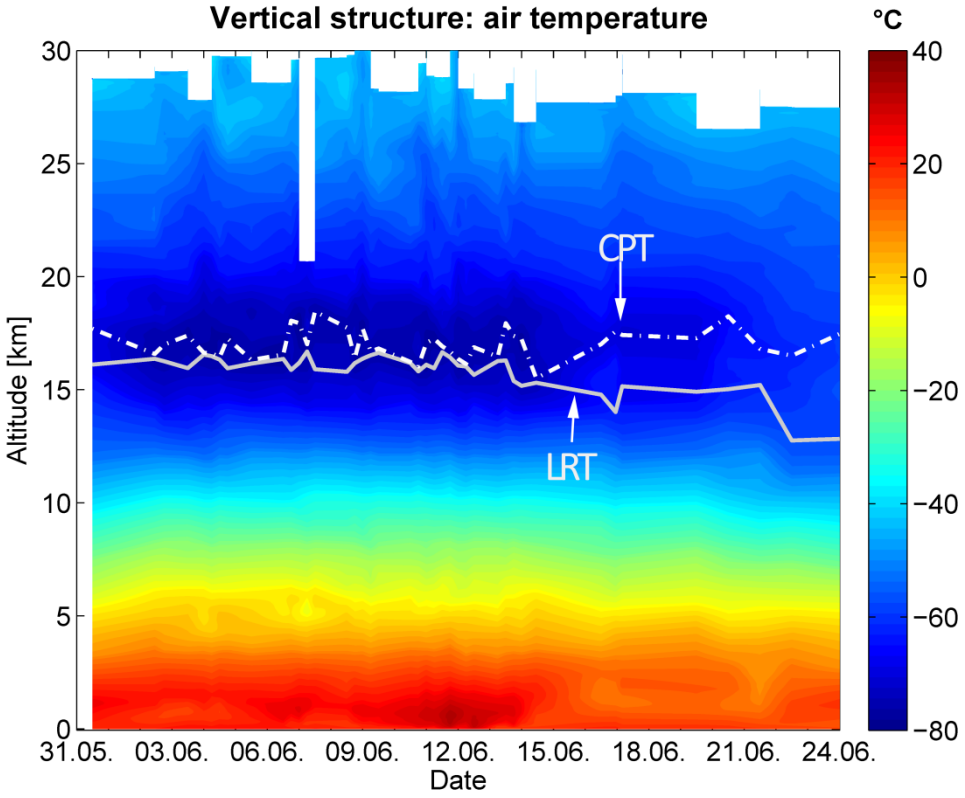

Figure 4-9: Vertical structure of air temperature measured by radiosondes with cold point tropopause (CPT) and lapse rate tropopause (LRT) during the DRIVE campaign 2010.

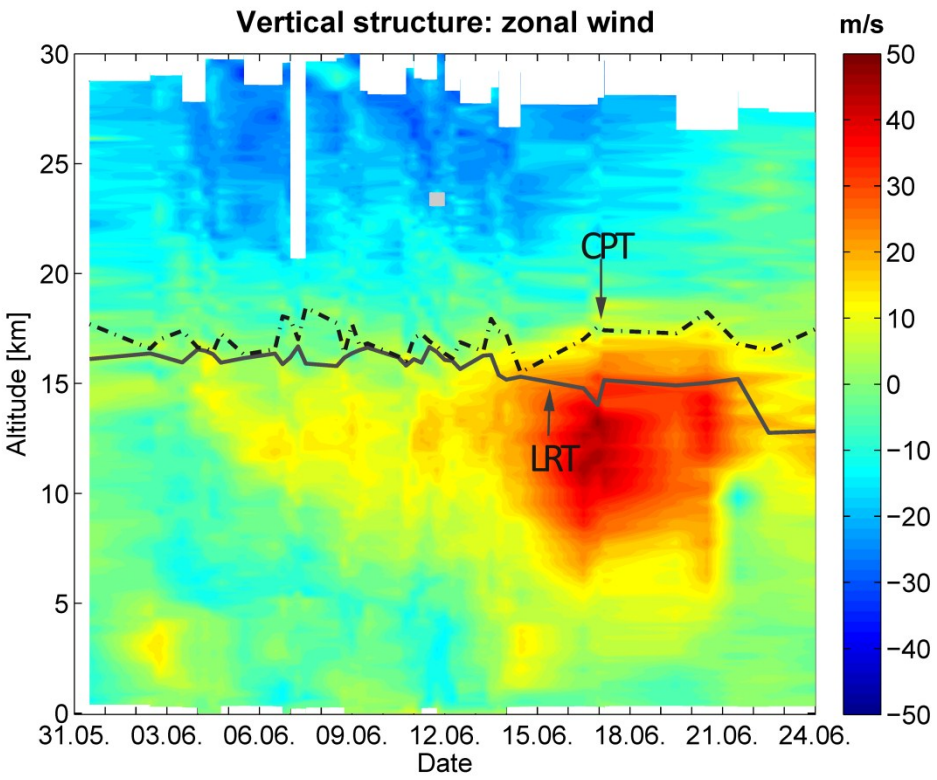

Figure 4-10: As Figure 4-9 for zonal wind. Positive values indicate westerly winds.

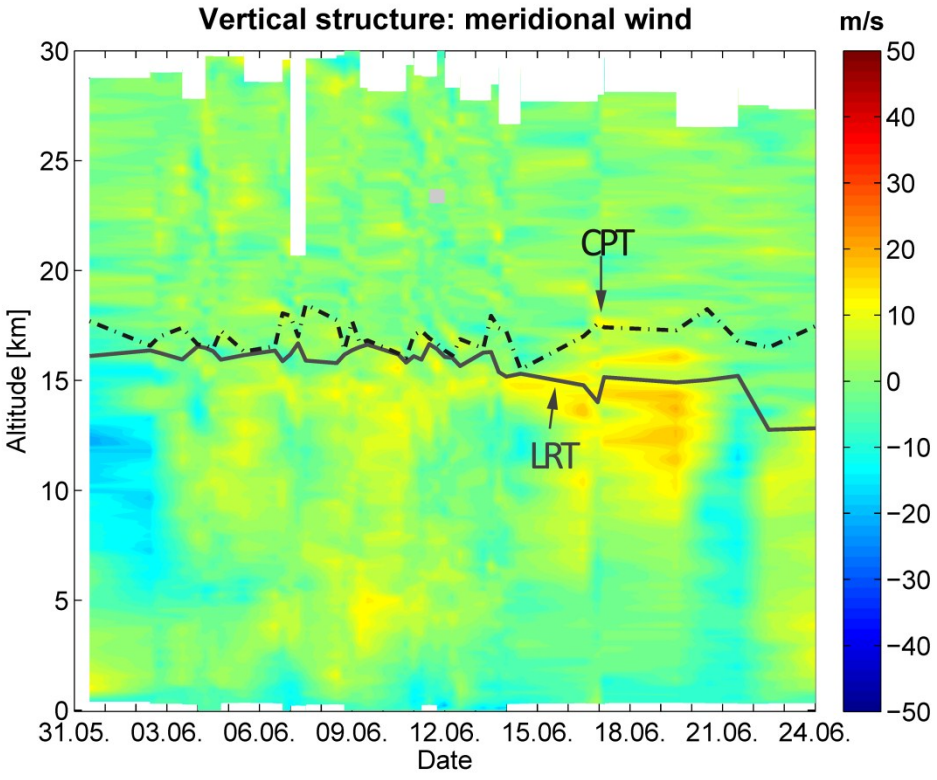

Figure 4-11: As Figure 4-9 for meridional wind. Positive values indicate southern winds.

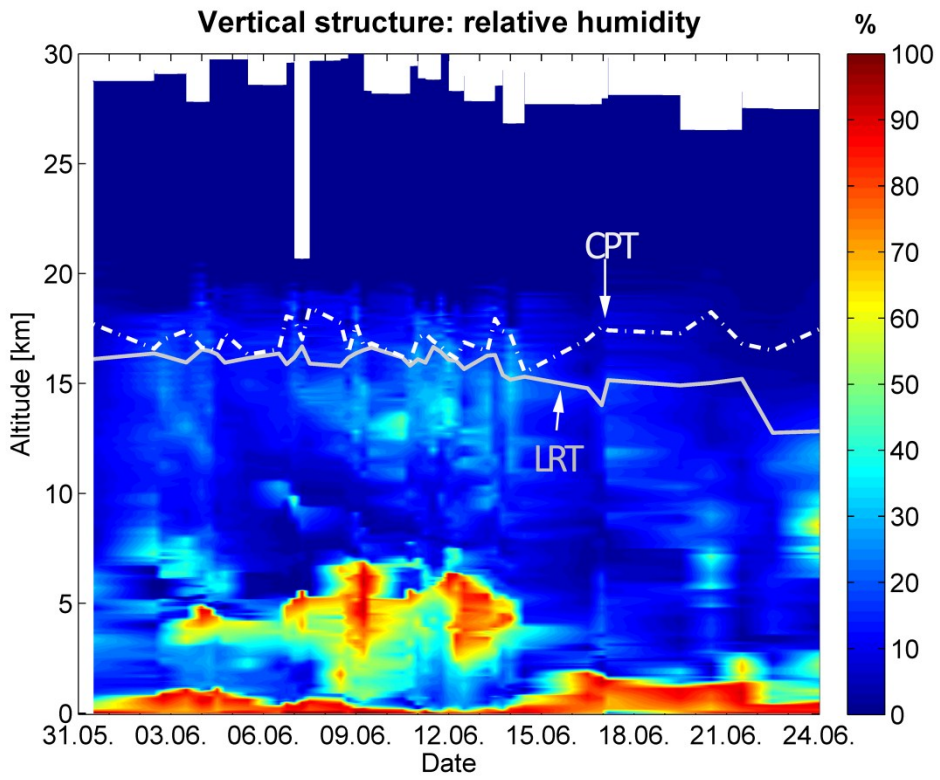

Figure 4-12: As Figure 4-9 for relative humidity.

This descent is also shown by the LRT on 21.06.2010 immediately after the STJ weakens. Although it is not central for this diploma thesis it is worth mentioning, that above 20 km of altitude the quasi-biennial oscillation (QBO) with easterly winds up to 35 m/s was determined by the radiosondes (Figure 4-10). Taking a closer look to the lower temperature profile of Figure 4-9, several temperature inversions from the ground up to 2 km of height, were detected by the radiosondes. Due to their height and regional appearance the inversions are identified as trade inversions. These inversions suppress vertical motion of air and are reflected in the vertical relative humidity profiles as well (Figure 4-12). The lower part of these measurements already shows a rough shape of the mixed layer height due to an intense decrease of relative humidity with height. From June 3 to June 14 several clouds can be distinguished from the vertical relative humidity profile. These clouds were observed by the scientific ship crew as well and identified as a number of different cloud types like cirrostratus, altostratus, cirrocumulus, altocumulus et cetera.

4.3.2. Mixed layer height

The mixed layer height for DRIVE is shown in Figure 4-13 and determined for all 41 radiosoundings after the approach described in section 2.2. It varies from about 200 m at the beginning of the cruise to a first maximum of 1200 m on June 3 2011. Afterwards it decreases to

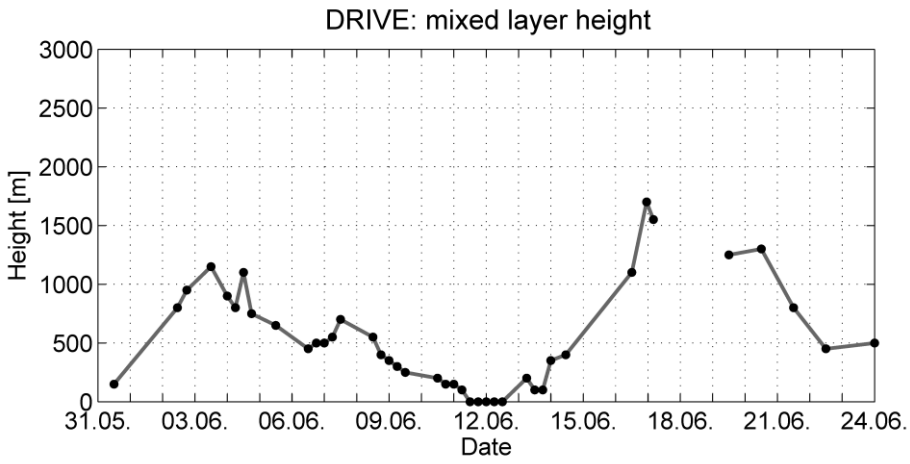

Figure 4-13: Mixed layer height, determined from radiosoundings during the DRIVE campaign 2010 with a gap between leg 2 and leg 3.

ground level on June 11 - 12 close to the Mauritanian coast until it increases again to its maximum of 1700 m on June 17 2011 00 UTC. During leg 3 the mixed layer drops from about 1300 m at the beginning to 500 m at the end. A typical radiosounding for the case of a convective boundary layer at 21° W and 18° N on 06.06.2010 18 UTC is shown in Figure 4-14. The upper left plot shows the vertical profiles of air temperature T and virtual potential temperature Θ_v. The trade inversion, which limits the vertical extension of the mixed layer height, starts at h^-= 400 m and ends at h^+= 800 m altitude. A sharp bend in the virtual potential temperature profile is found at the same altitude of the trade inversions lower limit. According to section 2.2.4 this first evidence for the mixed layer identifies its height at about 500 m. The upper right plot of Figure 4-14 shows the water vapor mixing ratio in kg water per kg of dry air. As a conserved quantity it is essential for determining the mixed layer height and in contrast to the relative humidity, which is measured by the radiosondes. At 400 m of altitude the water vapor mixing ratio shows a sudden decrease from about 0.0125 kg water per kg dry air to about 0.0035 kg water per kg dry air at 600 m. The upper limit of the mixed layer is identified from this plot at about 500 m. A vertical wind shear in the lower left plot of Figure 4-14 is found between 300 m and 600 m, identifying the height of the mixed layer at 400 – 500 m. The lower right and last plot shows the Richardson number (see section 2.2.3 for determination). The red star indicates the critical bulk Richardson number (0.25) at about 500 m height. This theoretical determination shows a good agreement with the practical determination of the mixed layer height. After all these evidences, the height of the mixed layer for this radiosounding is finally stated at about 500 m altitude. Another interesting radiosounding during DRIVE and especially during the time of several surface inversions from June 10 to June 13 is shown in Figure 4-15. This so-called stable boundary layer (section 2.2.2) suppresses vertical motion of air from the ground to about 500 m of altitude. Therefore the mixed layer height is set to be zero meters. The earlier mentioned recorded air temperature oscillations are as well reflected in the lower profiles of air- and virtual potential temperature. However they do not influence the temperature pattern of the lowest 3 km due to the small amplitude at this level.

A comparison of the determined mixed layer height and the observed relative humidity profile by radiosondes from 0 – 10 km height (Figure 4-16) shows a good agreement between the upper

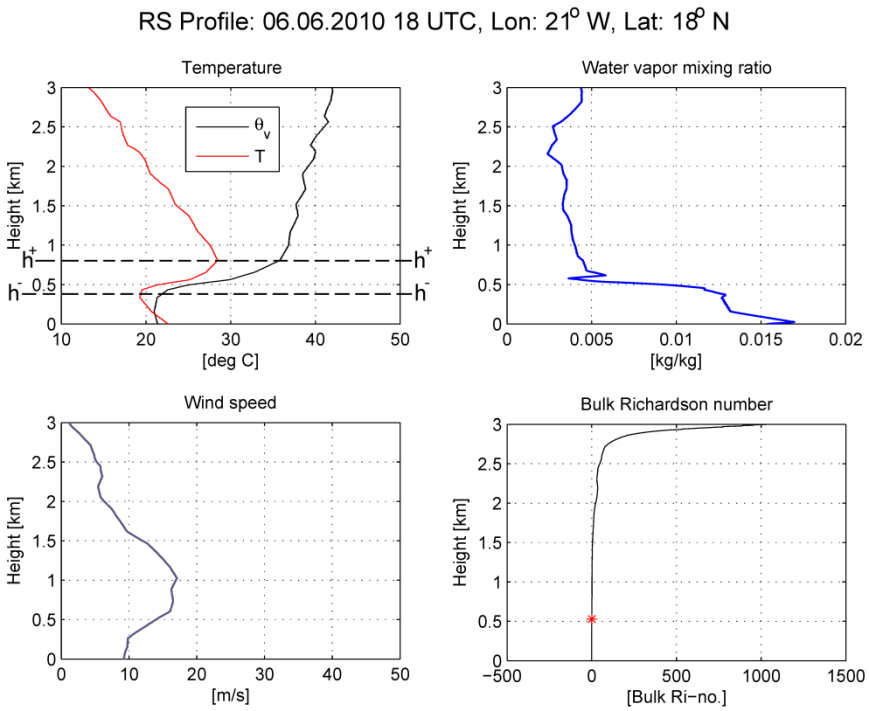

Figure 4-14: Radiosounding of the lowest 3 km of the atmosphere for the case of a convective boundary layer on June 6th 2010 18 UTC, 21° W and 18° N during the DRIVE campaign 2010. The red star indicates the critical bulk Richardson number.

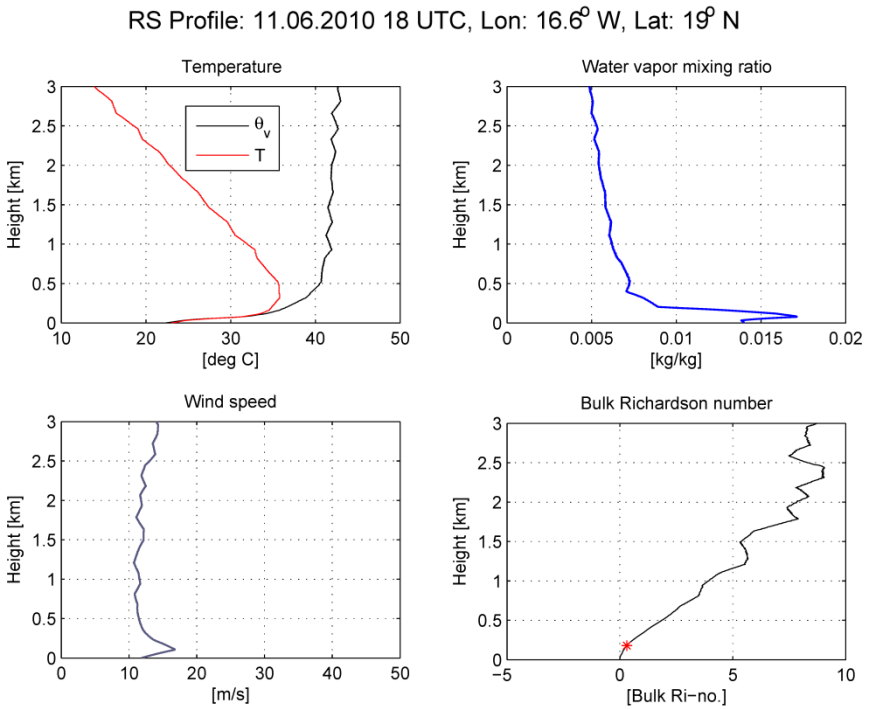

Figure 4-15: As Figure 4-14 for the case of a stable boundary layer on June 6th 2010 18 UTC, 21° W and 18° N during the DRIVE campaign 2010.

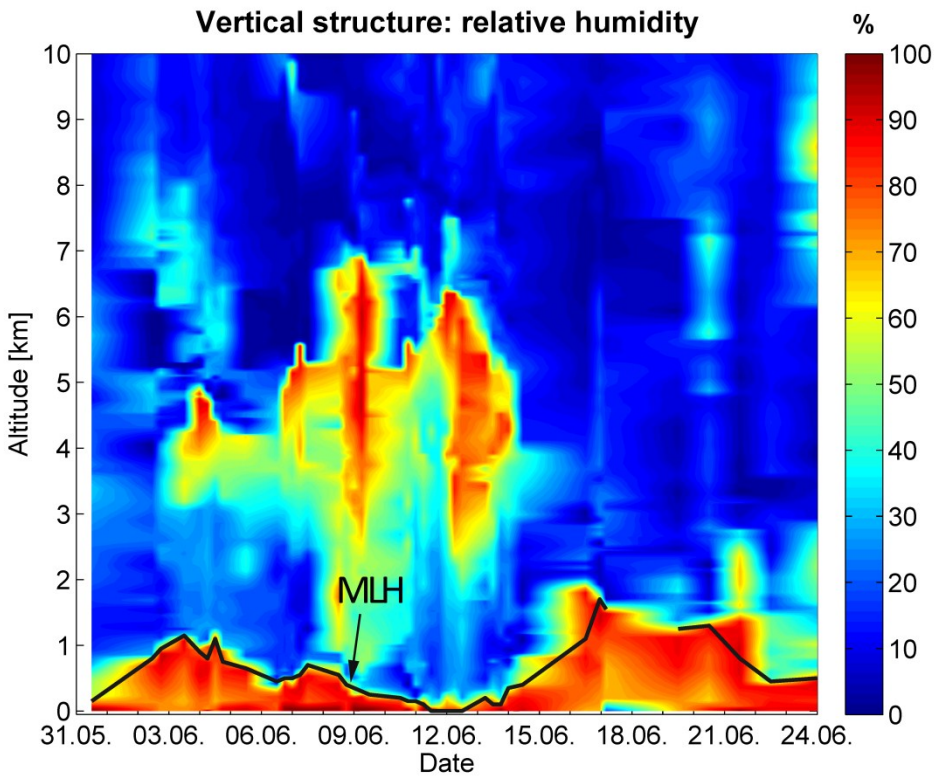

Figure 4-16: Vertical structure of relative humidity for the lowest 10 km measured by radiosondes and determined mixed layer height during the DRIVE campaign 2010.

limit of the mixed layer and the decrease of the relative humidity with height. Especially for leg 2 both parameters coincides very well. On June 16 and during leg 3 on June 21, there is a stronger deviation, probably caused by the lower temporal resolution of radiosonde measurements (one per day) at this time.

4.4. Data comparison

For the investigation of air masses and especially their origin it is important to investigate the reliability of the meteorological input data sets. For this reason wind speed and direction measurements from the ship and radiosondes are compared with the high-resolution ERA-Interim and, due to its use for the trajectory calculation by HYSPLIT, NCEP/NCAR Reanalysis Project 1 (NNRP-1) assimilation data. For detailed information about ERA-Interim and NNRP-1 see Chapter 3. The results are shown in Figure 4-17 for wind speed and Figure 4-18 for wind direction. The blue line indicates the ship measurements, the dark red line the ERA-Interim data and the light red line NNRP-1 data. The ship measurements were taken every second and are averaged for every minute. The gap between 17.06.2010 and 19.06.2010 is caused by the harbor time of the ship at Las Palmas between leg 2 and leg 3. The original ERA-Interim grid and the NNRP-1 grid are interpolated to 0.125° x 0.125° horizontal grids. For the comparison the closest grid point to the ships position is determined and plotted. Depending on the latitude, the

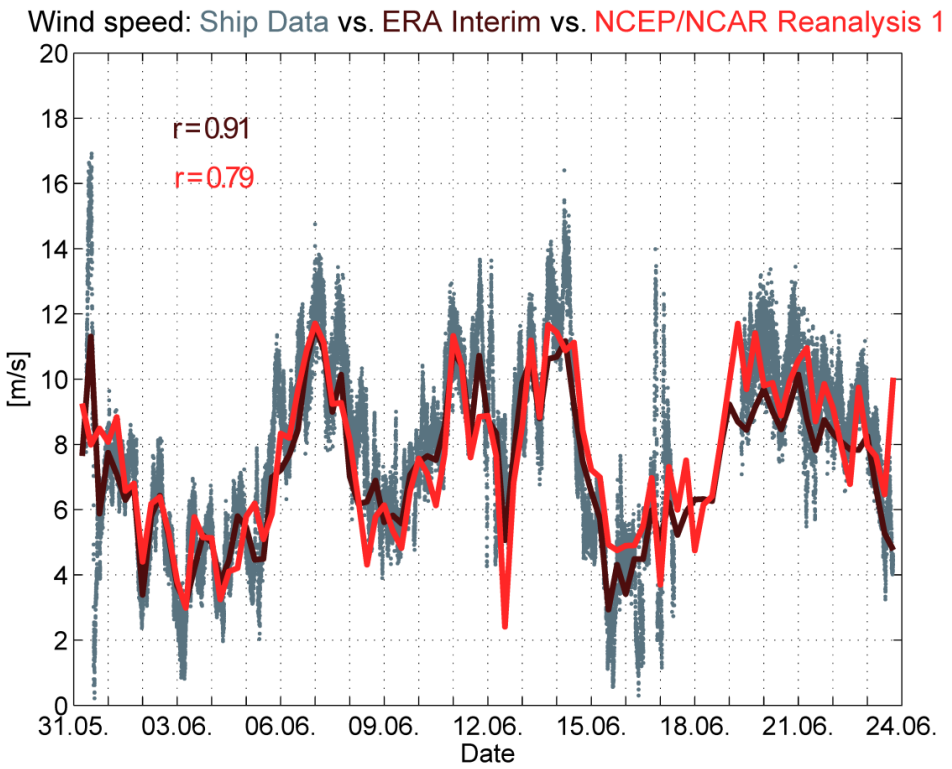

Figure 4-17: Wind speed comparison of ship measurement (blue) - ERA Interim (dark red) - NCEP/NCAR Reanalysis 1 (light red) during the DRIVE campaign 2010.

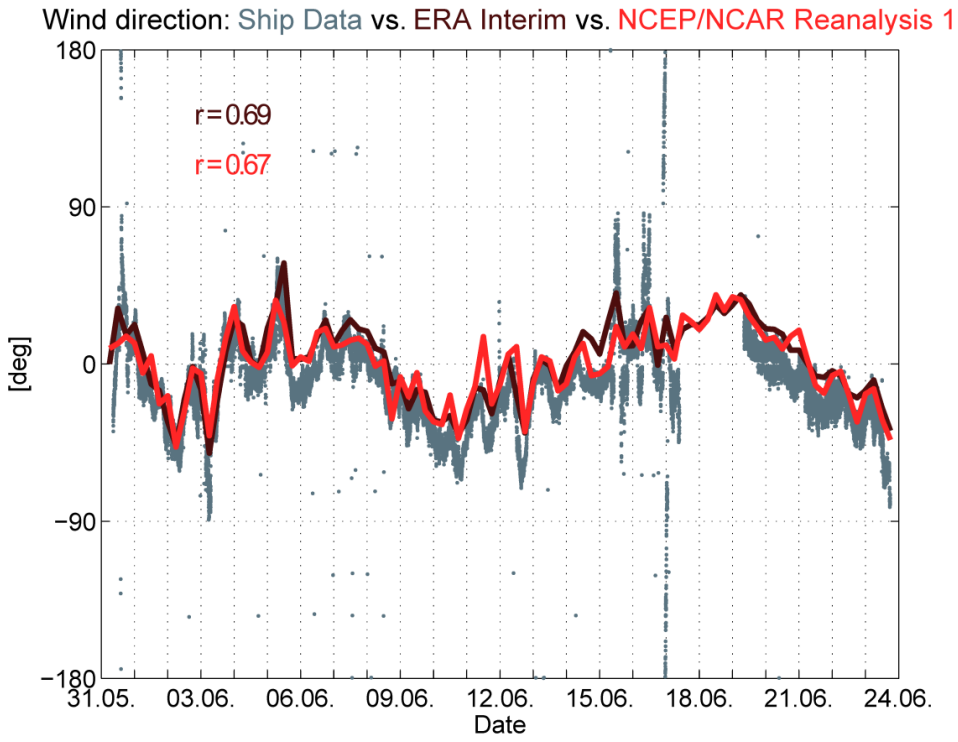

Figure 4-18: As Figure 4-17 for wind direction.

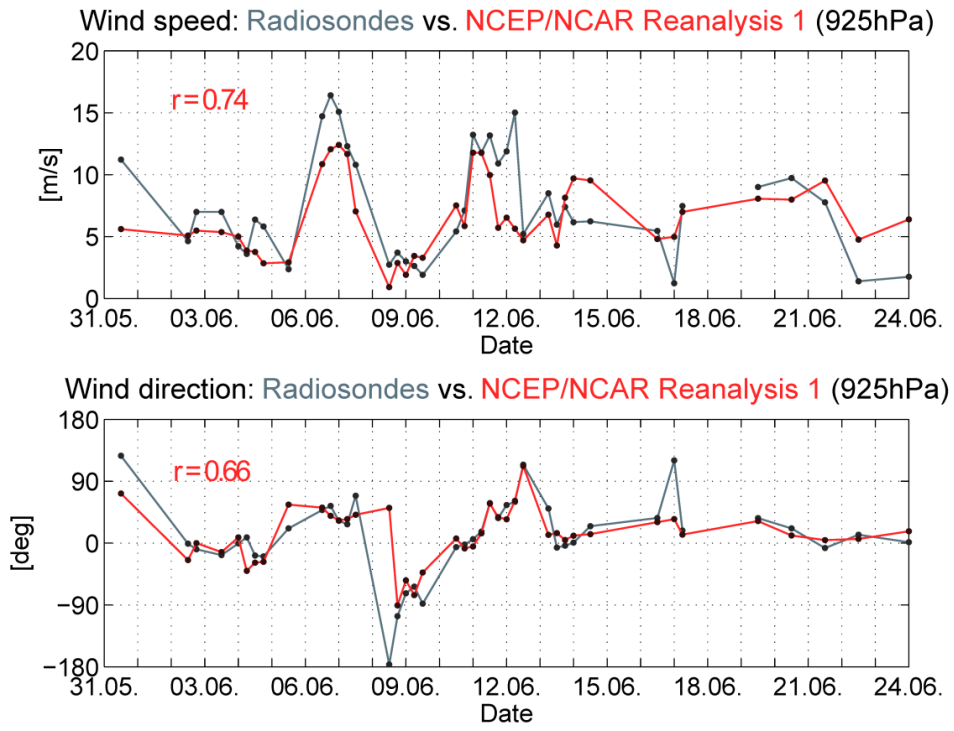

Figure 4-19: Comparison of wind speed and wind direction of radiosondes measurements and NCEP/NCAR Reanalysis Project 1 at 925 hPa pressure level during the DRIVE campaign 2010.

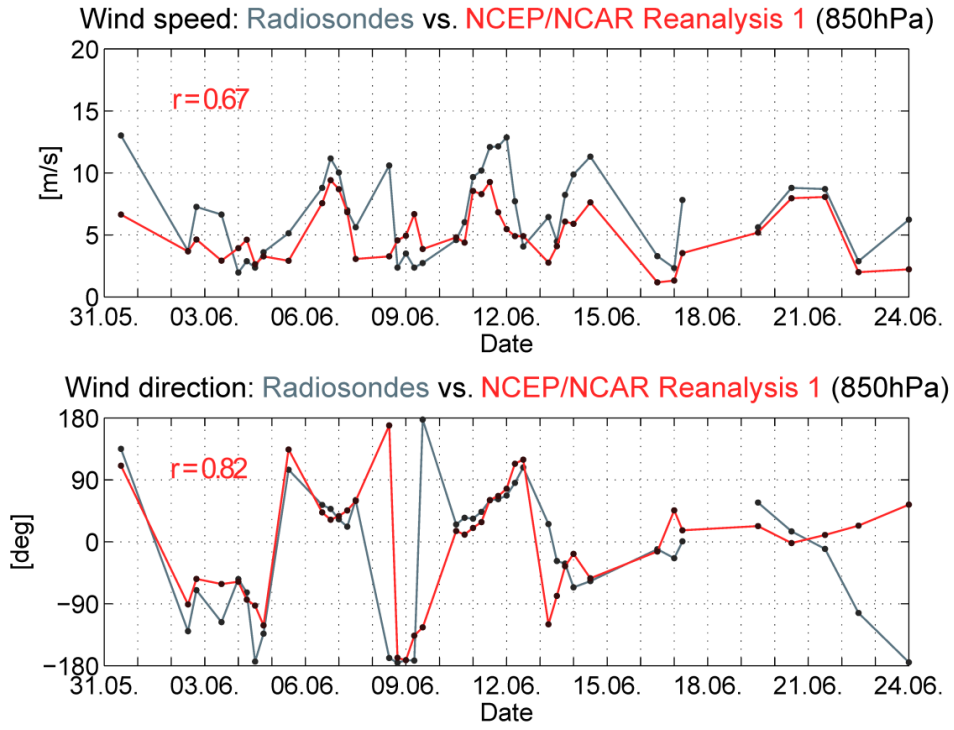

Figure 4-20: As Figure 4-19 for 850 hPa pressure level.

interpolated assimilation data grid points have a distance of 10 – 14 km to each other. Consequently the maximum distance between a grid point and the ships position is always within a range of 7 km. The wind fields show a good agreement for both data sets with the ship measurements. For wind speed the correlation coefficient of the ship data and ERA-Interim is r = 0.91 and r = 0.79 for ship data and NNRP-1 respectively. Both assimilations seem to underestimate the wind speed extremes. Due to the higher horizontal resolution of the ERA-Interim data, the extremes may be better resolved than for NNRP-1. Nevertheless both data sets do have their problems with the wind speeds on May 31, June 7, June 14 and June 16 on leg 2 and underestimate these by 2 – 6 m/s. During leg 3, which takes place in the extratropics, the wind speed is better resolved by NNRP-1. Here, ERA-Interim seems to underestimate the mean velocity by about 2 – 4 m/s. Besides the horizontal resolution, the temporal resolution also plays an important role in the comparison of the data sets. Averaging the wind speed measured by the ship to 6 hours results in improving correlation coefficients of r = 0.95 for ERA-Interim and r = 0.86 for NNRP-1 (Figure A-2). The wind direction comparison of the ship measurements and model data is shown in Figure 4-18 and for 6 hourly ship measurements in Figure A-3. The y axis shows the direction from -180° to 180° (0° = northerly, -90°/90° = westerly/easterly, -180° and 180° = southerly winds). For the once per minute average of the ship measurements, the correlation coefficients are r = 0.69 (ERA-Interim) and r = 0.67 (NNRP-1) and for the 6 hourly averaged measurements r = 0.94 (ERA-Interim) and r = 0.88 (NNRP-1). Both assimilations seem to simulate the surface winds quite well with regard to the temporal resolution. However, they occasionally overestimate the easterly wind component by up to 20°, which might by caused by the closeness to the coast. Despite the fact, that the original model data of ERA-Interim has a 2.5 times higher horizontal resolution than NNRP-1 the similar correlation coefficients for wind speed and direction are surprising. Unfortunately, the accuracy of the measuring instruments of the ship is unknown.

For the investigation of the air mass origin within the boundary layer by trajectory calculations, the wind measurements from radiosondes are compared with NNRP-1 data for the 925 hPa (Figure 4-19) and 850 hPa pressure levels (Figure 4-20). Now, the blue curve marks the observed wind from the radiosondes. To compare the NNRP-1 2.5° x 2.5° data with the radiosondes measurements, the model data are interpolated to a 0.125° x 0.125° horizontal grid on each pressure level. The closest grid point to the radiosonde position at each pressure level, with regard to the shift of the radiosonde, is taken. This results in a maximum distance of 7 km between the model grid point and radiosonde position. The correlation coefficients between radiosonde observations and NNRP-1 data at 925 hPa pressure level are r = 0.74 for wind speed and r = 0.66 for wind direction. For the 850 hPa pressure level the correlation results r = 0.67 (wind speed) and r = 0.82 (wind direction). In contrast to the surface comparison the assimilation data are not as accurate in determining the wind speed and direction at higher pressure levels. The correlation coefficients for wind speed are nearly similar, in contrast to the wind direction which shows a very high correlation. The higher coefficient for wind direction at 850 hPa might be caused by distorted radiosondes measurements near the surface, due to an interpolation of the lowermost radiosondes measurements from the first value, which was manually entered. This one was manually registered and the following values were interpolated until measurements and interpolated values of the radiosondes approximate. However, the wind speed seems though to be unaffected. Nevertheless, the curves roughly agree even though

meteorological assimilation data over the open ocean are quite rare. As the DRIVE radiosondes measurements were not delivered to the WMO data net, they were not assimilated in global meteorological data sets.

4.5. Trace gas measurements

During DRIVE, several anthropogenic and natural trace gases were analyzed. 5 of these anthropogenic and / or natural trace gases with life times of days to years are shown by Figure 4-21. The scales are color-coded and are found on the left side for n-butane and dichloromethane, and on the right side for bromoform, methyl iodide and halon-1211. With a life time of 2 – 7 days (Rudolph and Ehhalt, 1981) n-butane (red line) has the shortest life time. Two peaks were recorded, the first one with 189.2 ppt on 11.06.2010 during the 5th 24 h station and the second one on 13.06.2010 with 365 ppt. As an anthropogenic trace gas (Greenberg and Zimmermann, 1984; Field et al, 1992) with a life time of days, it must have local anthropogenic sources at these regions to explain the high measured mixing ratios. The purple line shows the methyl iodide recordings. With a life time of 5 days (Lovelock et al., 1973; Zafiriou, 1974) it also has a very short lifetime with natural and anthropogenic sources. The highest mixing ratios for methyl iodide are found at the end of the 4th 24 h station with 2.7 ppt and during the 5th and 6th 24 h stations with 2.7 – 3.3 ppt. Again local sources are possibly responsible for these peaks due

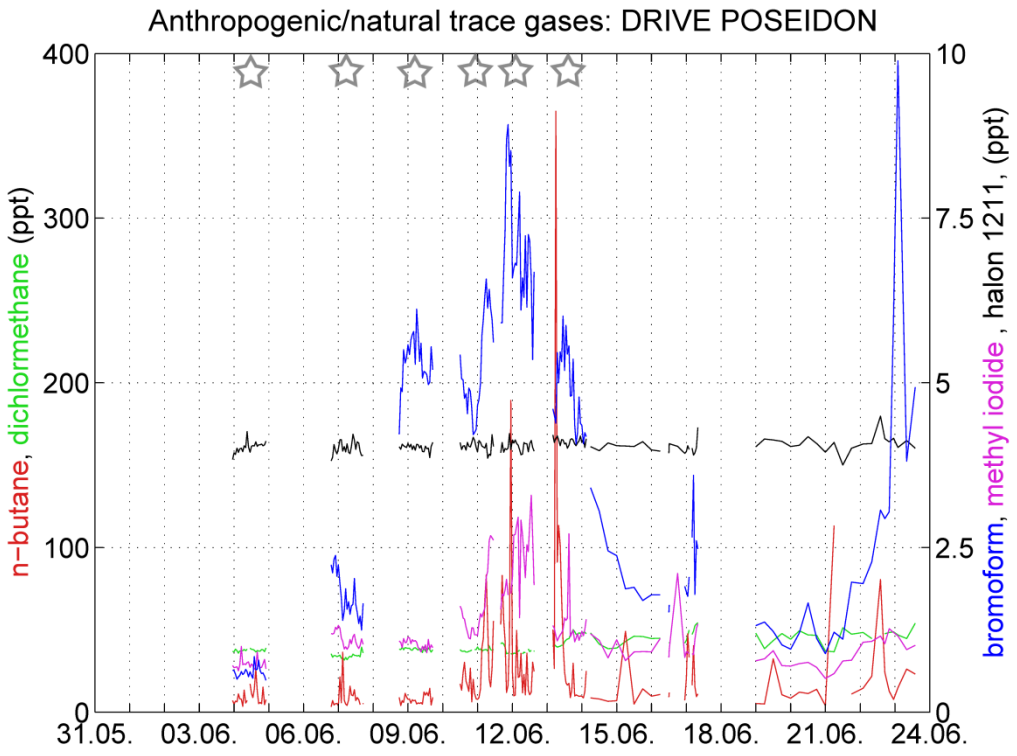

Figure 4-21: Anthropogenic and natural trace gases with different life times measured during the DRIVE campaign 2010. The stars indicate the 24 h stations.

to the short life time of less than a week. The next considered trace gas is bromoform (blue line) with a life time of 2-4 weeks (Barrie et al, 1988) and natural but also anthropogenic sources. Highest values for bromoform were recorded inshore. The analysis shows an increase from the beginning of the 3rd 24 h station to the maximum of 8.9 ppt during leg 2 at the beginning of the 5th 24 h station close to the Mauritanian coast on 11.06.2010. From this leg 2 maximum the recorded bromoform mixing ratios decreased to the end of leg 2. Comparing these three trace gases, no similar behavior is distinguishable for the first three 24 h stations. Contrary to that, nearly the same behavior is shown during the 4th 24 h station by all of them. First the mixing ratios decrease, until they increase again at the beginning of 11.06.2010 and reach their station maximum. This similar manner, with a correlation coefficient of r_4 = 0.76, indicates anthropogenic sources. In the following of station 4, the behavior of the curves does not agree anymore, probably due to decreasing influence of the anthropogenic sources. Except two coinciding peaks of bromoform and n-butane on 11.06.2010 23 UTC and 17.06.2010 06 UTC, which indicate anthropogenic sources, these trace gases do not show any similar behavior for the rest of leg 2. Therefore these observed mixing ratios may predominantly be caused by natural sources. The overall highest bromoform mixing ratio recorded during DRIVE was on June 24.06.2010 with 9.8 ppt on leg 3 close to Lisbon[4]. A possible anthropogenic influence on the atmospheric bromoform mixing ratio in this region may not be negligible. The last two trace gases with atmospheric life times in the order of 5 months for dichloromethane (McCulloch and Midgley, 1996) and about 20 years for halon-1211 (Solomon et al., 1995) have anthropogenic sources. Due to their relatively long lifetime, these two trace gases are a rather well mixed within the troposphere and the stratosphere. This is reflected in the mean dichloromethane mixing ratios of 40.1 ± 14.2 ppt and the mean halon-1211 mixing ratio of 4 ± 0.5 ppt, showing a rather calm behavior of these two long-lived trace gases. The bromoform, methyl iodide and dibromomethane measurements and their possible origins are further investigated in Chapter 5.

4.6. Trajectories

This section shall give a rough overview of the air mass origin using trajectory calculations for both legs of DRIVE. A detailed investigation for the 24 h stations is found in Chapter 5.2. To gain insight in the air mass history, backward trajectories are calculated with HYSPLIT for leg 2 (Figure 4-22) and 3 (Figure 4-23). The trajectories have a maximum runtime of 315 hours (13 days and 3 hours). In each figure the upper plot shows the horizontal distribution of the trajectories and the lower plot the vertical distribution starting on ground level. According to the trajectories, all surface ship measurements primarily originate from northern and north-western air masses below 2 km. At the beginning of leg 2 the trajectories mainly originate from the Azores and the Labrador Sea, and do not extend 250 m height. In the following, the trajectories are mainly influenced by a high pressure system located between the Azores and the coast of Portugal, which deflects the air up to 40° - 50° N, close to the coast of Portugal. Afterwards, the air is redirected, combination with the trade winds, southwards to the ship. Due to the high at

[4] Lisbon (38.7° N, 9.1° W), capital city of Portugal.

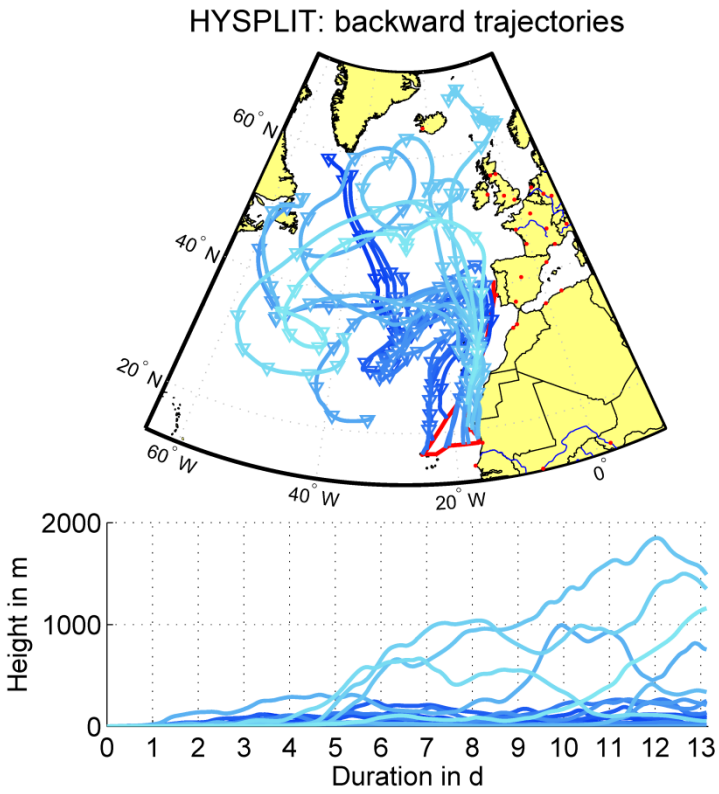

Figure 4-22: 315 h backward trajectories by HYSPLIT for leg 2, started every 24 hours at 12 UTC. Light blue indicates younger trajectories, dark blue older trajectories. The triangles mark one day.

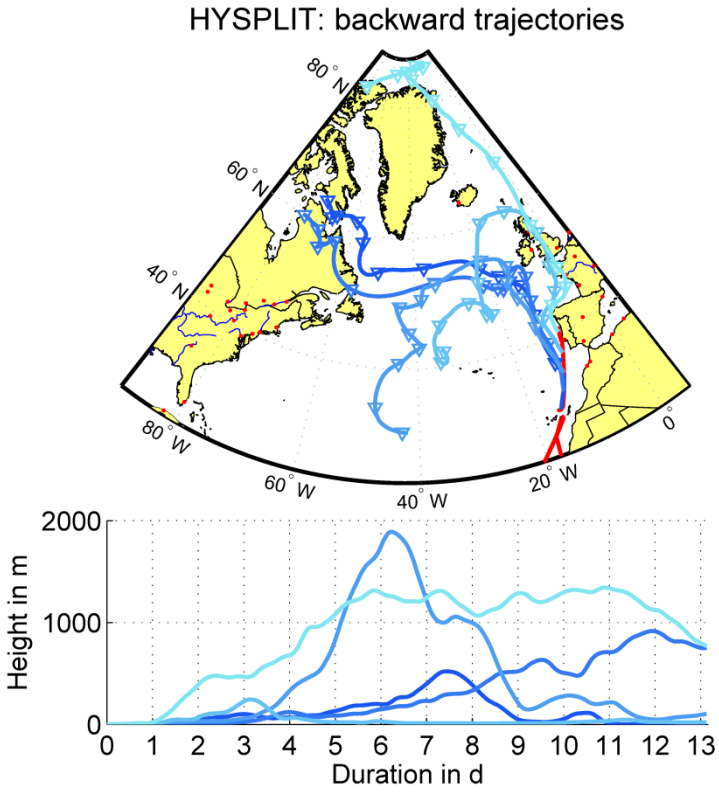

Figure 4-23: As Figure 4-22 for leg 3.

the Azores, these trajectories stay close to the ground for the whole duration. From the mid to the end of leg 2 the trajectories show a more varying origin, ranging from the Tropic of Cancer to the south of the Greenland Sea north of Iceland. Originated in heights of 1 – 2 km these trajectories descend to the surface, not later than 2 days before hitting the ship. Here, inversions as described in the investigation of the radiosondes measurements prevent the air masses from ascending. A similar situation is given for leg 3 (Figure 4-23). All trajectories stay close to the ground for at least one day before reaching the ship. The air masses show a high geographical variability as they origin from the North Atlantic, Northern Canada and the Arctic. A possible anthropogenic influence is also demonstrated by the last 2 trajectories which pass Great Britain and the northwest of France. According to Fogelqvist (1985) and Sturges et al (1992), Arctic air masses could also include bromoform emissions by ice algae, but these are highly speculative assumptions. Nevertheless, the ratio of dibromomethane and bromoform results in 0.27 close to Lisbon, indicating quite young sources. Due to the estuary of the Rio Tejo[5] at Lisbon, the observed bromine peak is more probably caused by this river input.

[5] Rio Tejo, longest river on the Iberian Peninsula, empties into the Atlantic Ocean at Lisbon.

5. Analysis of atmospheric VSLS variability

This chapter investigates the atmospheric distribution of three VSLS analyzed in air samples during the DRIVE campaign. lifetimes of these VSLS vary from days to months, giving first evidence about local and distant sources. For a first potential identification of these sources, trajectories are calculated. To evaluate influences on the VSLS, they are related to different meteorological data and compared with each other. Finally the results are discussed.

5.1. VSLS measurements

The main focus of the VSLS investigation now lies on leg 2, due to the main attention on the regional variability of halogen emissions from the open ocean to the upwelling area at the Mauritanian coast. A time series of the bromoform, dibromomethane and methyl iodide mixing ratios is shown in Figure 5-1 together with the mixed layer height. The regional and diurnal variability of these three compounds is further shown in Figure 5-2 (bromoform), Figure 5-3 (dibromomethane) and Figure 5-4 (methyl iodide). Station 1 and 2 are combined and identified as open ocean stations, station 4 – 6 as coastal stations. In addition the ratio of the dibromomethane and bromoform mixing ratios for leg 2 is shown in Figure 5-5. Due to the

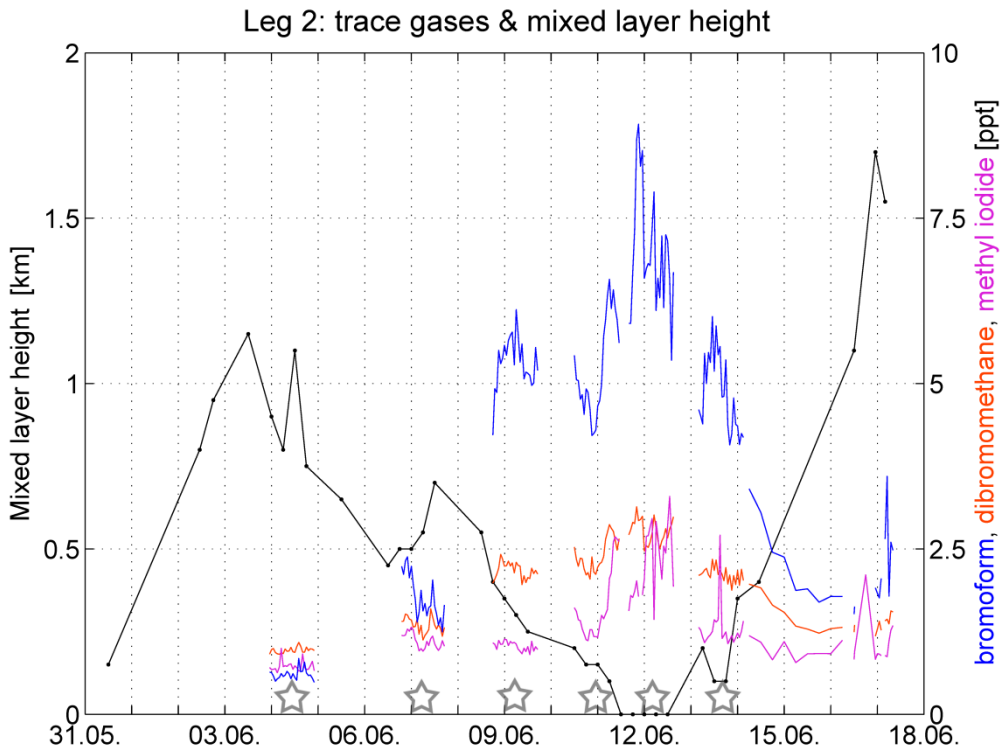

Figure 5-1: VSLS measurements of bromoform, dibromomethane, methyl iodide in ppt during leg 2. The VSLS have an hourly resolution at the 24 h stations and a 6 hourly resolution afterwards. In addition the determined mixed layer height in km is given. The stars indicate the 24 h stations.

differing lifetimes of both compounds (section 2.5), a first conclusion about the age of the encountered air masses can be derived. Marginal ratios up to 0.5 reflect younger and local sources of bromoform and dibromomethane, whereas higher ratios indicate older sources, as they are found over open ocean (Carpenter et al., 2003; Yokouchi et al., 2005; Quack et al., 2007). All trace gases show an increase of the atmospheric mixing ratios from the Cape Verde to the Mauritanian upwelling, followed by a decrease towards the Canary Islands. The lowest atmospheric mixing ratios for all trace gases were measured at the first 24 h station at the TENATSO. With a mean $CH_2Br_2/CHBr_3$ ratio of 1.63 typical open ocean air masses were observed. A first slight increase of the measured values (Figure 5-1) in combination with a decreasing mean $CH_2Br_2/CHBr_3$ ratio of 0.78 is distinguishable at the second 24 h station. At the third 24 h station, the trace gases, except for methyl iodide show an increase up to 4.22 – 6.12 ppt ($CHBr_3$) and 1.96 – 2.42 ppt (CH_2Br_2). A mean concentration ratio of 0.41, indicates younger emission sources. The fourth 24 h station shows approximately the same atmospheric mixing ratios and $CH_2Br_2/CHBr_3$ ratio as the third 24 h station. However, a diurnal variation seems to be adumbrated in the box for the fourth 24 h station in Figure 5-2, Figure 5-3 and Figure 5-4. The three VSLS show a marginal decrease from 12 UTC to 00 UTC followed by an increase from 06 UTC to 09 UTC on the following day, which also coincides with the sun rise initiating photochemical reactions. The fifth 24 h station shows the highest atmospheric mixing ratios measured during leg 2. Bromoform reaches mixing ratios of 8.92, dibromomethane of 3.14 and methyl iodide of 3.29 ppt. All measurements show minor variations, however the minimum for methyl iodide at 05 UTC seems to be an outlier, due to the high variation of nearly 1 ppt within

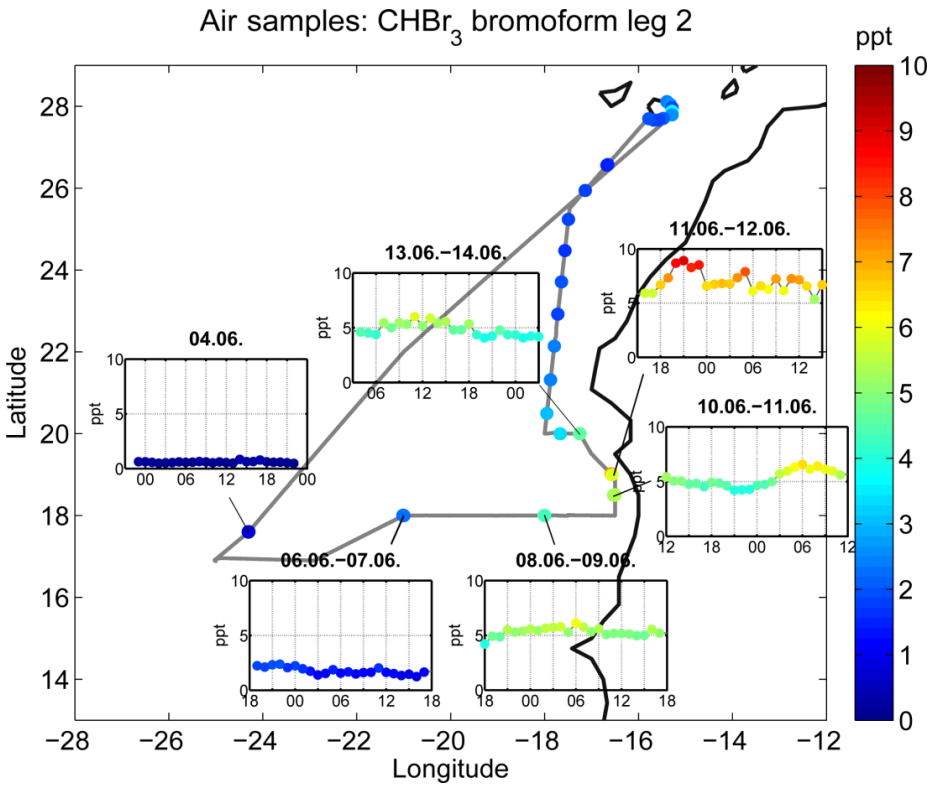

Figure 5-2: Atmospheric mixing ratio of bromoform in ppt measured by air samples during leg 2. The small boxes show the hourly measurements at the 24 h stations with UTC time at the x-axis; note the differing start times at the x-axes.

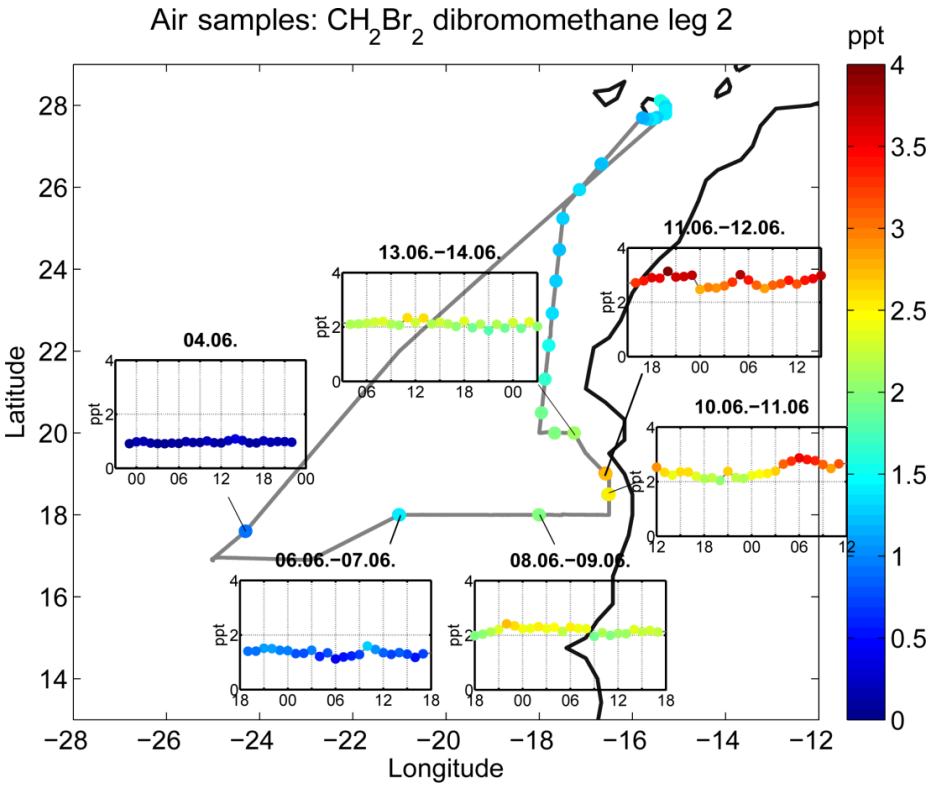

Figure 5-3: As Figure 5-2 for dibromomethane.

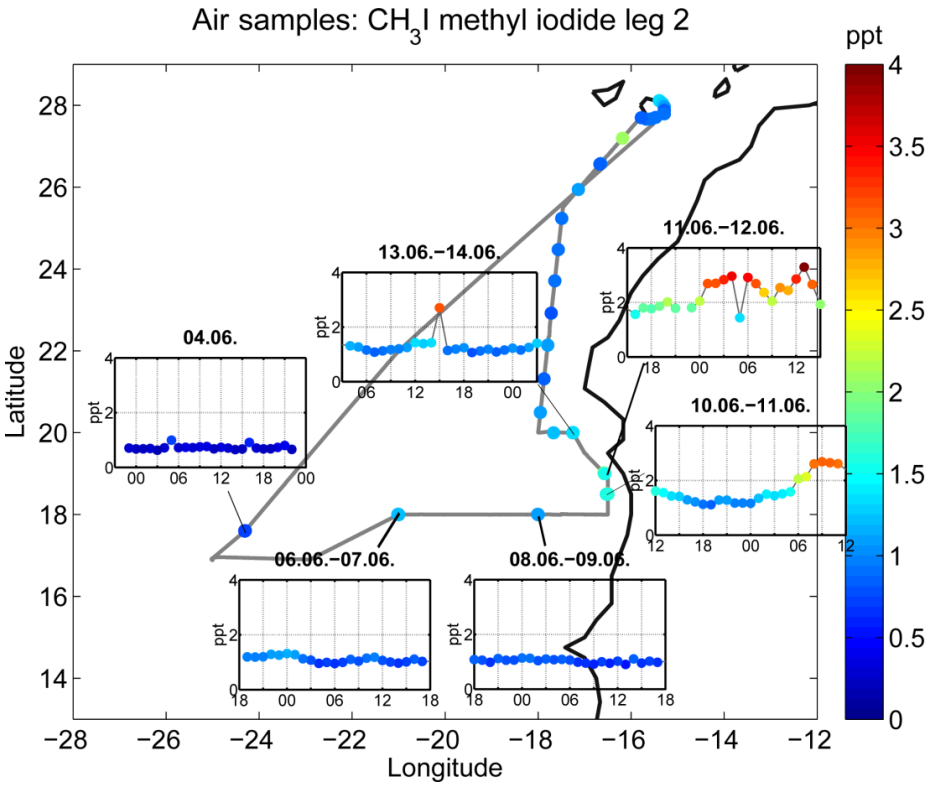

Figure 5-4: As Figure 5-2 for methyl iodide.

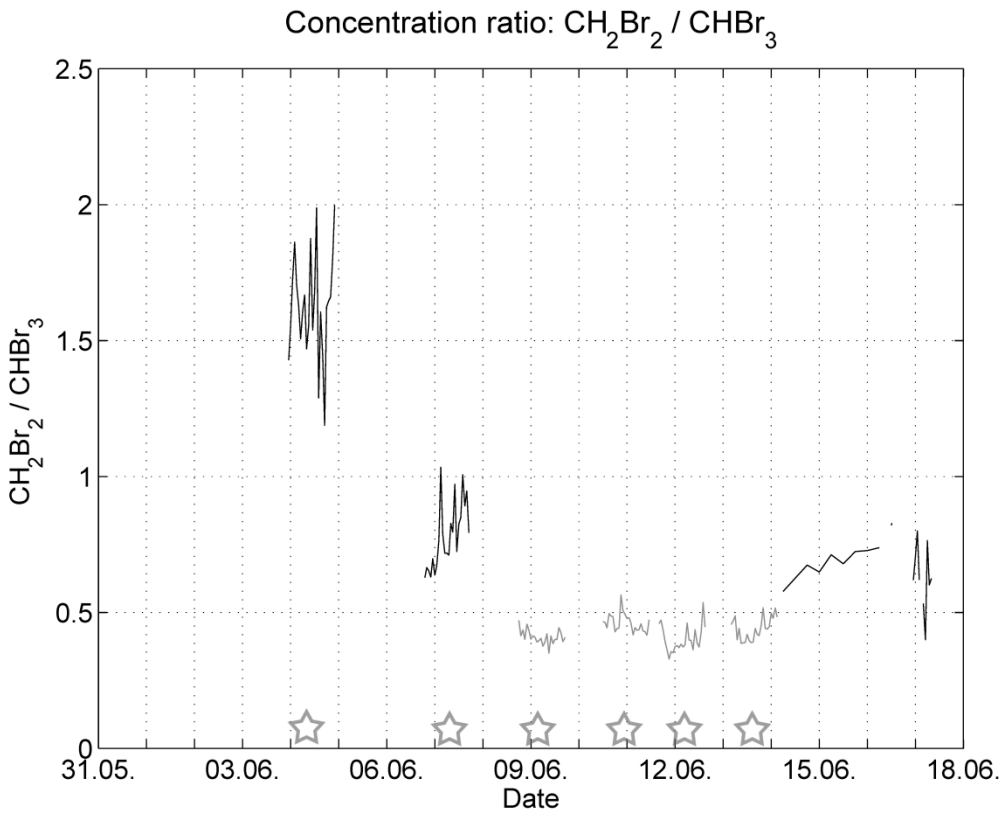

Figure 5-5: Concentration ratio (hourly at 24 h stations and 6 hourly afterwards) of CH_2Br_2 / $CHBr_3$. The coastal stations are grey, stars indicate the 24 h stations.

Table 2: Observed mixing ratios of bromoform ($CHBr_3$), dibromomethane (CH_2Br_2), their ratio and methyl iodide (CH_3I) for different regions. Open ocean combines station 1 and 2; coast combines station 3, 4, 5 and 6.

Parameter	Unit	Leg 2	Leg 2+3	Station 1	Station 2	Station 3	Station 4	Station 5	Station 6	Open ocean	Coast
$CHBr_3$ mean	ppt	3.91	3.75	0.60	1.77	5.32	5.25	7	4.85	1.17	5.60
$CHBr_3$ (min-max)	ppt	0.48 - 8.92	0.48 - 9.9	0.48 - 0.84	1.24 - 2.38	4.22 - 6.12	4.21 - 6.58	5.35 - 8.92	4.07 - 6.01	0.48 - 2.38	4.07 - 8.92
$CHBr_3$ stdv of mean	%	58	61	13	19	7	14	13	12	54	19
CH_2Br_2 mean	ppt	1.9	1.85	0.97	1.35	2.17	2.41	2.77	2.11	1.15	2.37
CH_2Br_2 (min-max)	ppt	0.91 - 3.14	0.89 - 3.14	0.91 - 1.09	1.12 - 1.59	1.96 - 2.42	2.04 - 2.87	2.47 - 3.14	1.87 - 2.34	0.91 - 1.59	1.87 - 3.14
CH_2Br_2 stdv of mean	%	33	34	5	9	6	10	7	5	18	13
CH_3I mean	ppt	1.30	1.25	0.73	1.11	1.03	1.62	2.30	1.28	0.91	1.55
CH_3I (min-max)	ppt	0.63 - 3.29	0.51 - 3.29	0.63 - 1	0.95 - 1.32	0.90 - 1.14	1.11 - 2.68	1.44 - 3.29	1.07 - 2.71	0.63 - 1.32	0.90 - 3.29
CH_3I stdv of mean	%	45	45	11	10	7	32	23	25	24	40
$CH_2Br_2/CHBr_3$ mean		0.68	0.69	1.63	0.78	0.41	0.46	0.40	0.44	1.21	0.43

an interval of two hours. Figure A-1 shows, that this station is directly influenced by cold, upwelling water. Local sources may cause such high mixing ratios intensified by surface inversions which suppress vertical air exchange. Although the lowest $CH_2Br_2/CHBr_3$ ratio of 0.40 during leg 2 was recorded at this station, this value is two to three times higher than ratios at other coastal areas (0.1 – 0.25), by Carpenter et al. (2003) and Yokouchi et al. (2005). Here, mixing with air masses, containing bromoform and dibromomethane with older sources (e. g. open ocean air masses) is a possible cause for the relative high $CH_2Br_2/CHBr_3$ ratio. At the last 24 h station a decrease of the trace gas mixing ratios is observed, while the distance to the coast is increasing. Again an outlier seems to occur in the methyl iodide measurements at 15 UTC, with regard to the remaining methyl iodide measurements during this station.

Table 2 summarizes the observed mixing ratios of bromoform, dibromomethane and methyl iodide for leg 2 and 3, each station, clustered stations and the whole cruise. In addition the ratio of dibromomethane and bromoform, as well as the standard deviations are given.

5.2. Analysis of air mass origin

This section analyzes the air mass history during leg 2, to distinguish potential source regions for atmospheric bromoform, dibromomethane and methyl iodide. The trajectories are calculated by HYSPLIT using NNRP-1 data. Figure 5-6 shows 5 day backward trajectories, started on the ground and at 1 km height. In comparison to the ground (see also section 4.6), the trajectories started at 1000 m height have a much higher horizontal and vertical (up to 7 km height) variability. Here the air masses have a strong eastern component and increased African continental influence. Especially close to the coast the trajectories are mainly distributed over land and might therefore influence the observed atmospheric mixing ratios.

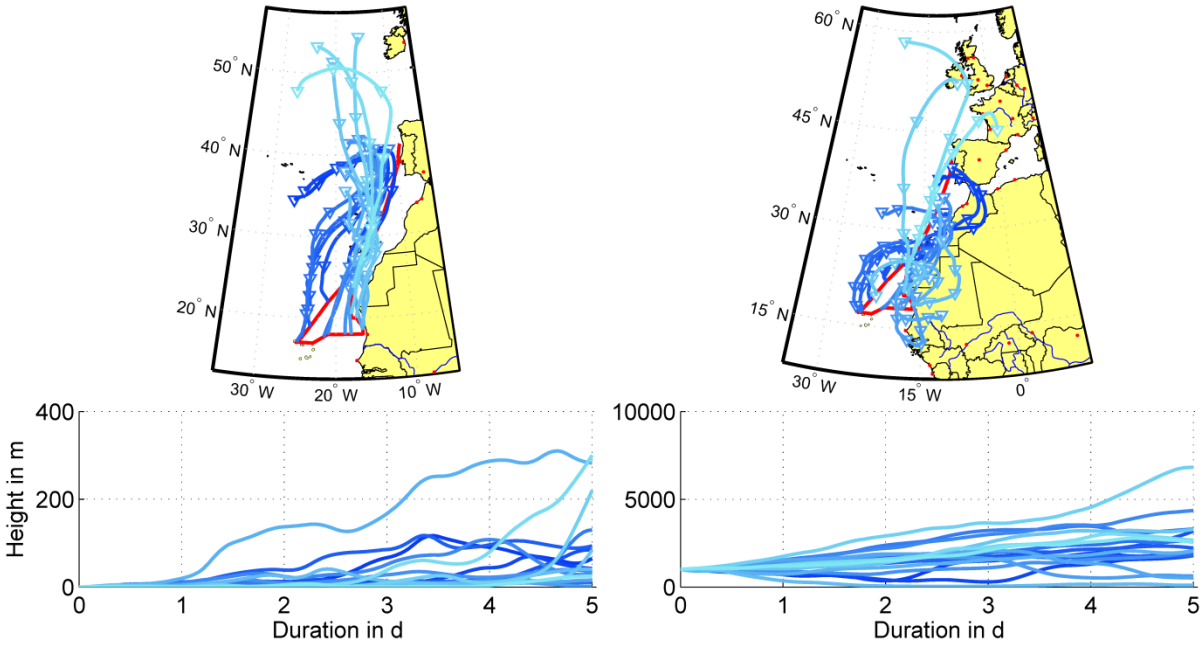

Figure 5-6: 5 day backward trajectories by HYSPLIT, started every 24 hours on the ground (left side) and at 1000 m height (right side) during leg 2.

5.2.1. 1st 24 h station

The backward trajectories and trace gas measurements for station 1 are shown in Figure 5-7. The trajectories have a total runtime of 48 hours and are color-coded. The starting time is shown by the legend in the lower plot. The trajectories indicate no influence by any coastal areas within range of the Mauritanian upwelling. This is also reflected by the trace gas concentrations, which had their minimum at this station. Also the ratio of dibromomethane and bromoform (1.62; Table 2) for the 1st 24 h station, indicate open ocean aged air masses, which is well represented by the trajectories.

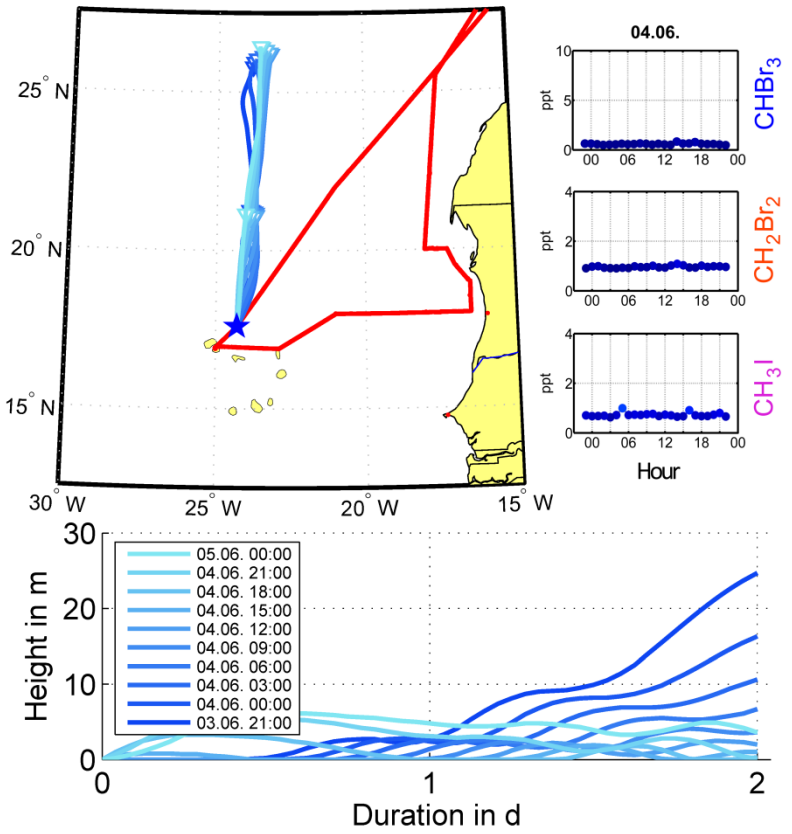

Figure 5-7: 2-day backward trajectories at the 1st 24 h station started every 3 hours at the ground from 03.06.2010 21 UTC (dark blue) to 05.06.2010 00 UTC (light blue). In addition the 24 h mixing ratios are shown in the upper right with corresponding UTC time.

5.2.2. 2nd 24 h station

A slight increase of the atmospheric VSLS mixing ratios was denoted for the first time at the second 24 h stations. They are shown in Figure 5-8 together with the associated trajectories. The backward trajectories have a much stronger eastern component, in contrast to the 1st 24 h station. Within one and a half day they pass the Canary Islands before approaching the ship position. A possible impact of the Canary Islands and their coastal regions on the air masses and atmospheric mixing ratios due to the low vertical distribution of the trajectories, with maximum

heights within 40 m altitude, is therefore not necessarily eliminated, as it was also supposed by Quack and Wallace (2004). Furthermore the decreased mean ratio for dibromomethane and bromoform of 0.78 indicates younger sources in comparison to the first 24 h station.

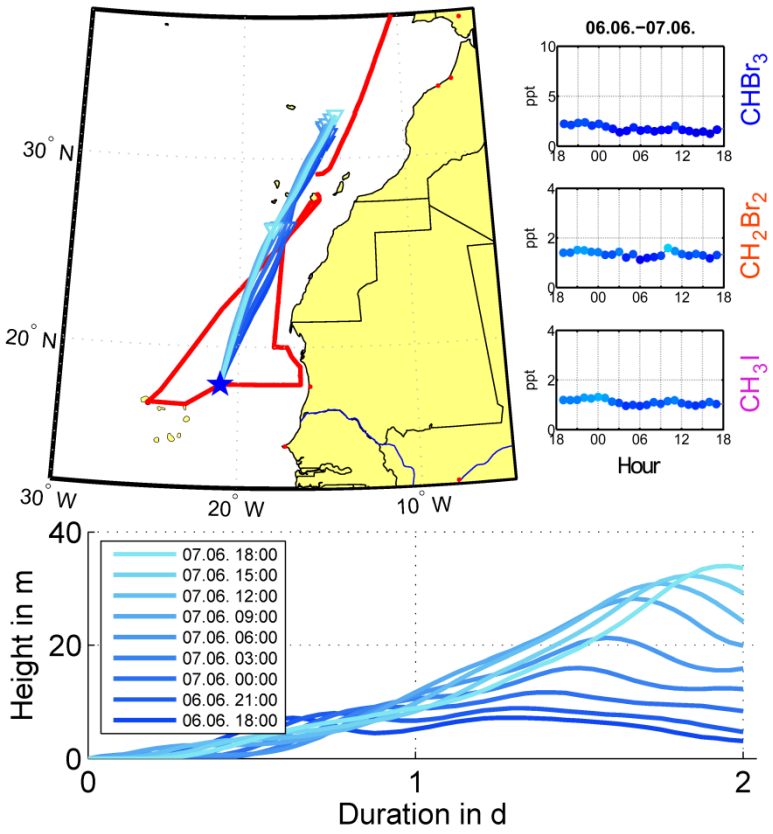

Figure 5-8: As Figure 5-7 for 2nd 24 h station from 06.06.2010 18 UTC (dark blue) to 07.06.2010 18 UTC (light blue).

5.2.3. 3rd 24 h station

The backward trajectories and atmospheric mixing ratios for the 3rd 24 h station are shown in Figure 5-9. The trajectories shift towards the east and get closer to the West African coast, while they still pass the Canary Islands. The approach to the Mauritanian upwelling and coastal regions is also reflected in the increase of the bromoform and dibromomethane mixing ratios. In contrast to methyl iodide the bromoform mixing ratios triple to a mean mixing ratio of 5.32 ppt and the dibromomethane mean mixing ratio increases by one and a half time to 2.17 ppt, reducing the ratio of the compounds to 0.4. The low heights of the trajectories with less than 25 m accumulate recent sea-air gas exchange of oceanic VSLS. In combination with the origin of the air masses over Gran Canaria and the Mauritanian upwelling with observed decreasing water temperatures, and the reduced dibromomethane and bromoform ratio, the trajectories indicate younger potential sources at these regions, where comparatively more bromoform than dibromomethane is emitted. Although the bromoform and dibromomethane mixing ratios do not reflect it, open oceanic influence on the air masses is still indicated by the trajectories.

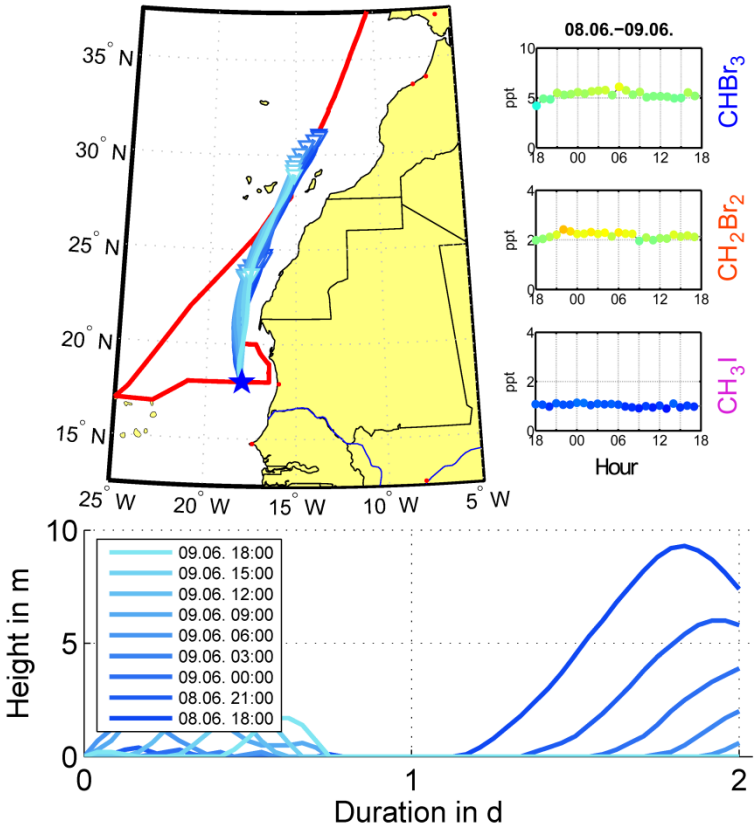

Figure 5-9: As Figure 5-7 for 3rd 24 h station from 08.06.2010 18 UTC (dark blue) to 09.06.2010 18 UTC (light blue).

5.2.4. 4th 24 h station

The backward trajectories for the 4th 24 h station with a total runtime of 48 hours in combination with the observed trace gases are shown in Figure 5-10. The high correlation of the wind direction with the variation of the trace gas measurements, as shown in Table 3, Table 4 and Table 5 respectively, is now obviously connected to a shift of the air masses over the Banc d'Arguin (Figure 5-10). The trace gases show an increase in the early morning hours which is connected to the shift of the trajectories towards the African continent, indicated by the lighter blue. Although this increase supposes potential nearby sources at, or at least near, the Banc d'Arguin, the mean concentration ratio of dibromomethane and bromoform for this station is just 0.46. This might by caused by mixing of the recently influenced air masses, with older air masses. According to the vertical extension of the trajectories, they seem to overflow the Banc d'Arguin very close to the ground. Taking a closer look at the trace gas measurements, the maximum of methyl iodide is reached about 3 hours later than the maxima for bromoform and dibromomethane, as well as the decrease in the following. There may be several reasons for the shift, including different source regions and photochemical reactions after sunrise, which is discussed later.

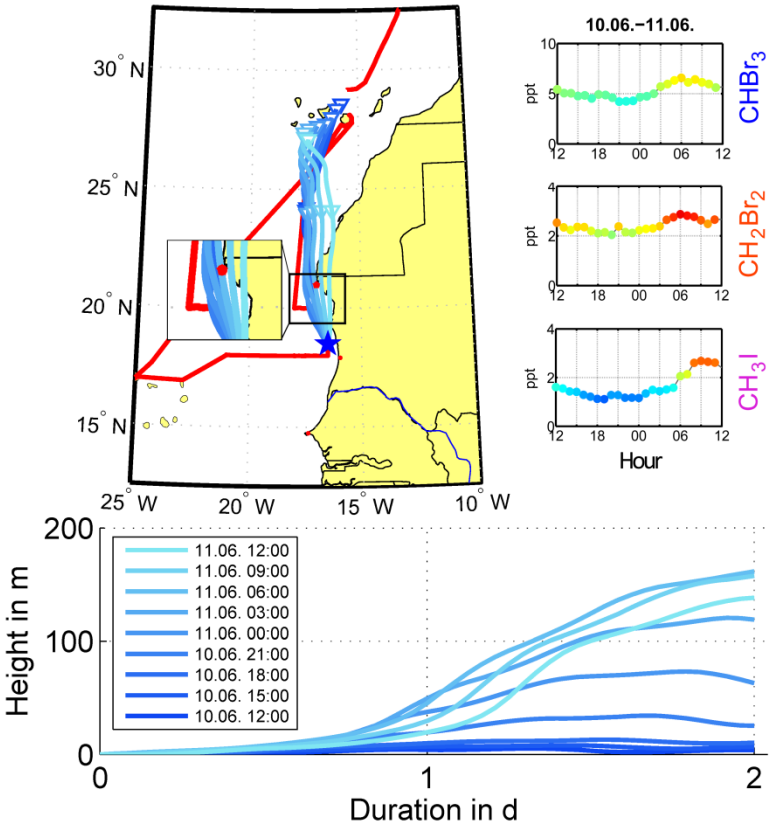

Figure 5-10: As Figure 5-7 for 4th 24 h station from 10.06.2010 12 UTC (dark blue) to 11.06.2010 12 UTC (light blue). The box shows a zoom of the Banc d'Arguin area with the red dot marking Nouadhibou[6].

5.2.5. 5th 24 h station

During the 5th 24 h station, the highest atmospheric mixing ratios of bromoform, dibromomethane and methyl iodide were measured during leg 2. Concentrations and trajectories are shown in Figure 5-11. The trajectories, originated at the Canary Islands, show a shift from the north-west over the Banc d'Arguin, as it was also observed at the end of the 4th 24 station, to the north-east and back again to the north-west. Thus, the air masses show little continental influence. Anthropogenic influence from Nouadhibou can also not be excluded. The shift of the trajectories seems not to be related to the variations of the VSLS mixing ratios. Although the mean dibromomethane and bromoform concentration ratio of 0.4 is not as low as it was observed in earlier studies at coastal regions, the correlation coefficients r = 0.16 (bromoform), r = -0.49 (dibromomethane) and r = 0.14 (methyl iodide) between the trace gases and the wind direction close to the Banc d'Arguin indicate local sources. As for the previous 24 h stations, mixing with less bromoform and trace gas concentrated air masses could result in the relative high mean ratio of dibromomethane and bromoform (0.40). The methyl iodide concentration at 05 UTC on 12.06.2010 has no distinguishable reason and may thus be an outlier.

[6] Nouadhibou (21° N, 17° W), city north of the Banc d'Arguin with about 84.000 inhabitants (2010) (World Gazetteer).

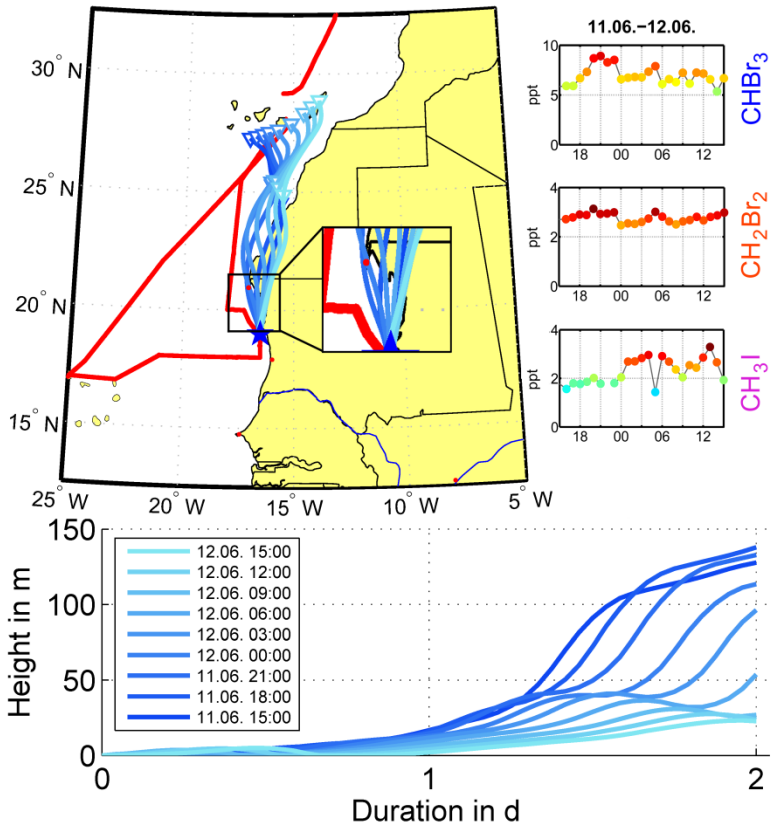

Figure 5-11: As Figure 5-7 for the 5th 24 h station from 11.06.2010 15 UTC (dark blue) to 12.06.2010 15 UTC (light blue).

5.2.6. 6th 24 h station

The last 24 h station is located to the west of the Banc d'Arguin. The according trajectories and trace gas measurements are shown in Figure 5-12. The maximum height of the trajectories within the last two days before reaching the ship is denoted by HYSPLIT at about 5 m. As shown in the Figure, the air masses are not influenced by the Banc d'Arguin anymore, but still enriched by atmospheric bromoform and dibromomethane. With regard to the atmospheric mixing ratios, which nearly have the same amount as for station 3, despite that second possible methyl iodide outlier at 15 UTC, and the origin of the trajectories, methyl iodide seems to be predominantly emitted at the Banc d'Arguin. In contrast to that, source regions for bromoform and dibromomethane seem to exist, besides the Banc d'Arguin, also at the coast of Western Sahara close to the upwelling regions, due to distribution of the trajectories at this coastline.

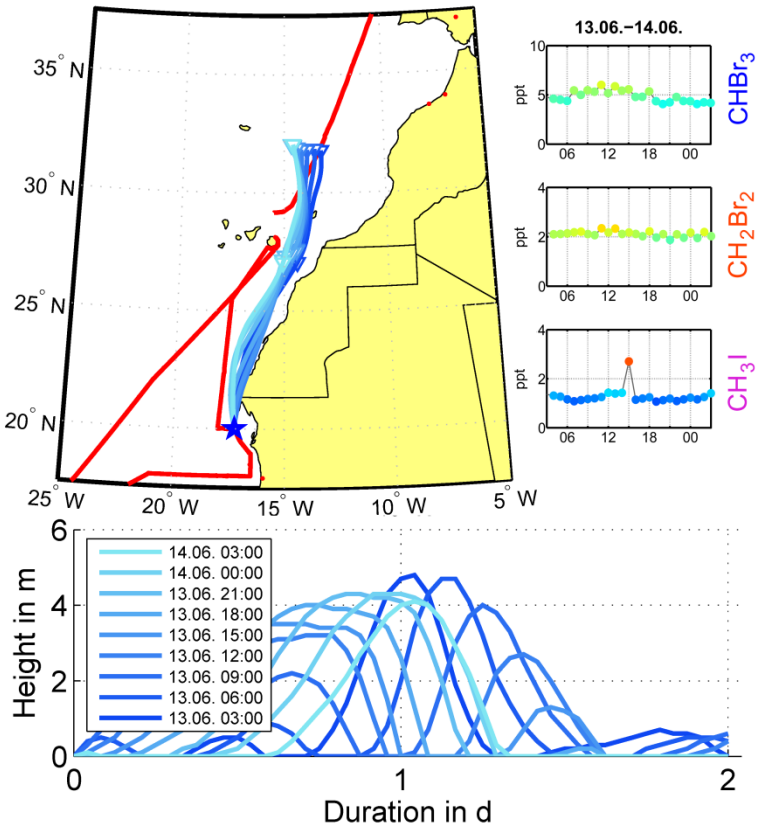

Figure 5-12: As Figure 5-7 for the 6th 24 h station from 13.06.2010 03 UTC (dark blue) to 14.06.2010 03 UTC (light blue).

5.3. Meteorological background

In this section, the meteorological measurements from the ship, the derived mixed layer height and the atmospheric mixing ratios of bromoform, dibromomethane and methyl iodide during leg 2 are compared to each other. The correlation coefficients of the three VSLS with the meteorological measurements are found in Table 3 for bromoform, Table 4 for dibromomethane and Table 5 for methyl iodide. The correlation coefficients of the mixed layer height are further found in the Appendix (Table 6). Significant general correlations and anti-correlations between the three VSLS and meteorological parameter are found for the air/water temperature difference ($CHBr_3$: r = 0.72, CH_2Br_2: r = 0.73, CH_3I: r = 0.73), the air pressure and the mixed layer height. The temperature difference in comparison with the trace gases is shown in Figure 5-13. Positive values indicate higher air temperatures and negative values higher water temperatures. Highest positive differences are reached from 11.06.2010 (begin of station 4) to 14.06.2010 (end of station 6) due to the cold upwelling water at this regions. The air/water temperature difference is relative to the sensible heat flux. The positive temperature difference creates a negative sensible heat transfer between air and water, which cools the lower air layers and thus creates surface inversions, or at least a stable stratification of the lower atmosphere. This suppresses the vertical movement of air and therefore reduces the volume of air which is available for mixing. As a result, for constant sources, the atmospheric mixing ratios increase.

Table 3: Correlation coefficients of bromoform ($CHBr_3$) with dibromomethane (CH_2Br_2), methyl iodide (CH_3I), mixed layer height (MLH), wind speed (w_{spd}), wind direction (w_{dir}), air pressure (p), relative humidity (U), air temperature (T_{air}), water temperature (T_{sea}) and temperature difference (ΔT) for the different parts of DRIVE. Station 1 and 2 are clustered to "Open ocean" and Station 3, 4, 5 and 6 to "Coast". Due to no distinguishable mixed layer height at station 5, a correlation coefficient cannot be determined. For the correlation of two parameters, the parameter with the higher resolution was averaged to an identical resolution of the second parameter (ship data: every minute, VSLS: hourly, MLH: 24 hourly, and 6 hourly at 24 h stations). High (anti) correlations are bold.

$CHBr_3$	Leg 2	Leg 2+3	Station 1	Station 2	Station 3	Station 4	Station 5	Station 6	Open ocean	Coast
CH_2Br_2	**0,97**	**0,97**	0,31	0,59	0,57	**0,89**	0,52	0,68	**0,93**	**0,84**
CH_3I	0,69	0,69	0,01	**0,76**	0,14	**0,76**	-0,33	0,33	**0,93**	**0,59**
MLH	**-0,94**	**-0,90**	-0,35	-0,68	-0,66	-0,61	/	**-0,70**	**-0,82**	**-0,75**
w_{spd}	0,30	0,23	0,17	0,03	-0,41	-0,01	0,18	-0,69	**0,88**	-0,14
w_{dir}	-0,53	-0,51	-0,42	0,16	-0,26	**0,85**	0,16	-0,18	0,05	0,06
p	**-0,84**	**-0,76**	-0,19	-0,01	-0,17	-0,32	-0,09	0,37	-0,64	-0,52
U	0,47	0,52	-0,07	0,61	0,64	**0,78**	0,47	-0,03	**0,93**	-0,14
T_{air}	-0,11	-0,03	0,31	0,10	-0,12	-0,58	-0,53	0,07	**-0,87**	0,40
T_{sea}	-0,56	-0,45	0,53	0,69	-0,55	-0,67	-0,37	-0,40	**-0,87**	-0,05
ΔT	**0,72**	**0,72**	0,14	-0,40	0,13	-0,07	-0,38	0,25	-0,46	**0,64**

Table 4: As Table 3 for dibromomethane.

CH_2Br_2	Leg 2	Leg 2+3	Station 1	Station 2	Station 3	Station 4	Station 5	Station 6	Open ocean	Coast
$CHBr_3$	**0,97**	**0,97**	0,31	0,59	0,57	**0,89**	0,52	0,68	**0,93**	**0,84**
CH_3I	**0,73**	**0,74**	-0,23	0,62	0,47	**0,74**	-0,43	0,20	**0,89**	**0,70**
MLH	**-0,94**	**-0,91**	**0,77**	0,32	-0,49	**-0,72**	/	-0,53	-0,69	**-0,80**
w_{spd}	0,34	0,27	0,30	-0,08	-0,04	-0,01	-0,05	-0,51	**0,86**	-0,02
w_{dir}	-0,57	-0,54	-0,26	0,11	-0,01	**0,81**	-0,49	-0,02	0,04	-0,16
p	**-0,87**	**-0,83**	0,21	0,23	-0,11	-0,27	-0,34	0,31	-0,55	**-0,71**
U	0,45	0,51	-0,50	0,22	0,76	**0,76**	0,09	0,19	**0,85**	-0,32
T_{air}	-0,06	0,05	0,54	0,17	-0,38	-0,54	-0,41	-0,05	**-0,83**	0,57
T_{sea}	-0,51	-0,38	0,52	0,38	-0,40	-0,69	0,23	-0,38	**-0,86**	0,12
ΔT	**0,73**	**0,73**	0,44	-0,11	-0,25	-0,03	-0,57	0,10	-0,35	0,63

Table 5: As Table 3 for methyl iodide.

CH_3I	Leg 2	Leg 2+3	Station 1	Station 2	Station 3	Station 4	Station 5	Station 6	Open ocean	Coast
$CHBr_3$	0,69	0,69	0,01	**0,76**	0,14	**0,76**	-0,33	0,33	**0,93**	0,59
CH_2Br_2	**0,73**	**0,74**	-0,23	0,62	0,47	**0,74**	-0,43	0,20	**0,89**	0,70
MLH	-0,57	-0,63	-0,61	-0,46	**0,77**	**-0,90**	/	-0,40	**-0,83**	**-0,79**
w_{spd}	0,29	0,24	-0,04	0,09	0,06	-0,18	-0,30	-0,23	**0,85**	0,07
w_{dir}	-0,31	-0,30	-0,23	0,06	0,15	**0,83**	0,14	-0,33	0,01	0,00
p	-0,66	-0,65	-0,24	0,08	-0,10	0,20	0,44	0,07	-0,61	-0,52
U	0,16	0,22	0,11	0,52	0,48	0,69	0,01	0,02	**0,89**	-0,37
T_{air}	0,17	0,24	-0,20	0,22	-0,51	-0,15	0,51	0,08	**-0,85**	0,47
T_{sea}	-0,32	-0,21	-0,17	0,54	-0,27	-0,63	0,14	0,04	**-0,85**	-0,01
ΔT	0,73	0,74	-0,17	-0,18	-0,48	0,27	0,48	0,07	-0,44	0,69

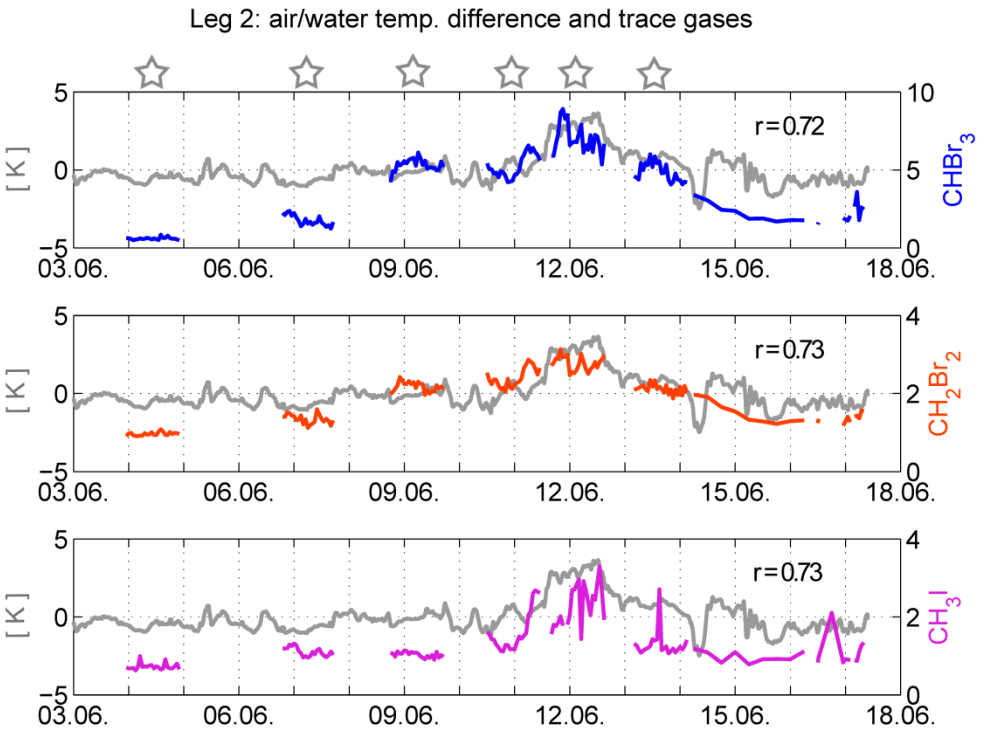

Figure 5-13: Hourly averaged air/water temperature difference from ship measurements (grey line) in comparison with hourly atmospheric mixing ratios of bromoform (blue), dibromomethane (orange) and methyl iodide (pink) in ppt from June 3rd to June 18th 2010.

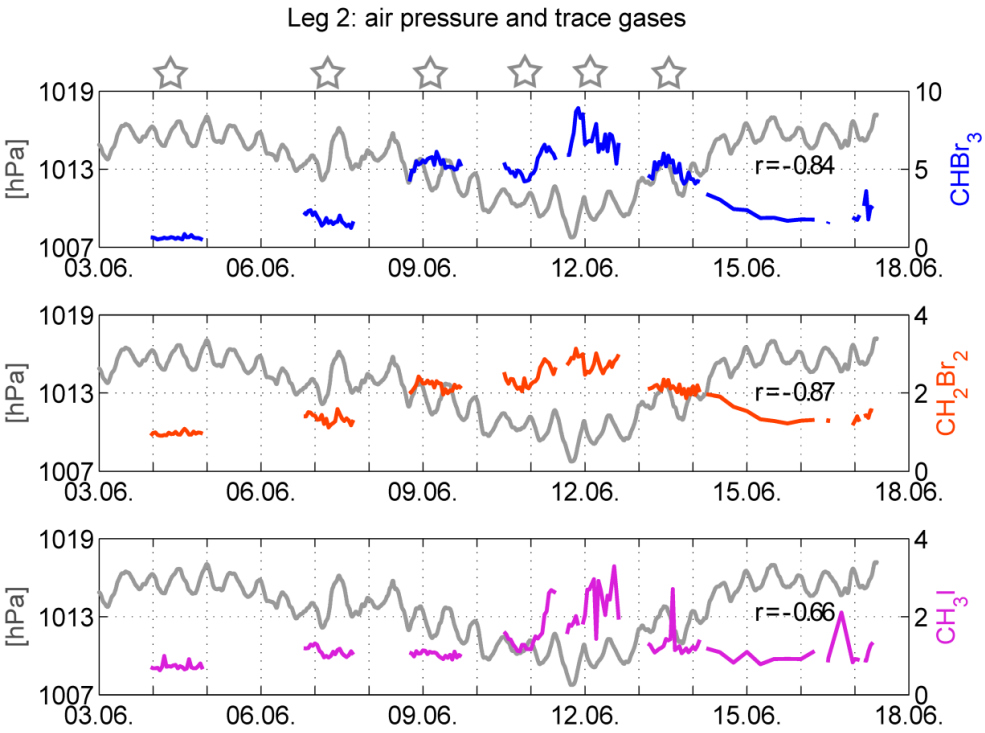

Figure 5-14: As Figure 5-13 for air pressure.

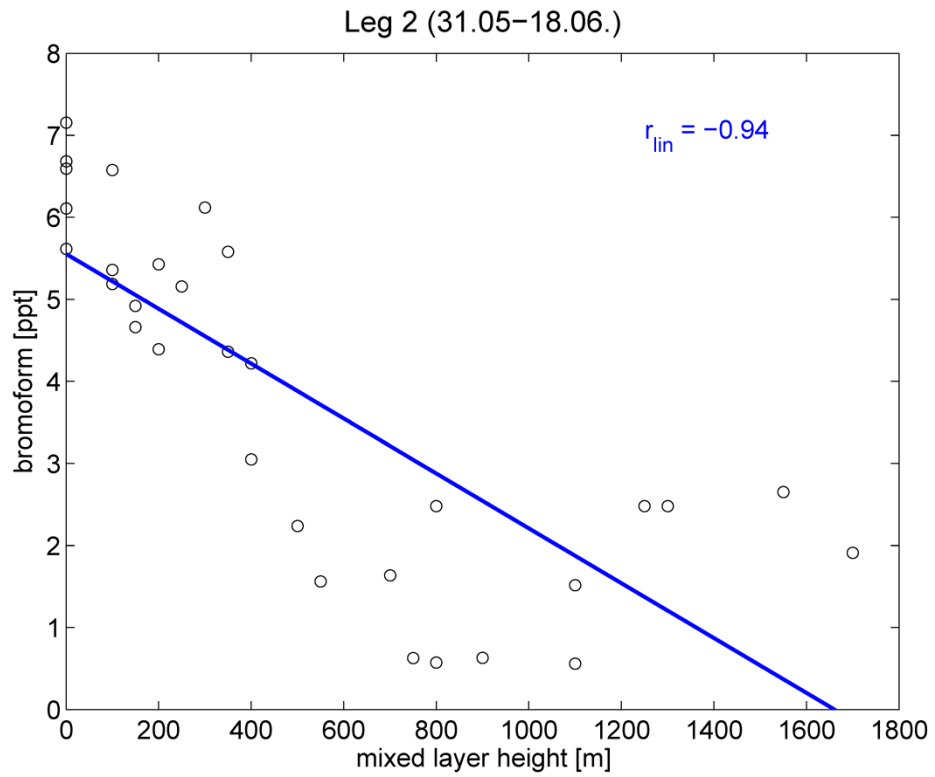

Figure 5-15: Scatterplot of the mixed layer height and in situ bromoform atmospheric mixing ratio during leg 2 (6 hourly at 24 h stations, else 24 hourly). The blue line stands for the linear regression.

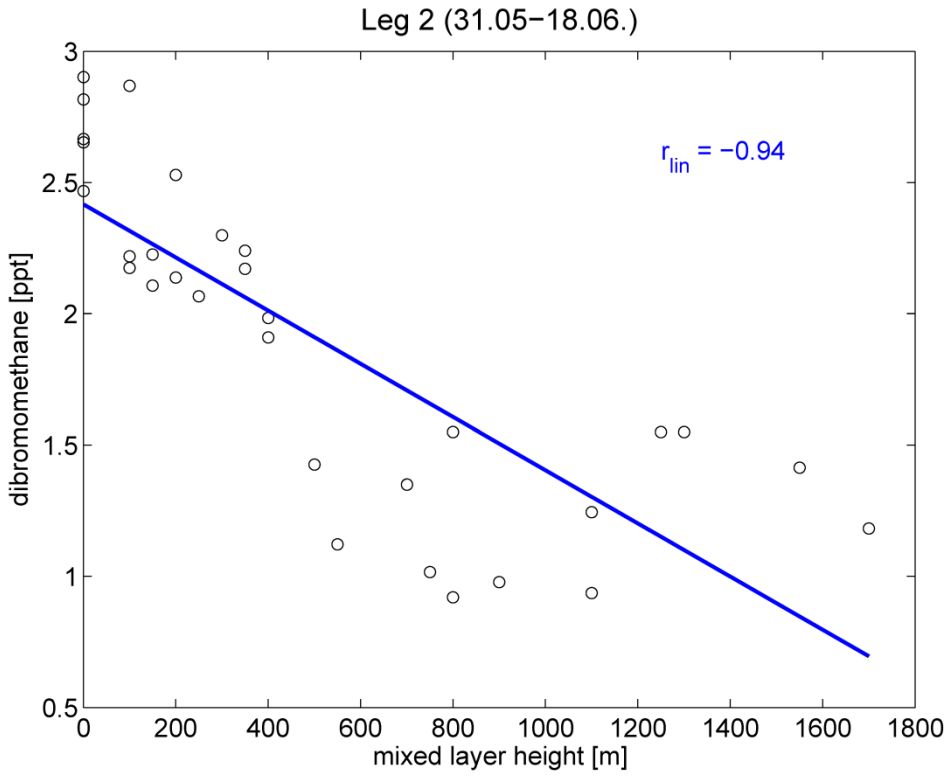

Figure 5-16: As Figure 5-15 for dibromomethane.

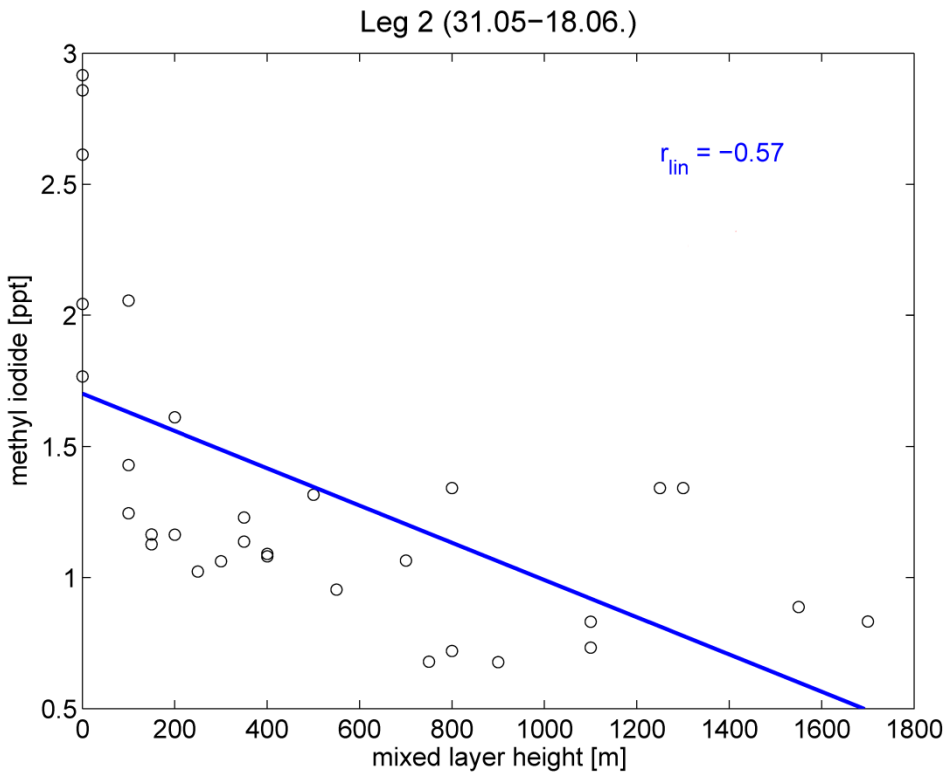

Figure 5-17: As Figure 5-15 for methyl iodide.

Additional correlation coefficients for each 24 h station range from -0.57 to 0.47 and thus showing no significant relation. The comparison of the air pressure and the trace gases is shown in Figure 5-14. The high anti-correlation ($CHBr_3$: r = -0.84, CH_2Br_2: r = -0.87, CH_3I: r = -0.66) is caused by the low pressure system over the African continent as mentioned in section 4.2 which dropped the air pressure at the same time, higher VSLS concentrations were observed. In addition there is no connection between the 24 h station measurements and the air pressure. A comparison of bromoform, dibromomethane and methyl iodide with the mixed layer height is shown in Figure 5-1. Obviously higher VSLS concentrations agree with a lower mixed layer height (MLH) and vice versa. The corresponding correlations with correlation coefficients are shown in Figure 5-15 ($CHBr_3$), Figure 5-16 (CH_2Br_2) and Figure 5-17 (CH_3I), respectively. Highest anti-correlations are found for bromoform (r_{lin} = -0 .94) and dibromomethane (r_{lin} = -0 .94). Although a correlation coefficient of r_{lin} = -0.57 (methyl iodide) is not negligible it is quite less than the coefficients for bromoform and dibromomethane. Methyl iodide does no respond to changes in the mixed layer height, as distinct as it is observable for bromoform and dibromomethane. This might be caused by the different lifetimes and of these VSLS. Figure A-4 shows the comparison of wind speed ship measurements and the trace gases. The correlation coefficients for the trace gases are r = 0.30 ($CHBr_3$), r = 0.34 (CH_2Br_2) and r = 0.29 (CH_3I). The low agreement is also distinguishable from the plot. Therefore it is questionable if local sources are distinct enough to cause the increase of the atmospheric mixing ratios of the trace gases on their own. In general, higher wind speeds should lead to an increase of the air-sea gas exchange, but at the same time leads to an increase of air masses from far away.

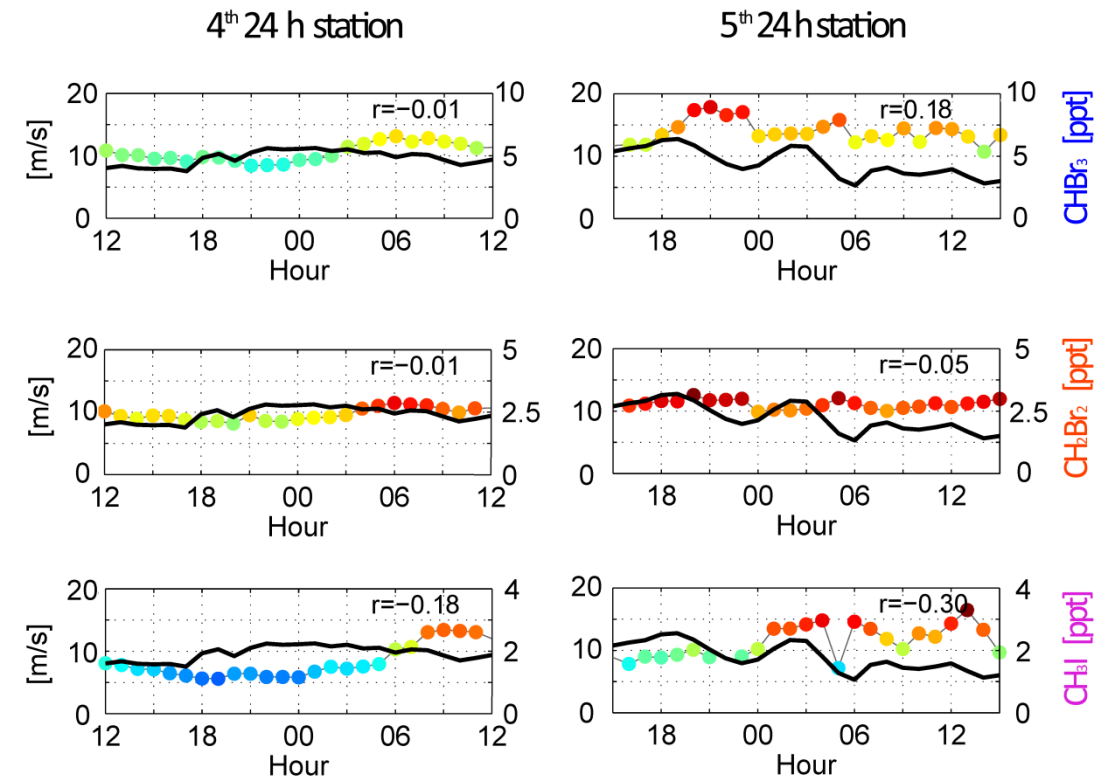

Figure 5-18: Comparison of hourly averaged wind speed measurements (black line) and hourly trace gases (colored dots) during station 4 and 5. The time is given in UTC.

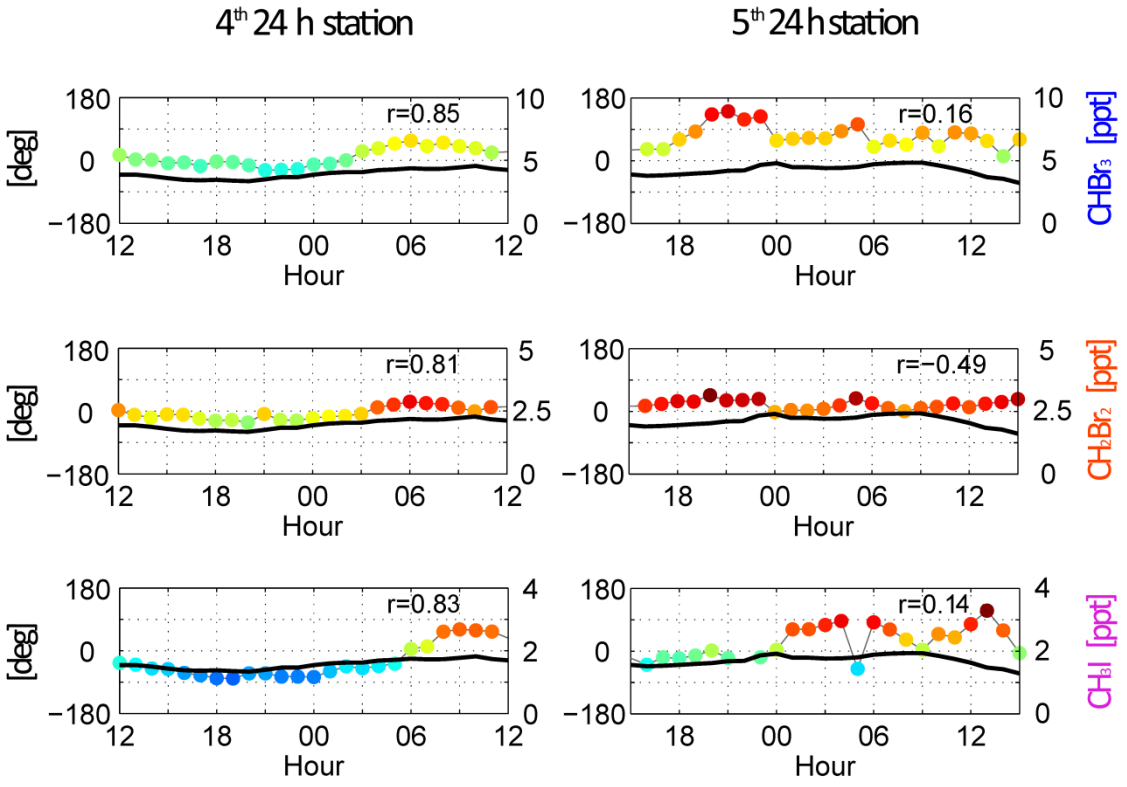

Figure 5-19: As Figure 5-18 for wind direction.

Dividing the 24 h stations into an open ocean cluster and a coastal cluster, results in surprisingly high correlation coefficients of the wind speed for the open ocean cluster ($CHBr_3$: r = 0.88, CH_2Br_2: r = 0.86 and CH_3I: r = 0.84) and no correlations at the coastal station cluster. But taking a closer look to Figure 5-18, especially the comparison of wind speed with the trace gases during station 5, a time lag between wind speed changes and the trace gas concentrations of about 3 hours seem to exist for bromoform and dibromomethane. A separate correlation, regarding the time shift of 3 hours, results in correlation coefficients of r = 0.50 ($CHBr_3$), r = 0.55 (CH_2Br_2) and r = -0.51 (CH_3I). This could also be caused by the low mixed layer height, which suppresses effective vertical mixing.

Due to the regional variability of the trace gases, an overall comparison with the wind direction is meaningless, but as Figure 5-19 shows, the above assumed diurnal variations of the trace gases during the 4th 24 h station are highly correlated to the wind direction (r = 0.85 ($CHBr_3$), r = 0.81 (CH_2Br_2) and r = -0.83 (CH_3I)). With an increasing eastern component of the wind direction, the mixing ratios of bromoform, dibromomethane and methyl iodide increase. In contrast to that, no connection between wind direction and trace gases is distinguishable at the 5th 24 station. This independency seems to result from local sources, which would also explain the high variability of bromoform, dibromomethane and methyl iodide at this station.

5.4. Tracer – Tracer correlations

The scatter plot for the correlation of bromoform and dibromomethane during leg 2 is shown in Figure 5-20. Both trace gases show a nearly exact positive linear correlation with a coefficient of r = 0.97. Due to their same natural marine sources, the high correlation over the open ocean and near coastal regions (Station 4 – 6) is characteristic for these bromocarbons and was also reported by other authors (e. g. Yokouchi et al., 1997; Quack et al., 2007) for atmospheric mixing ratios. The correlation of bromoform and methyl iodide is further shown in Figure 5-21. The blue line is the linear regression with a correlation coefficient of r_{lin} = 0.69. The distribution of the scatter points resembles a quadratic behavior. For this reason a quadratic regression is calculated and illustrated by the red line. With a correlation of r_{qua} = 0.71, both coefficients are yet quite similar. The same procedure is done for dibromomethane and methyl iodide (Figure 5-22). The linear regression results in a correlation coefficient of r_{lin} = 0.73 (blue line) and the quadratic regression in r_{quq} = 0.77 (red line). Although the similar correlations of bromoform / dibromomethane with methyl iodide are not surprising due to the high correlation of bromoform and dibromomethane themselves, such high correlation for bromocarbons and iodocarbons are very unusual. Yokouchi et al. (1997) could not distinguish any correlation between both halocarbons as well as Palmer (2010), who reports a correlation coefficient of determination between bromoform and methyl iodide of $r^2 \approx 0$. For leg 2 the correlation coefficient of determination is $r^2 \approx 0.5$ for bromoform ($r^2 \approx 0.6$ for dibromomethane), showing that only 50 – 60 % of the methyl iodide variations are explained by the (slightly better fitting) quadratic regression.

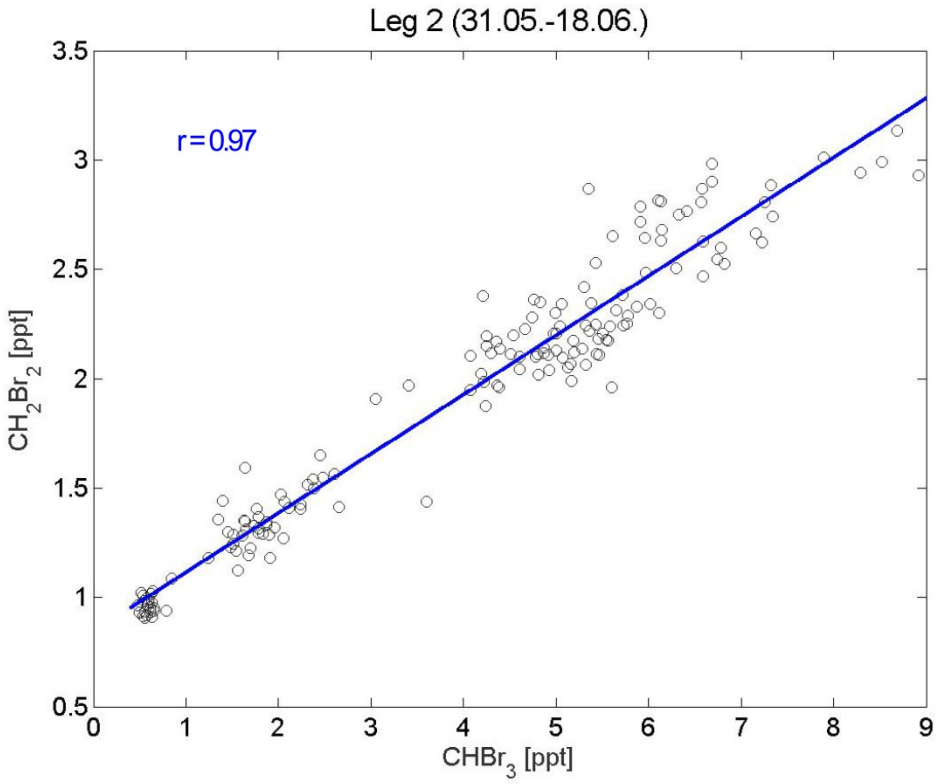

Figure 5-20: Scatterplot of bromoform and dibromomethane atmospheric mixing ratios during leg 2 (6 hourly at 24 h stations, else 6 hourly).

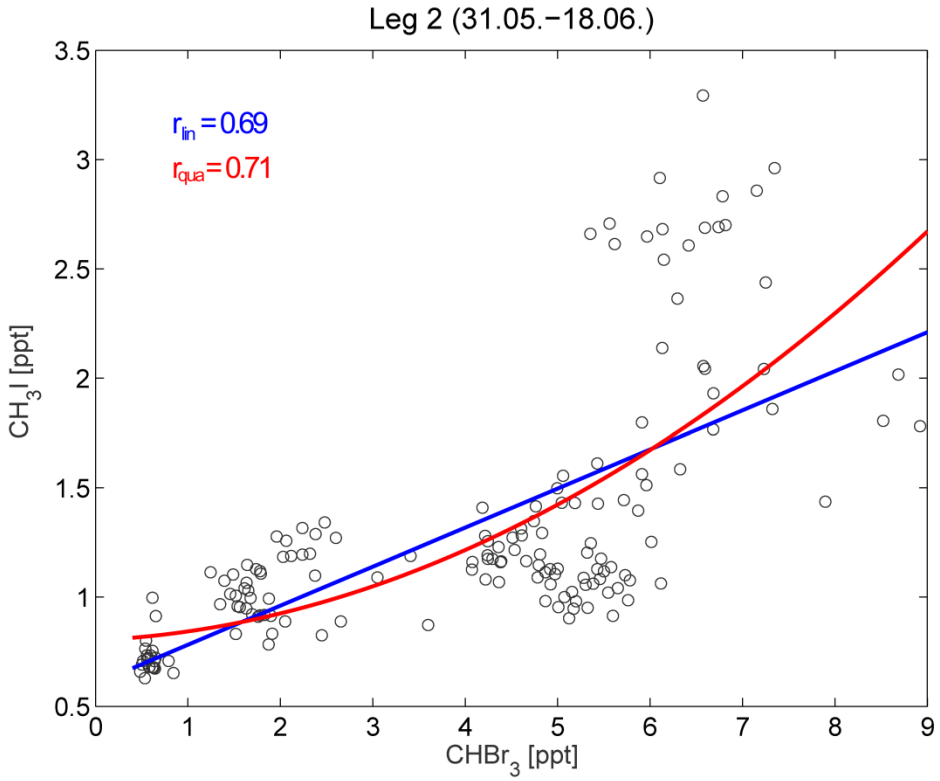

Figure 5-21: Scatterplot of bromoform and methyl iodide atmospheric mixing ratios during leg 2. The blue line stands for the linear and the red line for the quadratic regression.

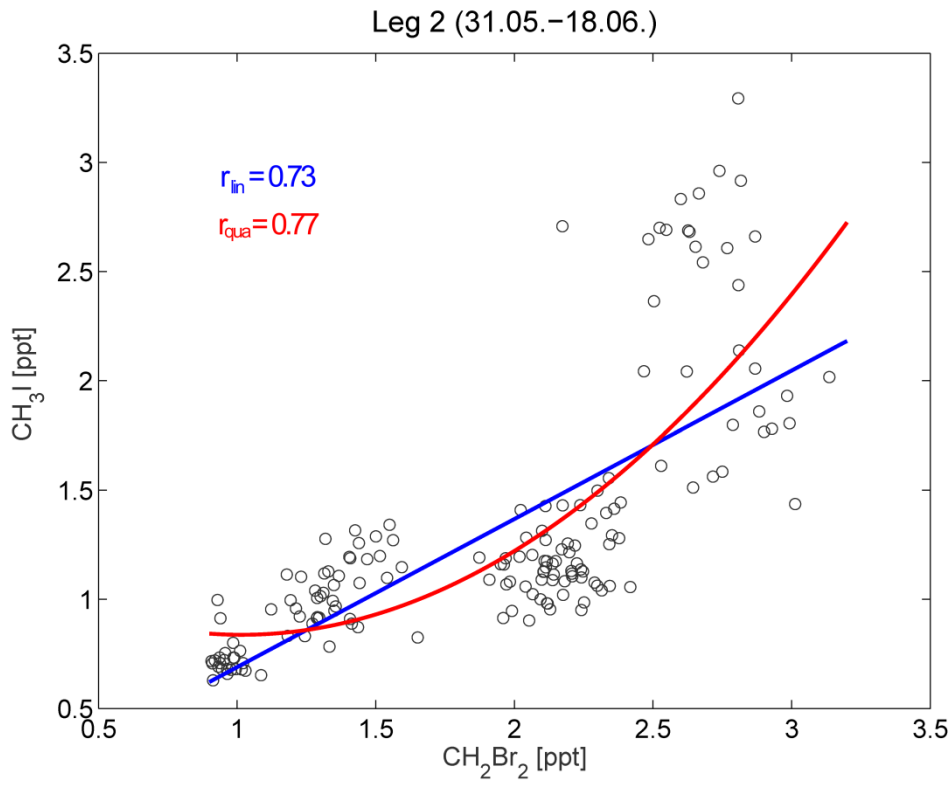

Figure 5-22: As Figure 5-21 for dibromomethane and methyl iodide.

5.5. Discussion

Given the complexity of physical and chemical processes playing a role during the DRIVE campaign it is rather difficult to access the main variability of the atmospheric VSLS. Observations at the first two stations close to Cape Verde reflect the expected open ocean VSLS mixing ratios of ~ 1 ppt. O'Brien et al. (2009) measured mixing ratios of bromoform, ranging from 2.0 – 43.7 ppt, dibromomethane (0.7 – 8.8 ppt) and methyl iodide (0.5 – 31.4 ppt) at the Cape Verde Observatory from May 30 to June 15 2007, which are up to 10 times higher as our detected values. A comparison of the backward trajectories of both campaigns at and respectively close to Cape Verde shows the different origins of the air masses at this region. The lower mixing ratios observed by O'Brien et al. (2009) coincide with northerly trajectories coming from the open ocean, in good agreement with our analysis of stations 1 and 2, whereas the highest values origin from the Mauritanian upwelling. A comparison with the P320/1 ship campaign during March/April 2005 (Quack et al., 2007) reveals similar mean mixing ratios for bromoform (near station 3: P320: *5.8 ppt*, P399: *5.3 ppt*; near stations 4/5: P320: *7.7 ppt*, P399: *5.3 ppt – 7 ppt*; near station 6: P320: *3.7 ppt*, P399: *4.85 ppt*) and dibromomethane (near station 3: P320: *2.3 ppt*, P399: *2.17 ppt*; near station 4/5: *2.6 ppt*, P399: *2.4 ppt – 2.8 ppt*; near station 6: P320: *2.0 ppt*, P399: *2.1 ppt*). Although this earlier campaign took place at the beginning of spring and the DRIVE campaign operated at the end of spring, the observed atmospheric mixing ratios agree very well. Comparing the $CH_2Br_2/CHBr_3$ ratio of both campaigns reveals similar bromocarbon ratios as well (near station 3: P320: *0.40*, P399: *0.41*; near station 4/5: P320: *0.35*, P399: *0.40 – 0.46*; near station 6: P320: *0.54*, P399: *0.44*). Given the

similar meteorology during the P320 campaign (e. g. mean wind direction: northerly winds (5°), mean wind speed: 9.3 m/s) compared to the P399 cruise the good overall agreement of the VSLS observations may not be surprising.

A better insight of potential sources and source regions in the area of the Mauritanian upwelling can be obtained at the coastal stations. At the 3rd 24 h station increased mean mixing ratios of bromoform (5.3 ppt) and dibromomethane (2.2 ppt) contrast a constant low mean methyl iodide mixing ratio (1.0 ppt). The trajectory analysis revealed air masses originating over the Canary Islands and over observed upwelling water during the previous 2 days. Consequently with regard to the mean ratio of $CH_2Br_2/CHBr_3$ = 0.41 the brominated halocarbons must have a biological source at this station in contrast to methyl iodide, probably causing these different mixing ratios. For station 4 the diurnal variations of the observed mixing ratios is striking, highly correlated with an eastward shift of the wind direction (sea breeze) leading to air mass origin from the Banc d'Arguin. The increase of the mixing ratios of bromoform and dibromomethane is denoted about 4 h before sunrise. In contrast, the methyl iodide mixing ratios directly increase after sunrise, suggesting a photochemical reaction triggered by the sunlight, which is however highly speculative. Although the increase of methyl iodide coincides with the sunrise, it does not explain the decrease of the mixing ratios in the following hours and the variability at other 24 h stations. In addition, the mixed layer height decreases during this fourth 24 h station and might therefore influence the increase of the bromoform, dibromomethane and methyl iodide mixing ratios as well. In contrast to that these mixing ratios decrease in the last hours of the fourth 24 h station, coinciding with a decreasing mixed layer height, indicating sources beneath. During the 5th 24 h station local sources must have caused the high variations in the mixing ratios due to a very low constant mixed layer height. The corresponding trajectories (Figure 5-11) and especially those in the zoom over the Banc d'Arguin, all indicate influence of these coastal shallow waters, but also continental influence, as they pass the coast of Western Sahara and Mauritania. The increase of the correlation coefficients of wind speed and VSLS by adjusting for the observed time lag of 3 hours to r = 0.50 ($CHBr_3$), r = 0.55 (CH_2Br_2) and r = -0.51 (CH_3I) further approves the assumption of local sources. An increase of the wind speed may have increased the air-sea gas exchange which may cause the increased mixing ratios after the time lag at decreasing wind speed. The 6th 24 station shows a similar pattern as the 3rd station. Mixed layer height (100 m – 200 m, Figure 5-1), mean atmospheric mixing ratios (4.85 ppt ($CHBr_3$), 2.11 ppt (CH_2Br_2) and 1.28 ppt (CH_3I)) and trajectories show nearly the same behavior. The air masses, which show no influence of the Banc d'Arguin anymore, as seen in the trajectory pathways, show similar VSLS mixing ratios as station 3.

The sources for the bromocarbons can be related to air masses originated at the west coast of Mauritania and Western Sahara, which can't be distinguished from each other, while the source for methyl iodide seems to be connected to air masses originated at the Banc d'Arguin, but, according to the trajectories also over land. Williams et al. (2007) already reported unexpected coincidental correlations between Saharan dust input and emission of methyl iodide in the North East Atlantic. Due to the earlier mentioned wind direction bias of about 20 degrees between model and ship measurements, Saharan dust input, as pointed out by the trajectories seems not to influence the methyl iodide concentrations in our case and was not observed by the scientific crew either. The increase of the methyl iodide mixing ratios could therefore be connected to increased methyl iodide emission from seawater at the area of the Banc d'Arguin.

Distinguishing a meteorological parameter, which mainly influences the atmospheric mixing ratios, the mixed layer height seems to have the strongest relation to the observed VSLS mixing ratio. Less available volume of air for mixing, leads to an increase of volume mixing ratios for constant sources. This is reflected by the high anti-correlations (Table 3, Table 4, Table 5) between the mixed layer height and the VSLS. Note however, that for this correlation calculation 6 hourly VSLS mixing ratios had to be compared with the 6 hourly mixed layer height values. A higher temporal resolution of the mixed layer height would gain an increased insight in this relation and may change this highly significant result. However parameters as air/water temperature difference, wind speed and wind direction have an influence on the mixed layer height itself and thus they are not independent from each other. In addition the strength of a VSLS source itself is also very important. The maximum bromoform mixing ratio (~ 10 ppt) was observed close to Lisbon with a corresponding mixed layer height of about 500 m (not shown) in contrast to less mixing ratios at lower mixed layer heights. A consideration of the local conditions (strength of the sources) is therefore also important as shown by the Rio Tejo.

6. Conclusion

This thesis investigates the variability of VSLS mixing ratios during the DRIVE campaign in the tropical East Atlantic during end of spring 2010. The focus lies on three very short lived halocarbons, which contribute to ozone depletion in the troposphere and stratosphere, in particular their regional and diurnal variability. Measurements of air and water temperature, humidity, wind speed, - direction and air pressure have been taken by the ship. In addition regular air samples and radiosonde launches complemented the investigations.

The cruise was mainly exposed to moderate weather with mean wind speeds of 4 – 5 Bft and a mean wind direction of NNW, in contrast to the climatological trade wind regime with winds from the north-east. Consequently continental influence, for example Saharan dust input, is not identifiable and was also not observed on board. The changeover between tropical and extra-tropical air masses is indicated by the radiosonde profiles at the beginning of leg 3 at about 30° N. The radiosonde measurements are further used for the determination of the mixed layer height, which varies from the ground to about 1700 m, depending on the location. The lowest mixed layer height is observed at the Mauritanian upwelling, coinciding with a decrease of the water temperature. The cold water creates negative sensible heat fluxes, resulting in stable stratification of the lower atmosphere and thus a decrease of the mixed layer height.

An increase of the atmospheric VSLS mixing ratios (bromoform: 0.48 – 8.9 ppt; dibromomethane: 0.91 – 3.14 ppt; methyl iodide: 0.63 – 3.29 ppt) is found close to the West African coast, at the area of the Mauritanian upwelling with high expected biological productivity, coinciding with an increase of the VSLS concentrations in the water (not investigated in this study). The observed mean mixing ratios of bromoform (5.6 ppt) and dibromomethane (2.37 ppt), as well as the ratio of these bromocarbons (0.43), confirm recent observations by Quack et al. (2007) during spring 2005 in this region. In comparison to that study, an even higher correlation between both bromocarbons of 0.97 is found. Surprisingly high correlations between the brominated carbons, and methyl iodide ($r = 0.69$ for bromoform and $r = 0.74$ for dibromomethane) are observed in contrast to earlier studies (Yokouchi et al., 1997; Palmer, 2010). For the evaluation of the atmospheric mixing ratios, the three VSLS are compared and correlated with the mixed layer height. All three VSLS show high anti-correlations ($CHBr_3$: $r = -0.90$, CH_2Br_2: $r = -0.90$, CH_3I: $r = -0.63$) for the whole campaign. Highest mean mixing ratios ($CHBr_3$: 7 ppt, CH_2Br_2: 2.8 ppt, CH_3I: 2.3 ppt) coincide with the lowest mixed layer height (ground level) at the 5th 24 h station.

For the investigation of air mass origin, HYSPLIT is used to calculate 2 – 13 day backward trajectories using NCEP/NCAR Reanalysis Project 1 assimilation data. To evaluate these trajectories, ship measurements of wind speed and direction are compared with ERA-Interim and NCEP/NCAR Reanalysis Project 1 meteorological assimilations. The corresponding correlation coefficients for 6-hourly surface wind speed averages are $r = 0.95$ (ERA-Interim) and $r = 0.86$ (NNRP-1) and for wind direction $r = 0.94$ (ERA-Interim) and $r = 0.88$ (NNRP-1), indicate a good agreement between assimilation models and ship measurements, although the radiosoundings were not delivered to the WMO global data net. The trajectories indicated predominantly air masses originated over the North Atlantic. For the first two 24 h stations the

mean ratios of the dibromomethane and bromoform mixing ratio (1st station: 1.63, 2nd station: 0.78) indicate open ocean air masses, which are also reflected by the trajectories. An increase of the mean atmospheric mixing ratios of the bromocarbons (3rd station: bromoform: 5.32 ppt, dibromomethane: 2.17 ppt) is observed as the ship and trajectories approach the West African coast, coinciding with a decrease of the mixed layer height. A high correlation between the wind direction and the VSLS mixing ratios (> 0.8) is found for station 4. The eastern shift of the trajectories over the Banc d'Arguin National Park may pass potential source regions. At the 5th 24 h station local sources could have contributed to the high mean mixing ratios and the strong variability of the VSLS ($CHBr_3$: 5.4 – 8.9 ppt, CH_2Br_2: 2.5 – 3.14 ppt, CH_3I: 1.4 – 3.9 ppt). A correlation of the wind speed and the mixing ratios, regarding a time lag of three hours resulted in correlation coefficients of r = 0.50 ($CHBr_3$), r = 0.55 (CH_2Br_2) and r = -0.51 (CH_3I). The 6th 24 h station again revealed similar results, as the 3rd station for mixing ratios and trajectories. According to the trajectories with regard to the wind direction bias, the methyl iodide mixing ratios seems to be related to air masses origin from the coastal areas of Western Sahara and Mauritania as well as the Banc d'Arguin.

Finally the variability of the VSLS mixing ratios over the Mauritanian upwelling seems to be predominantly influenced by changes in the mixed layer height. In contrast to earlier studies, which always indicate an increase of VSLS mixing ratios by a changes in the wind direction and therefore a change in source region for the air masses, this study reveals a strong influence of the mixed layer height on the VSLS mixing ratios. The mixed layer height, which is lower in upwelling areas due to a stable boundary layer (Smedman et al., 1997), might be the main reason for the increase in the atmospheric mixing ratios from ocean emitted VSLS species derived during drive. Increases in sources or strong source regions are not necessarily the only cause for the atmospheric mixing ratios increase as suggested earlier by Quack et al. (2004, 2007).

List of Figures

List of Tables

A. Appendix

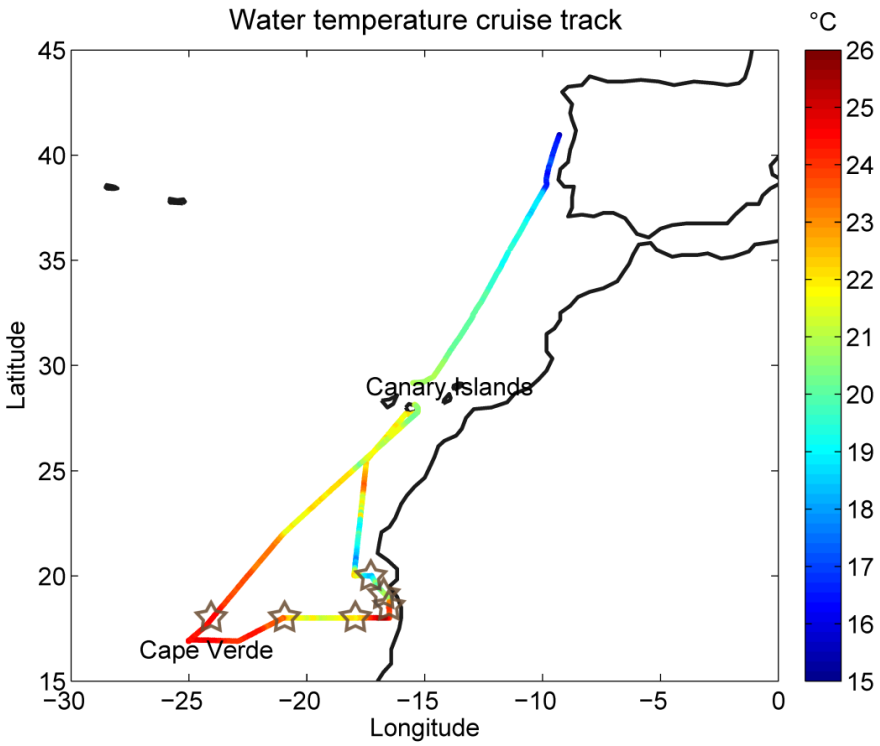

Figure A-1: Cruise track of water temperature measured on POSEIDON during the DRIVE campaign 2010. The stars indicate 24 h stations.

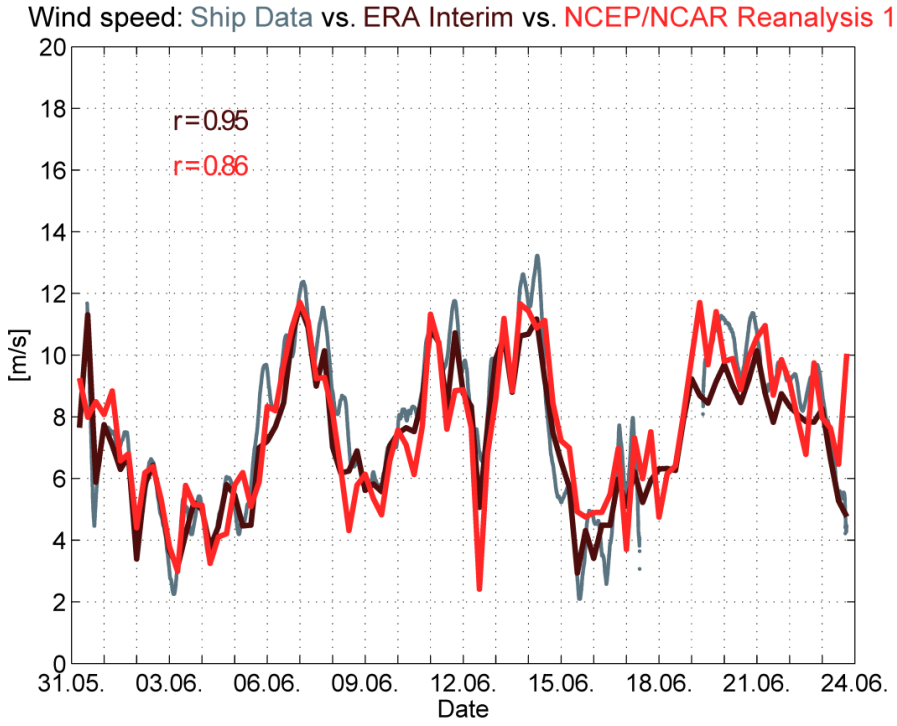

Figure A-2: As Figure 4-17 for 6 hourly averaged ship measurements.

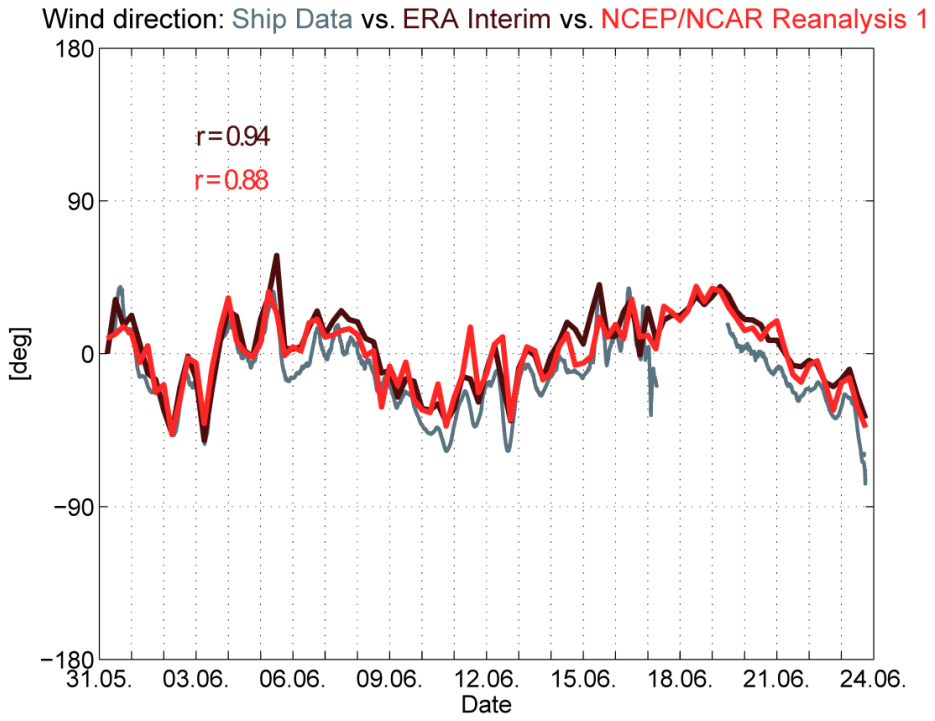

Figure A-3: As Figure 4-18 for 6 hourly averaged ship measurements.

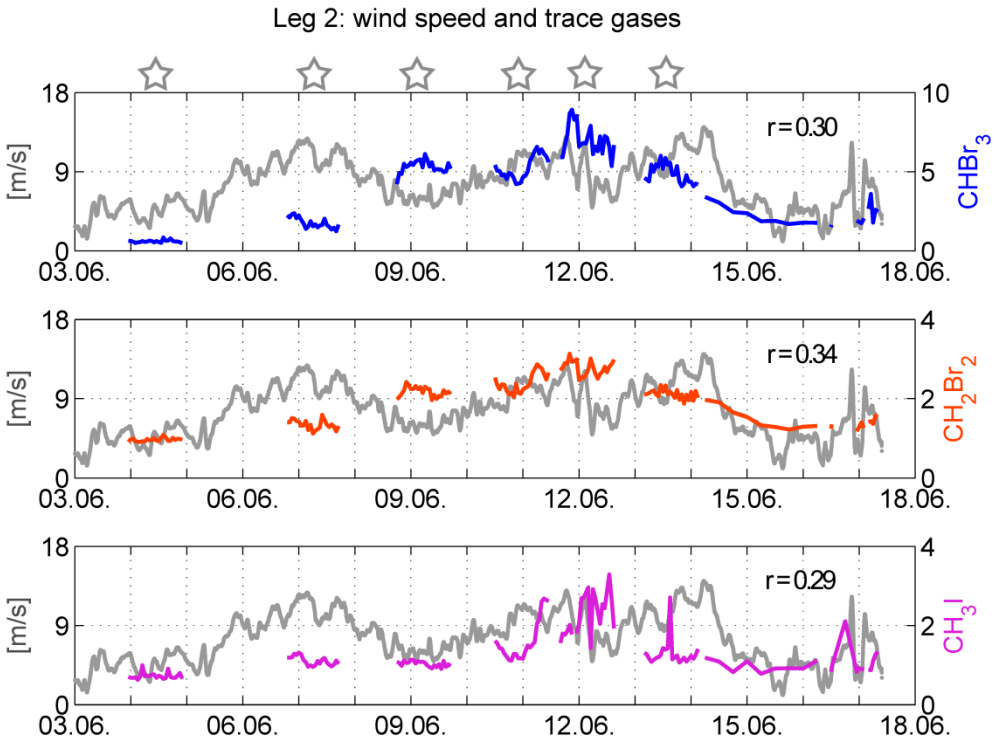

Figure A-4: As Figure 5-13 for wind speed.

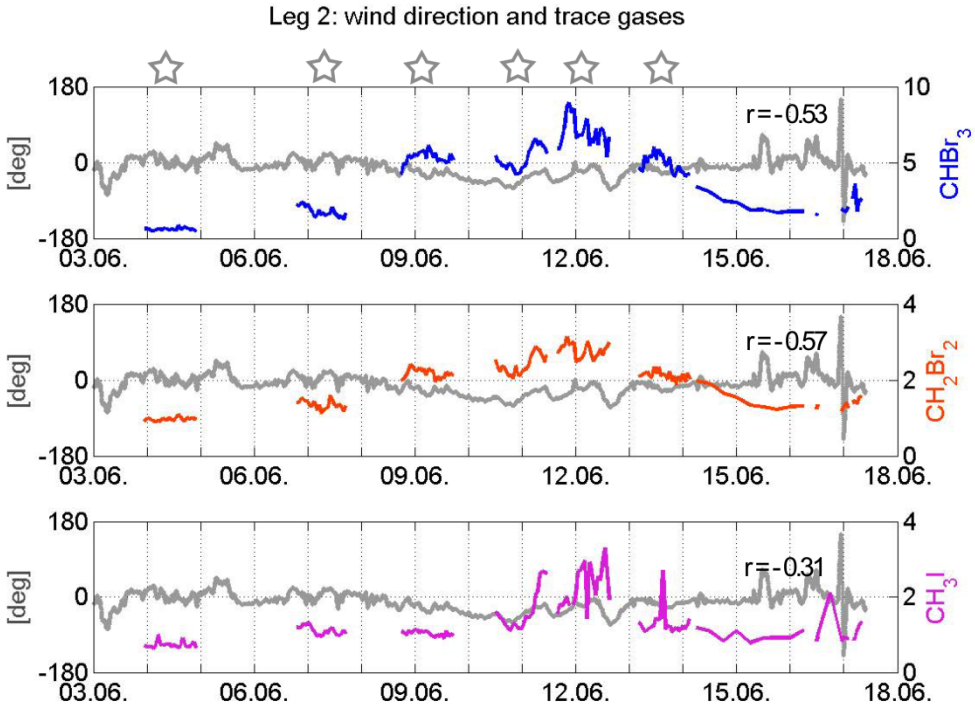

Figure A-5: As Figure 5-13 for wind direction

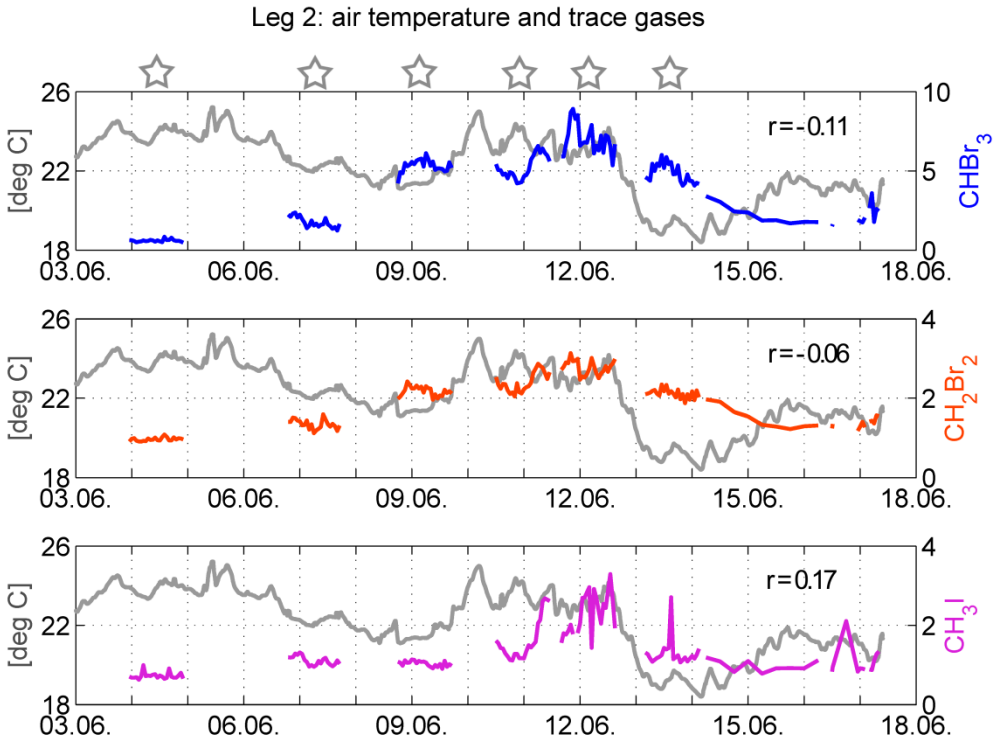

Figure A-6: As Figure 5-13 for air temperature.

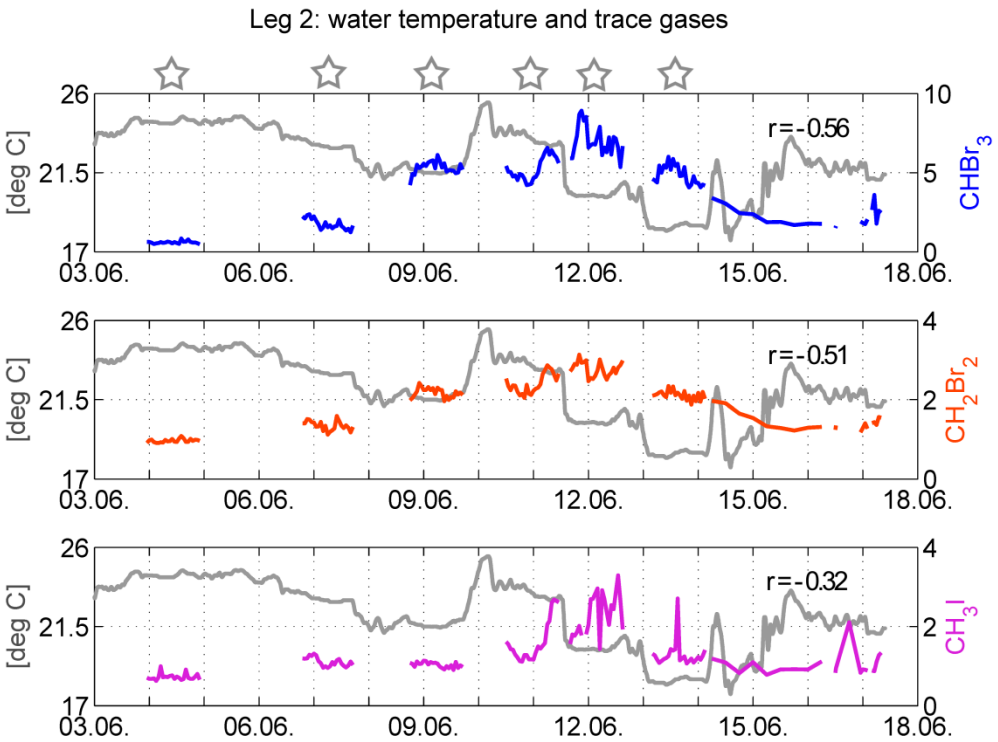

Figure A-7: As Figure 5-13 for water temperature.

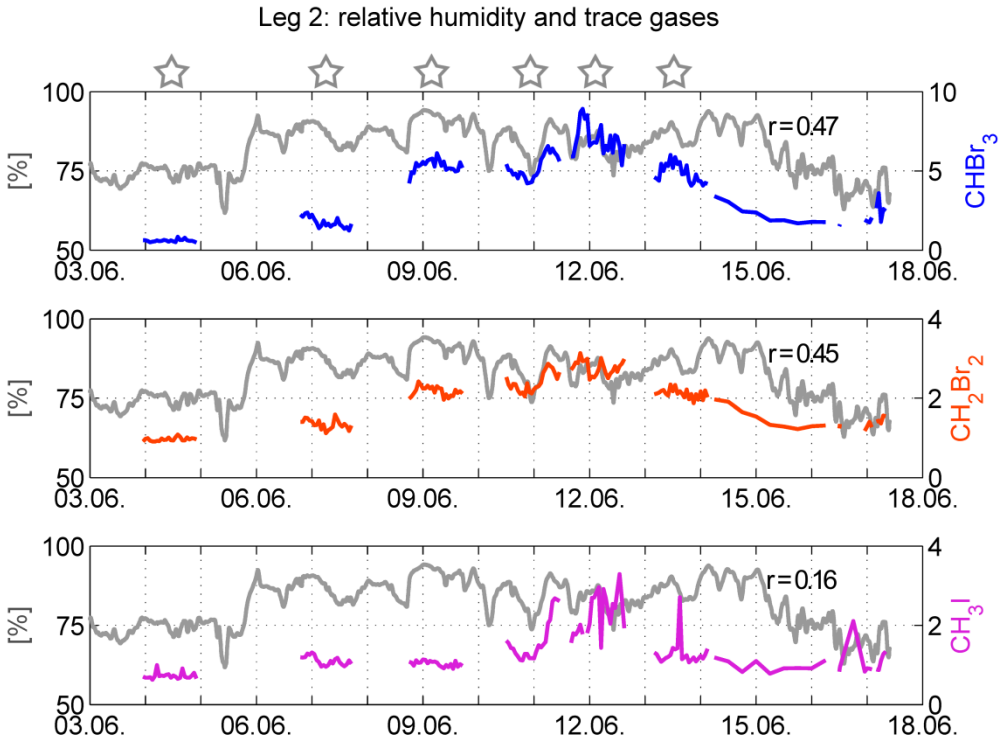

Figure A-8: As Figure 5-13 for relative humidity.

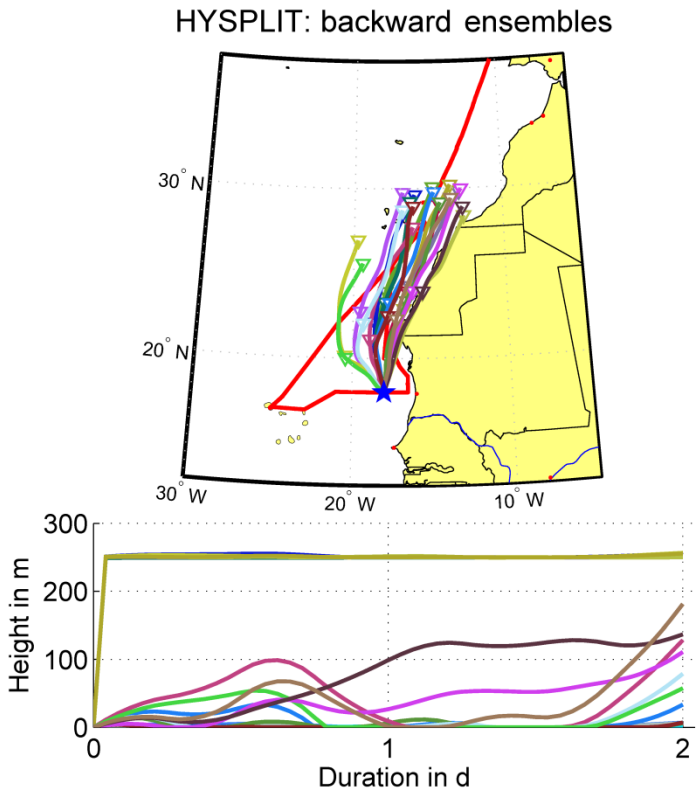

Figure A-9: 2 day HYSPLIT backward trajectory ensembles at the 3rd 24 h station on 09.06.2010 06 UTC.

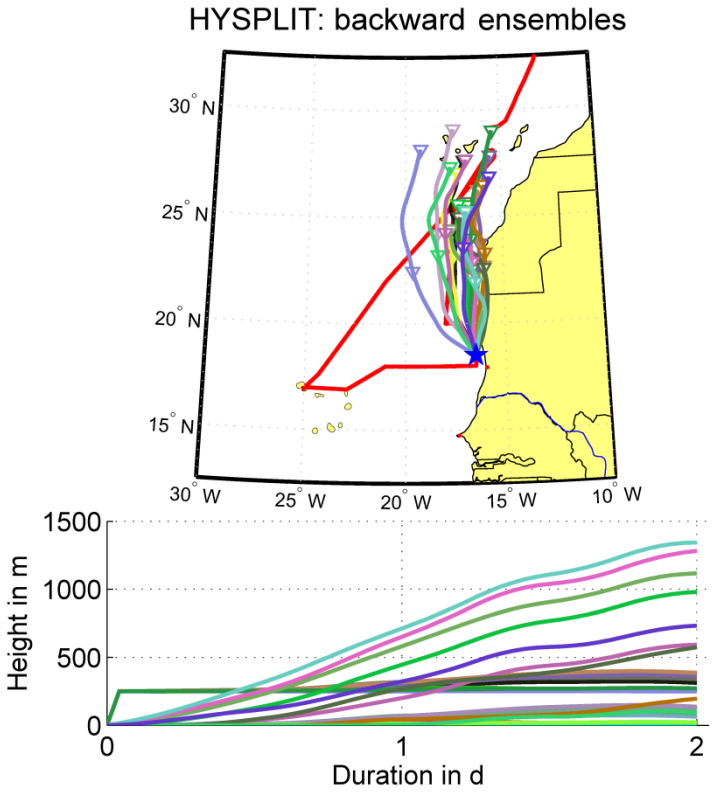

Figure A-10: As Figure A-9 at the 4th 24 h station on 11.06.2010 00 UTC.

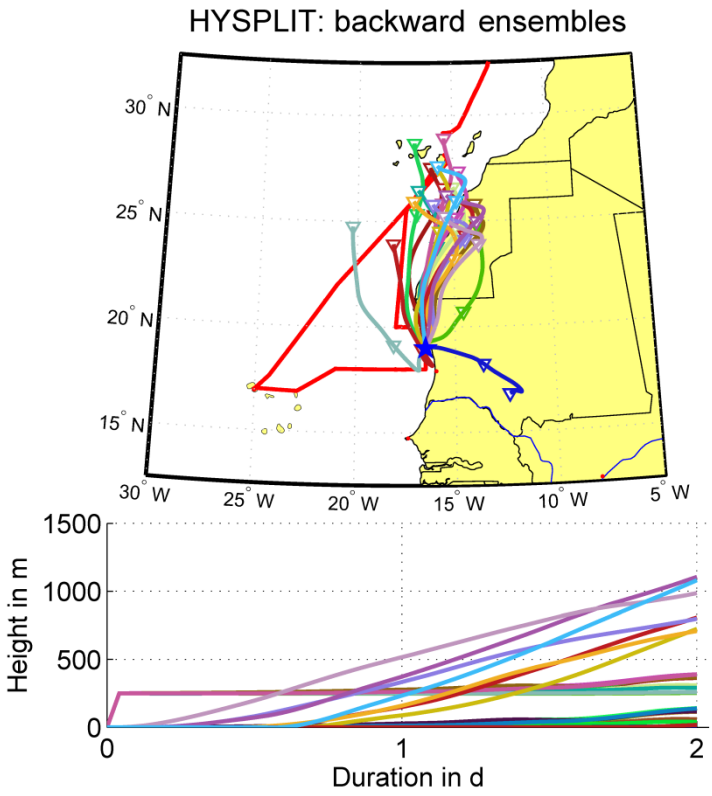

Figure A-11: As Figure A-9 at the 5th 24 h station on 12.06.2010 00 UTC.

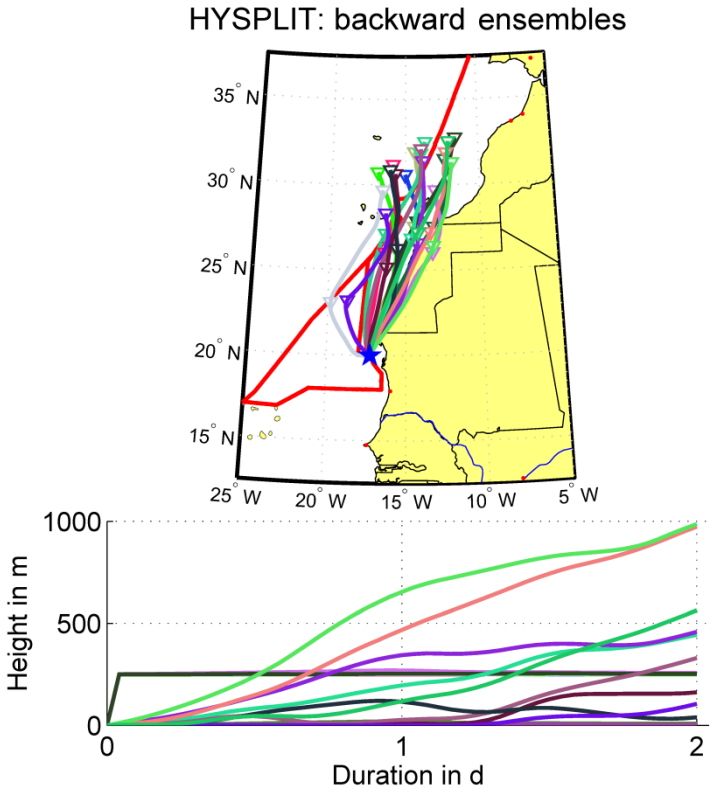

Figure A-12: As Figure A-9 at the 6th 24 h station on 13.06.2010 15 UTC.

Table 6: As Table 3 for mixed layer height.

MLH	Leg 2	Leg 2+3	Station 1	Station 2	Station 3	Station 4	Station 5	Station 6	Open ocean	Coast
$CHBr_3$	**-0,94**	**-0,90**	-0,35	-0,68	-0,66	-0,61	/	**-0,70**	**-0,82**	**-0,75**
CH_2Br_2	**-0,94**	**-0,91**	**0,77**	0,32	-0,49	**-0,72**	/	-0,53	-0,69	**-0,80**
CH_3I	-0,57	-0,63	-0,61	-0,46	**0,77**	**-0,90**	/	-0,40	**-0,83**	**-0,79**
w_{spd}	-0,55	-0,47	-0,29	-0,23	**0,94**	-0,38	/	0,25	**-0,80**	-0,25
w_{dir}	0,58	0,56	-0,19	-0,02	0,35	-0,46	/	0,46	-0,11	0,07
p	0,77	**0,76**	**0,93**	**0,91**	-0,38	0,13	/	0,36	**0,80**	0,65
u	-0,68	**-0,70**	-0,47	**-0,96**	-0,17	-0,27	/	0,51	**-0,76**	0,63
T_{air}	0,01	-0,08	0,21	-0,06	**-0,86**	-0,47	/	-0,60	0,52	-0,50
T_{sea}	0,40	0,25	-0,02	-0,69	-0,01	**0,78**	/	0,09	0,64	0,04
ΔT	-0,63	-0,60	0,26	0,81	**-0,95**	**-0,75**	/	**-0,73**	0,06	**-0,76**

Bibliography

Anderson, J. G., Brune, W. H., & Proffitt, M. H. (1989). *Ozone Destruction by Chlorine Radicals Within the Antarctic Vortex: The Spatial and Temporal Evolution of ClO–O3 Anticorrelation Based on in Situ ER-2 Data.* JOURNAL OF GEOPHYSICAL RESEARCH, VOL. 94, NO. D9. doi:10.1029/JD094iD09p11465

Barrie, L. A., Bottenheim, R. C., Crutzen, P. J., & Rasmussen, R. A. (1988). *Ozone destruction and the chemical reactions at polar sunrise in the lower Arctic atmosphere.* Nature.

Bell, N., Hsu, L., Jacob, D. J., Schultz, M. G., Blake, D. R., Butler, J. H., et al. (2002). *Methyl iodide: Atmospheric budget and use as a tracer of marine convection in global models.* Journal of Geophysical Research, Vol. 107, No. D17. doi:10.1029/2001JD001151

Blake, N. J., Blake, D. R., Swanson, A. L., Atlas, E., Flocke, F., & Rowland, F. S. (2003). *Latitudinal, vertical, and seasonal variations of C1-C4 alkyl nitrates in the troposphere over the Pacific Ocean during PEM-Tropics A and B: Oceanic and continental sources.* JOURNAL OF GEOPHYSICAL RESEARCH, VOL. 108, NO. D2. doi:10.1029/2001JD001444

Carpenter, L. J., & Liss, P. S. (2000). *On temperate sources of bromoform and other reactive organic bromine gases.* JOURNAL OF GEOPHYSICAL RESEARCH, VOL. 105, NO. D16.

Carpenter, L. J., Liss, P. S., & Penkett , S. A. (2003). *Marine organohalogens in the atmosphere over the Atlantic and Southern Oceans.* J. Geophys. Res., 108(D9). doi:10.1029/2002JD002769

Davis, D., Crawford, J., Liu, S., McKeen, S., Bandy, A., Thornton, D., et al. (1996). *Potential impact of iodine on tropospheric levels of ozone and other critical oxidants.* JOURNAL OF GEOPHYSICAL RESEARCH, VOL. 101, NO. D1.

Dee, D. P., Uppala, S. M., Simmons, A. J., Berrisford, P., Poli, P., Kobayashi, S., et al. (2011). *The ERA-Interim reanalysis: configuration and performance of the data assimilation system.* Quarterly Journal of the Royal Meteorological Society. doi:10.1002/qj.828

DeMore, W. B., Sander, S. P., Golden, D. M., Hampson, R. F., Kurylo, M. J., Howard, C. J., et al. (1997). *Chemical Kinetics and Photochemical Data for Use in Stratospheric Modelling.* Evaluation number 12. JPL Publ.

Draxler, R. R., & Hess, G. D. (2004). *Description of the HYSPLIT 4 modelling system.* NOAA Technical Memorandum.

Dvortsov, V. L., Geller, M. A., Solomon, S., Schauffler, S. M., Atlas, E. L., & Blake, D. R. (1999). *Rethinking reactive halogen budgets in the midlatitude lower stratosphere.* (V. 2. GEOPHYSICAL RESEARCH LETTERS, Ed.) doi:10.1029/1999GL900309

Etling, D. (2008). *Theoretische Meteorologie.* Berlin: Springer-Verlag.

Field, R. A., Goldstone, M. E., Lester, J. N., & Perry, R. (1992). *The sources and behaviour of tropospheric anthropogenic volatile hydrocarbons.* Atmospheric Environment. Part A. General Topics. doi:10.1016/0960-1686(92)90290-2

Fogelqvist, E. (1985). *CARBON TETRACHLORIDE. TETRACHLOROETHYLENE, 1,1,1-TRICHLOROETHANE AND BROMOFORM IN ARCTIC SEAWATER.* JOURNAL OF GEOPHYSICAL RESEARCH, VOL. 90, NO. C5. doi:10.1029/JC090iC05p09181

Greenberg, J. P., & Zimmermann, P. R. (1984). *Nonmethane Hydrocarbons in Remote Tropical, Continental, and Marine Atmospheres.* JOURNAL OF GEOPHYSICAL RESEARCH, VOL. 89, NO. D3.

Hagen, E. (2000). *Northwest African upwelling scenario.* Baltic Sea Research Institute. Warnemuende: Oceanologica Acta, Vol. 24.

Highwood, E. J., & Hoskins, B. J. (1998). *The tropical tropopause.* Quart. J. Roy. Meteor. Soc.

Kalnay, E., Kanamitsu, M., Kistler, R., Collins, W., Deaven, D., Gandin, L., et al. (1996). *The NCEP/NCAR 40-year reanalysis project.* Bulletin of the American Meteorological Society. doi:10.1175/1520-0477(1996)077<0437:TNYRP>2.0.CO;2

Kistler, R., Kalnay, E., Collins, W., Saha, S., White, G., & Woollen, J. (2001). *The NCEP-NCAR 50-year reanalysis: Monthly means CD-ROM and documentation.*

Klose, B. (2008). *Meteorologie: Eine interdisziplinäre Einführung in die Physik der Atmosphäre.* Springer-Verlag.

Kraus, H. (2000). *Die Atmosphäre der Erde: Eine Einführung in die Meteorologie.* Springer-Verlag.

Kurylo, M. J., Rodriguez, J. M., Andrea, M. O., Atlas, E. L., Blake, D. R., Butler, J. H., et al. (1999). *Chapter 2: Short-lived ozone-related compounds in Scientific Assessment of Ozone Depletion, 1998 edited by C. A. Ennis.* Geneva: Word Meteorological Organization.

Labitzke, K. G. (1999). *The stratosphere: phenomena, history, and relevance.* Berlin: Springer-Verlag.

Leser, H., Hönninger, G., & Platt, U. (2003). *MAX-DOAS measurements of BrO and NO2 in the marine boundary layer.* GEOPHYSICAL RESEARCH LETTERS, VOL. 30, 1537. doi:10.1029/2002GL015811

Lovelock, J. E., Maggs, R. J., & Wade, R. J. (1973). *Halogenated Hydrocarbons in and over the Atlantic.* Nature 241. doi:10.1038/241194a0

Manley , S. L., & de la Cuesta, J. L. (1997). *Methyl Iodide Production from Marine Phytoplankton Cultures.* Limnology and Oceanography, Vol. 42, No. 1.

Manley, S. L., & Dastoor, M. N. (1987). *Methyl halide (CH3X) production from the giant kelp, Macrocystis, and estimates of global CH3X production by kelp.* Limnology and Oceanography, Vol. 32, No. 3.

Manley, S. L., & Dastoor, M. N. (1988). *Methyl iodide (CH3I) production by kelp and associated microbes.* Marine Biology, Vol. 98, No. 4. doi:10.1007/BF00391538

Manley, S. L., Goodwin, K., & North, W. J. (1992). *Laboratory production of bromoform, methylene bromide, and methyl iodide by macroalgae and distribution in nearshore sourthern Californial waters.* Limnology and Oceanography.

McCulloch , A., & Midgley, P. M. (1996). *The production and global distribution of emissions of trichloroethene, tetrachloroethene and dichloromethane over the period 1988–1992.* Atmospheric Environment Volume 30, Issue 4. doi:10.1016/1352-2310(09)50032-5

McElroy, M. B., Salawitch, R. J., Wofsy, S. C., & Logan, J. A. (1986). *Reductions of Antarctic ozone due to synergistic interactions of chlorine and bromine.* NATURE VOL. 321.

McGivern, W. S., Francisco, J. S., & North, S. W. (2002). *Investigation of the atmospheric oxidation pathways of bromoform: Initiation via OH/Cl reactions.* J. Phys. Chem.

McGivern, W. S., Sorkhabi, O., Suits, A. G., Deresckei-Kovacs, A., & North, S. W. (2000). *Primary and secondary processes in the photodissociation of CHBr3.* J. Phys. Chem.

Minas, H. J., D., R. C., & Codispoti, L. A. (1982). *Nutrients and primary production in the upwelling region off Northwest Africa.* Rapp. P.-V. Reun. Cons Int. Explr. Mer.

Mittelstaedt, E. (1986). *Upwelling regions* (Vols. Landoldt-Börnstein, Vol. 3). Berlin: Springer Verlag.

Montzka, S. A., Butler, J. H., Hall, B. D., Mondeel, D. J., & Elkins, J. W. (2003). *A decline in tropospheric organic bromine.* Geophysical Research Letters. doi:10.1029/2003GL017745

Moore, R. M., & Groszko, W. (1999). *Methyl iodide distribution in the ocean and fluxes to the atmosphere.* Journal of Geophysical Research, Vol 104, No. C5. doi:1998JC900073

Moore, R. M., & Zafiriou, O. C. (1994). *Photochemical production of methyl iodide in seawater.* J. Geophysical Res.

Moore, R. M., Groszko, W., & Niven, S. (1996b). *Ocean-atmosphere exchange of methyl chloride: Results fron N.W. Atlantic and Pacific Ocean studies.* J. Geophys. Res., Vol. 101.

Moortgat, G. K., Meller, R., & Schneider, W. (1993). *Temperature dependence (256K - 296K) of the absorption cross-sections of bromoform in the wave-length range 285 - 360 nm.* The Tropospheric Chemistry of Ozone in the Polar Regions, edited by H. Niki and R. H. Becker, pp. 359-370. New-York: Springer-Verlag.

National Acadamy of Sciences. (2008). *Earth Observations from Space: The First 50 Years of Scientific Achievements.* Washington, D.C.: National Acadamies Press.

Nielsen, J. E., & Douglass, A. R. (2001). *A simulation of bromoform's contribution to stratospheric bromine.* J. Geophys. Res, 106.

O'Brien, L. M., Harris, N. R., Robinson, A. D., Gostlow, B., Warwick, N., Yang, X., et al. (2009). *Bromocarbons in the tropical marine boundary layer at the Cape Verde Observatory – measurements and modelling.* Atmos. Chem. Phys. Discuss., 9.

Palmer, C. J. (2010). *Contrasting the surface ocean distribution of bromoform and methyl iodide; implications for boundary layer physics, chemistry and climate.* IOP Conference Series: Earth and Environmental Science, Vol. 13, No. 1. doi:10.1088/1755-1315/13/1/012004

Parrish, D. F., & Derber, J. C. (1991). *The National Meteorological Center's spectral statistical-interpolation analysis system.* Monthly Weather Review.

Quack, B., & Wallace, D. W. (2003). *Air-sea flux of bromoform: Controls, rates and implications.* Global Biogeochemical Cycles. doi:10.1029/2002GB001890

Quack, B., Atlas, E., Petrick, G., & Wallace, D. W. (2007). *Bromoform and dibromomethane above the Mauretanian upwelling: Atmospheric distributions and oceanic emissions.* Journal of Geophysical Research, Vol. 112. doi:10.1029/2006JD007614

Quack, B., Atlas, E., Petrick, G., Stroud, V., Schauffler, S., & Wallace, D. W. (2004). *Oceanic bromoform sources for the tropical atmosphere.* GEOPHYSICAL RESEARCH LETTERS, VOL. 31, L23S05. doi:10.1029/2004GL020597

Rasmussen, R. A., Khalil, M. A., Gunawardena, R., & Hoyt, S. D. (1982). *Atmospheric Methyl Iodide (CH3I).* Journal of Geophysical Research, Vol. 87, No. C4.

Roe, J. M., & Jasperson, W. H. (1981). *A Temperature Lapse Rate Definition of the Tropopause Based on Ozone.*

Roedel, W., & Wagner, T. (2011). *Physik unserer Umwelt: Die Atmosphäre.* Springer-Verlag.

Rudolph, J., & Ehhalt, D. H. (1981). *Measurements of C2-C5 Hydrocarbons Over the North Atlantic.* J. Geophys. Res., 86.

Salawitch, R. J. (2006). *Atmospheric chemistry: Biogenic bromine.* Nature.

Salawitch, R. J., Weisenstein, D. K., Kovalenko, L. J., Sioris, C. E., Wennberg, P. O., Chance, K., et al. (2005). *Sensitivity of ozone to bromine in the lower stratosphere.* Geophysical Research Letters, VOL. 32, L05811. doi:10.1029/2004GL021504

Sawadogo, S., Brajard, J., Niang, A., Lathuiliere, C., Crepon, M., & Thiria, S. (2009). *Analysis of the Senegalo-Mauritanian upwelling by processing satellite remote sensing observations with topological maps.* International Joint Conference on Neural Networks. doi:10.1109/IJCNN.2009.5178623

Schauffler, S. M., Atlas, E. L., Blake, D. R., Flocke, F., Lueb, R. A., Lee-Taylor, J. M., et al. (1999). *Distributions of brominated organic compounds in the troposphere and lower stratosphere.* JOURNAL OF GEOPHYSICAL RESEARCH, VOL. 104, NO. D17. doi:10.1029/1999JD900197

Schemainda, R., Nehring, D., & Schulz, S. (1975). *Ozeanologische Untersuchungen zum Produktionspotential der nordwestafrikanischen Wasserauftriebsregionen 1970-1973.* Geodätische Geophysikalische Veröffentlichungen IV(16): 1-88.

Schönwiese, C. D. (2003). *Klimatologie.* Stuttgart: Ulmer Verlag.

Seibert, P., Beyrich, F., Gryning, S.-E., Joffre, S., Rasmussen, A., & Tercier, P. (1997). *Mixing Height Determination for Dispersion Modelling.* COST710 Working Group 2.

Signorini, S. R., Murtugudde, R. G., McClain, C. R., Christian, J. R., Picaut, J., & Busalacchi, A. J. (1999). *Biological and physical signatures in the tropical and subtropical Atlantic.* JOURNAL OF GEOPHYSICAL RESEARCH, VOL. 104, NO. C8.

Sinnhuber, B. M., & Folkins, I. (2006). *Estimating the contribution of bromoform to stratospheric bromine and its relation to dehydration in the tropical tropopause layer.* Atmospheric Chemistry and Physics 6, 12.

Smedman, A.-S., Bergström, H., & Grisogono, B. (1997). *Evolution of stable internal boundary layers over a cold sea.* JOURNAL OF GEOPHYSICAL RESEARCH, VOL. 102, NO. C1. doi:10.1029/96JC02782

Solomon, S., Garcia, R. R., & Ravishankara, A. R. (1994). *On the role of iodine in ozone depletion.* JOURNAL OF GEOPHYSICAL RESEARCH, VOL. 99, NO. D10. doi:10.1029/94JD02028

Solomon, S., Wuebbels, D., Isaksen, I., Kiehl, J., Lal, M., Simon, P., et al. (1995). *Ozone depletion potentials, global warming potentials, and future chlorine/bromine loading.* Scientific Asessment of Ozone Depletion.

Stull, R. B. (1988). *An Introduction to Boundary Layer Meteorology.* Dordrecht: Kluwer Academic Publishers.

Sturges, W. T., Cota, G. F., & Buckley, P. T. (1992). *Bromoform emission from Arctic ice algae.* Nature 358. doi:10.1038/358660a0

Sturges, W. T., Oram, D. E., Carpenter, L. J., & Penkett, S. A. (2000). *Bromoform as a source of stratospheric bromine.* Geophysical Research Letters.

Tanhua, T., Fogelqvist, E., & Bastürk, Ö. (1996). *Reduction of volatile halocarbons in anoxic seawater, results from a study in the Black Sea.* Marine Chemistry, Vol. 54. doi:10.1016/0304-4203(96)00005-9

Tokarczyk, R., & Moore, R. M. (1994). *Production of volatile organohalogens by phytoplankton cultures.* GEOPHYSICAL RESEARCH LETTERS, VOL. 21, NO. 4. doi:285-288

Tomczak, M., & Godfrey, J. S. (2005). *Regional oceanography: an introduction.*

Vogel, T. M., Criddle, C. S., & McCarty, P. L. (1987). *Transformations of halogenated aliphatic compounds.* Environ. Sci. Technol.

Warwick, N. J., Pyle, J. A., Carver, G. D., Yang, X., Savage, N. H., O'Connor, F. M., et al. (2006). *Global modeling of biogenic bromocarbons.* JOURNAL OF GEOPHYSICAL RESEARCH, VOL. 111, D24305. doi:10.1029/2006JD007264

Williams, J., Gros, V., Atlas, E., Maciejczyk, K., Batsaikhan, A., Schöler, H. F., et al. (2007). *Possible evidence for a connection between methyl iodide emissions and Saharan dust.* JOURNAL OF GEOPHYSICAL RESEARCH, VOL. 112, D07302. doi:10.1029/2005JD006702

WMO. (1995). *Scientific Assessment of Ozone Depletion.* Geneva: World Meteorological Organization.

WMO. (1999). *Scientific Assessment of Ozone Depletion.* Geneva: World Meteorological Organization.

WMO. (2003). *Scientific Assessment of Ozone Depletion.* Geneva: World Meteorological Organization.

WMO. (2007). *Scientific Assessment of Ozone Depletion.* Geneva: World Meteorological Organization.

WMO. (2011). *Scientific Assessment of Ozone Depletion.* Geneva: World Meteorological Organization.

Wofsy, S. C., McElroy, M. B., & Yung, Y. L. (1975). *The chemistry of atmospheric bromine.* GEOPHYSICAL RESEARCH LETTERS, VOL. 2, NO. 6. doi:10.1029/GL002i006p00215

Wolff, W. J., & Smit, C. J. (1990). *THE BANC D'ARGUIN, MAURITANIA, AS AN ENVIRONMENT FOR COASTAL BIRDS.* Research Institute for Nature Management.

Yang, X., Cox, R. A., Warwick, N. J., Pyle, J. A., Carver, G. D., O'Connor, F. M., et al. (2005). *Tropospheric bromine chemistry and its impacts on ozone: A model study.* J. Geophys. Res., 110, D23311. doi:10.1029/2005JD006244

Yokouchi, Y., Hasebe, F., Fujiwara, M., Takashima, H., Shiotani, M., Nishi, N., et al. (2005). *Correlations and emission ratios among bromoform, dibromochloromethane, and dibromomethane in the atmosphere.* Journal of Geophysical Research, Vol. 110. doi:10.1029/2005JD006303

Yokouchi, Y., Mukai, H., Yamamoto, H., Otsuki, A., Saitoh, C., & Nojiri, Y. (1997). *Distribution of methyl iodide, ethyl iodide, bromoform, and dibromomethane over the ocean (east and southeast Asian seas and the western Pacific).* JOURNAL OF GEOPHYSICAL RESEARCH, VOL. 102, NO. D7. doi:10.1029/96JD03384

Yung, Y. L., Pinto, J. P., Watson, R. T., & Sander, S. P. (1980). *Atmospheric Bromine and Ozone Perturbations in the Lower Stratosphere.* Journal of the Atmospheric Sciences, 37 (2). doi:10.1175/1520-0469(1980)037

Zafiriou, O. C. (1974). *Sources and Reactions of OH and Daughter Radicals in Seawater.* JOURNAL OF GEOPHYSICAL RESEARCH, VOL. 79, NO. 30. doi:10.1029/JC079i030p04491

Zhou, Y., Mao, H., Russo, R. S., Blake, D. R., Wingenter, O. W., Haase, K. B., et al. (2008). *Bromoform and dibromomethane measurements in the seacoast region of New Hampshire, 2002-2004.* JOURNAL OF GEOPHYSICAL RESEARCH. doi:10.1029/2007JD009103

Acknowledgements

Zum Abschluss möchte ich die Gelegenheit nutzen und all jenen danken, die mich bei dieser Arbeit unterstützt haben.

In erster Linie gilt der Dank hierbei Frau Prof. Dr. Kirstin Krüger für die Vergabe des Themas, der guten Betreuung und der Korrektur der Arbeit, sowie Frau Dr. Birgit Quack für die Zweitkorrektur.

Des Weiteren gilt mein Dank der gesamten Arbeitsgruppe Krüger für die hilfreichen Anregungen während der Gruppensitzungen und dem BMBF für die finanzielle Unterstützung der Poseidon-Fahrt P399 im Rahmen des Verbundprojektes SOPRAN II (FKZ 03F0611A).

Auch möchte ich mich bei Annika und Greg für das Kontrolllesen und den hilfreichen Tipps während der ersten „englischen Schritte“, bedanken.

Vielen Dank auch an Franziska und Helmke, für die Luftprobennahmen, den Radiosondenaufstiegen und die Beantwortung chemischer Fragen, sowie Elliot Atlas für die Analyse der atmosphärischen Mischungsverhältnisse.

Schließlich danke ich auch meinen Eltern für die Ermöglichung des Studiums und der ausdauernden Unterstützung.

Erklärung

Hiermit bestätige ich, dass ich die vorliegende Diplomarbeit selbstständig verfasst und keine anderen als die angegebenen Quellen und Hilfsmittel verwendet habe.

Ich versichere, dass diese Arbeit noch nicht zur Erlangung eines Diplomgrades an anderer Stelle vorgelegen hat.

Kiel, Juli 2011

_____

(Steffen Fuhlbrügge)